UNIVERSITEIT VAN PRETORIA
UNIVERSITY OF PRETORIA
YUNIBESITHI YA PRETORIA

THE INFLUENCE OF AGEING TREATMENT ON THE MICROSTRUCTURAL EVOLUTION AND THE MECHANICAL PROPERTIES OF THE TI-6AL-4V ALLOY

by

Mosimanegape Stephen Masete

Submitted in partial fulfilment of the requirements for the degree of

Master of Science (Applied Science) (Metallurgy)

in the

Department of Materials Science and Metallurgical Engineering

Faculty of Engineering, Built Environment and Information Technology

Supervisors:

University of Pretoria: Prof. Roelf Mostert and Prof. Charles Siyasiya.

CSIR: Kalenda Mutombo.

February 2017

Acknowledgements

The author would like to acknowledge the Department of Science and Technology (DST) for funding this work, the Council for Scientific and Industrial Research (CSIR) and the Light Metals team for affording me the studentship and for the use of their facilities.

My appreciation goes to my CSIR supervisor, Kalenda Mutombo for his guidance, technical knowledge, time and patience during my studies.

I also give thanks to the University of Pretoria supervisors, Prof. Roelf Mostert and Prof. Charles Siyasiya for their fruitful discussion, guidance and support.

Dr Sagren Govender is thanked for his support and encouragement during key performance indicator reviews.

I would also like to gratefully acknowledge the expertise of Chris McDuling and Erich Guldenpfennig for their contributions in mechanical testing, Pierre Rossouw for the material supply and heat treatment facilities, Grobbies and his team for the machining of samples for tensile, fracture toughness and fatigue crack growth, Martin Williams for the design and mechanical testing support and Levy Chauke for the supply of consumables used in the preparation of metallographic samples.

My colleagues at the CSIR are also acknowledged for their support and advice, Dr Ronald Machaka, Dr Silethelwe Chikosha, Dr Chris Machio, Dr Hilda Chikwanda, Dr Ulyate Curle, Peter Malesa, Sam Papo, Mandy Seerane, Linda Mahlatji, Johannes Jordaan, Mary Mojalefa, Christelle Stearn and Rebecca Mwelase.

Dedication

I dedicate the success of my studies to:

The Lord Almighty for the strength during difficult times, protection, guidance and his blessings.

My wife, Dikeledi, and daughter, Retshegofetse for putting up with me during stressful times and long periods of absence while going through my studies.

My family for support and encouragement, my mother (Julia), sister (Lesego), brother (Frank), and all the Masete, Mokgatlhe, Mlamla, Moaisi, and Mothibedi families, as well as friends.

"Bahurutshe!
Ditshwene ke naiwa mmele makopong ga ke naiwe ke sireletswa ke seriba"

Abstract

The Ti-6Al-4V alloy is used in aerospace parts and its microstructure and properties can be controlled by solution treatment or solution treatment followed by ageing. However, there are different views on whether solution treatment above the beta transus temperature followed by ageing can improve the microstructure and mechanical properties of the Ti-6Al-4V alloy.

This study investigated the influence of ageing treatment conditions (ageing time, temperature and cooling rate) on the microstructural evolution and the response of the mechanical properties.

Specimens of the Ti-6Al-4V alloy were solution-treated at 1050 °C for 30 minutes in a furnace in an oxygen atmosphere and water-quenched (WQ), or furnace-cooled (FC) to room temperature. The specimens were subsequently aged at temperatures of 500 °C to 900 °C for 0.5 hours to 48 hours, followed by either FC or WQ. Microstructural analysis, hardness measurements, tensile properties, fracture toughness, and fatigue crack growth rate were determined.

The ageing temperatures of 500 °C to 650 °C produced greater hardness, yield strength, and ultimate tensile strength with optimum ageing times of 0.5 hours for samples that were solution-treated and WQ. As ageing temperature and time increased, hardness, yield strength and ultimate tensile strength decreased due to the increase in the volume fraction of the α-phase and the dissolution of the martensitic needles. The best strength-ductility balance was obtained from specimens that were solution-treated and WQ, followed by ageing at 900 °C for 24 hours and FC.

Ageing of samples that were solution-treated and FC (colony lamellar) showed hardness, yield strength, and ultimate tensile strength to increase as ageing time and temperature increased. The increase was attributed to the increase in the beta content with ageing and subsequent martensitic phase transformation after quenching.

Solution treatment and WQ followed by ageing was found to result in improved mechanical properties of the Ti-6Al-4V alloy for use in the aerospace industry.

The colony lamellar specimens gave greater fracture toughness values than the fully martensitic specimens. In addition, the fatigue crack growth resistance was superior for the colony lamellar specimens than for the fully martensitic specimens. The random orientation of the α/β-colonies in the lamellar microstructure led to crack branching and formation of secondary cracks, resulting in higher fracture toughness and fatigue crack growth resistance. The fully martensitic morphology had brittle fractures leading to smoother fracture surfaces. The aged, fully martensitic specimens gave rise to greater fracture toughness than the fully martensitic specimens due to the larger α-plates, while the fatigue crack growth resistance was found to be similar.

List of figures

List of tables

List of abbreviations

%EL	Percentage Elongation
%RA	Percentage Reduction in Area
AC	Air Cooled
AT	Ageing Treatment
BSEI	Backscattered Electron Image
CMOD	Crack Mouth Opening Displacement
CT	Compact Tension
EBSD	Electron Backscattered Diffraction
EDS	Electron Diffraction Spectrometry
ELI	Extra Low Interstitials
FC	Furnace Cooled
FCGR	Fatigue Crack Growth Rate
GB	Grain boundary
HiPping	Hot Isostatic Pressing
LVDT	Linear Variable Differential Transformer
OM	Optical Microscope
SEI	Secondary Electron Image
SEM	Scanning Electron Microscope
SEVNB	Single Edge V-Notch Beam
S-N curve	Stress and Number of cycles curve
ST	Solution Treatment
ST/AC	Solution Treatment and Air Cooled
ST/FC	Solution Treatment and Furnace Cooled
ST/WQ	Solution Treatment and Water Quenched
UTS	Ultimate Tensile Strength
WQ	Water Quenched
YS	0.2% Yield Strength

Nomenclature

α	Secondary alpha (hexagonal phase)
α''	Alpha double prime (orthogonal martensite)
α'	Alpha prime (hexagonal martensite)
α_2	Alpha 2 (Ti_3Al)
α_p	Primary alpha
a	Crack length
B	Sample thickness
C	Paris constant for crack growth rate
da/dN	Fatigue crack growth rate
$d\sigma/d\varepsilon$	Strain-hardening rate
J_{1C}	Mode I J-Integral fracture toughness
K	Strength coefficient
K_1	Mode 1 stress intensity factor
K_C	Critical stress intensity factor
K_{1C}	Mode I plane strain fracture toughness
K_{1Q}	Mode 1 Conditional fracture toughness
m	Paris constant
N	Number of cycles
$P_{min,}\ P_{max}$	Minimum and Maximum load during a fatigue cycle
P_Q	Conditional load
n	Strain-hardening exponent
R	Load ratio (P_{min}/P_{max})
T_β	Beta transus temperature
W	Sample width
β	Beta phase (body centred cubic phase)
ΔK	Change in stress intensity factor
ΔK_{th}	Threshold stress intensity factor

ΔP	Load amplitude ($P_{max-} P_{min}$)
ε	True strain
σ	True stress
σ_{ys}	0.2% Yield Strength
$\frac{d\sigma}{d\varepsilon}$	Strain-hardening rate
d	average grain diameter

Table of contents

CHAPTER 1 Introduction

Titanium and its alloys are employed in many applications, including medical implants, automotive, defence, sports and aerospace parts [1][2][3][4][5]. The high strength to weight ratio of titanium alloys is attractive in the aerospace applications because it results in weight saving [3]. The most common titanium alloy is a two-phase alpha-beta (α/β) Ti-6Al-4V alloy which has exceptional mechanical properties, low density and good corrosion resistance [3][6][2]. This alloy is used for turbine engine parts and structural components in aircraft. The mechanical properties of the Ti-6Al-4V alloy can be optimised during thermo-mechanical processing and heat treatment [7][8].

One of the areas where Ti-6Al-4V alloy is used is the aircraft engine for the fan blades. The fan blades are exposed to temperatures below 400 °C where the Ti-6Al-4V would not be negatively affected. The fan blades experience a fatigue loading of high frequencies and varying stress ratios. The fatigue crack initiation, crack propagation and crack growth in Ti-6Al-4V alloy parts are of interest in the design of durable structures. The conventional method of assessing fatigue life is by using the stress and the number of cycles (S-N) curve and investigation of crack initiation and propagation. The S-N curve method would not apply where a structure has a pre-existing crack. The fracture mechanics approach becomes useful in determining the threshold stress intensity required to cause an existing crack to propagate. Determination of the fatigue crack growth rate and fracture toughness properties is essential for structures with pre-existing cracks.

The Ti-6Al-4V alloy is used in the annealed or solution-treated or solution-treated and aged condition [3][6]. These heat treatments affect the microstructure and mechanical properties of the alloy, resulting in limited use of the Ti-6Al-4V alloy at higher service temperatures. Solution heat treatment of the Ti-6Al-4V alloy at different temperatures, times and cooling rates has been widely reported [4][5][7][8][9][10][11][12]. Most authors [4][7][8] preferred to do only solution treatment at a temperature below the beta transus (T_β). Reda et al. [8] suggested solution-treating the Ti-6Al-4V alloy at temperatures below the β-transus to avoid grain coarsening and the greater volume fraction of fine martensitic needles.

There are limited data on ageing treatment of the Ti-6Al-4V alloys. In addition, there are various schools of thought on whether the ageing treatment can improve the microstructure and mechanical properties. Literature sources propose that finding the optimum solution treatment conditions is better, so as to avoid ageing treatment which adds to manufacturing costs [4][8][10]. Other sources proposed the need for ageing to improve ductility, especially where the solution-treated alloy was water-quenched [7][5]. Youssef et al [7] solution-treated the Ti-6Al-4V alloy above the β-transus temperature and only considered one ageing temperature (500 °C) and time (24 hours). The authors found hardness to increase after ageing treatment. Zeng and Bieler [5] studied the microstructural evolution of primary alpha (α_p), secondary alpha (α_s), beta (β), hexagonal martensite (α') and orthorhombic martensite (α'') phases during heat treatment of Ti-6Al-4V wire alloy and showed that formation of metastable phases like α'' and β form during ageing. The authors [5] indicated that this transformation depended on the temperature and chemical composition of the alloy. Zeng and Bieler [5] did not indicate how these phases affected mechanical properties of the alloy. Carreon et al [13] studied ageing of Ti-6Al-4V alloy at temperatures of 515 °C, 545 °C and 575 °C for ageing times over one minute up to 576 hours and precipitated nanometer-sized α_2-particles within the α-phase. The morphology stayed the same for all the ageing times.

After ageing times of 100 hours, there was saturation in precipitation of α_2-phase hence the hardness stayed the same for up to 576 hours ageing time. Gil et al reported the hardness to increase with increasing ageing temperature (400 to 800 °C) for the fully martensitic morphology [14]. The results of Gil et al [14] contradict those of Carreon et al [13].

References to the effect of ageing treatment in the mechanical properties of interest in the aerospace industry (strain-hardening, fatigue crack growth rate, and fracture toughness) are scarce. Fatigue crack growth rate and fracture toughness of the microstructural morphology produced by solution treatment without ageing is widely reported in the literature. These morphologies are the lamellar, equiaxed, bimodal and the fully martensitic morphology. However, the effect of ageing on hardness of the Ti-6Al-4V alloy is extensively covered in the literature. Some papers looked at fracture toughness and fatigue, but these were mainly to understand the effect of other treatments such as welding, irradiation and laser treatment on mechanical properties [15][16]. Experimental data for the ageing of the Ti-6Al-4V alloy specimens that have been solution-treated above the beta transus is also limited.

This dissertation aims to answer the following questions.

- How does the microstructure of the Ti-6Al-4V alloy evolve at various ageing temperatures, ageing times and cooling rates for specimens that are solution-treated above the beta transus temperature?
- How does the ageing condition affect the tensile properties, fracture toughness and the fatigue crack growth resistance of the Ti-6Al-4V alloy?
- Can an optimised microstructural morphology with better tensile properties, fatigue crack growth rate, and fracture toughness than the fully martensitic morphology or lamellar morphology be produced by ageing?

The objective of this project was to study the effect of ageing conditions (temperature, time and cooling rate) on the microstructure (grain size, lath size, α/β content, α/β-colony size) and the mechanical properties (hardness, tensile properties, fracture toughness and the fatigue crack growth rate) of the Ti-6Al-4V alloy solution treated above the beta transus. The study is needed to develop an understanding that will aid in the design of a Ti-6Al-4V alloy with optimised fatigue crack growth resistance or fracture toughness or tensile properties used in aircraft fan blades.

The dissertation has seven chapters. Chapter 1 has an introductory section providing background and the project motivation. Chapter 2 is a survey of literature on Ti-6Al-4V alloy's heat treatment, microstructure evolution and the mechanical properties. Chapter 3 details the methodology followed in conducting this research. The results are reported in Chapter 4. Discussion of the results is provided in Chapter 5. Chapter 6 contains conclusions, while Chapter 7 gives recommendations for future work.

CHAPTER 2 Literature review

The chapter reviews the literature on heat treatment, microstructure and mechanical properties of the Ti-6Al-4V alloy solution treated above the beta transus temperature. The review presents prior knowledge of microstructural features of the Ti-6Al-4V alloy, the microstructural evolution and the resulting microstructures after heat treatment. The related mechanical properties of the alloy, with emphasis on tensile properties, fracture toughness and fatigue crack growth rate resistance are reviewed. The current gaps in the literature on microstructure and mechanical properties of the alloy are identified and used as motivation for the current project.

2.1 Solution-treatment of the Ti-6Al-4V alloy

Thermomechanical processing of titanium alloys is utilised to modify and control the microstructure and, consequently, the mechanical properties [9][17][18]. Heat treatment process can be used to produce the optimal combination of ductility and machinability, to increase strength, as well as to optimise fracture toughness, fatigue and creep strength, and also to reduce residual stresses. The main solution treatment variables are temperature, time and cooling rate. Solution treatment can be performed below or above the beta (β) transus temperature of the Ti-6Al-4V [18][19]. Solution treatment below the beta transus reduces the energy cost and limits the grain growth of the alloy. The highest ductilities are obtained from solution treatment below the beta transus, followed by furnace-cooling, while the highest possible strengths are obtained from solution treatment above the beta transus, followed by water-quenching [8]. The β-transus temperature of Ti-6Al-4V depends on the chemical composition and impurity levels of the alloy, and ranges between 990 °C to 1000 °C [8][7] [20][18][21]. The ternary phase diagram (Figure 2.1) of the Ti-6Al-4V alloy shows the β-transus temperature to be about 1000 °C [19]. For a Ti-6Al-4V alloy, the β-phase is shown to be stable above 1000 °C, while the α plus β-phases are stable below 1000 °C. The solution treatment dwell times of 10 to 60 minutes are frequently used, while the cooling rates are water-quenching (WQ), air-cooling (AC) or furnace-cooling (FC) [7] [8][18][19].

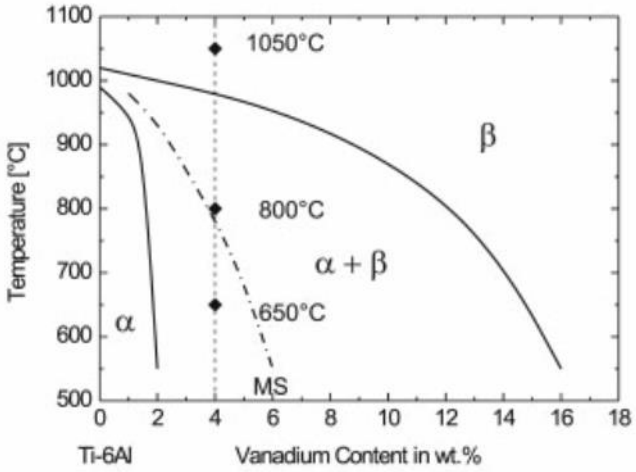

Figure 2.1: Schematic ternary phase diagram of the Ti-6Al-V alloy [19]

The continuous cooling transformation diagram of the Ti-6Al4V alloy (Figure 2.2) shows various phases that can form during cooling from above the β-transus temperature[22]. The martensitic phase (α′) forms when cooling at a rate above 18 °C/s. As the cooling rate

decreases down to 3.5 °C/s, a martensitic phase, plus a combination of α and β, forms. The decrease in cooling rates leads to a reduction in martensitic volume fraction while the α-phase volume fraction increases [22]. Colony lamellar microstructures consisting of stable α and β-phases form at cooling rates below 2 °C/s.

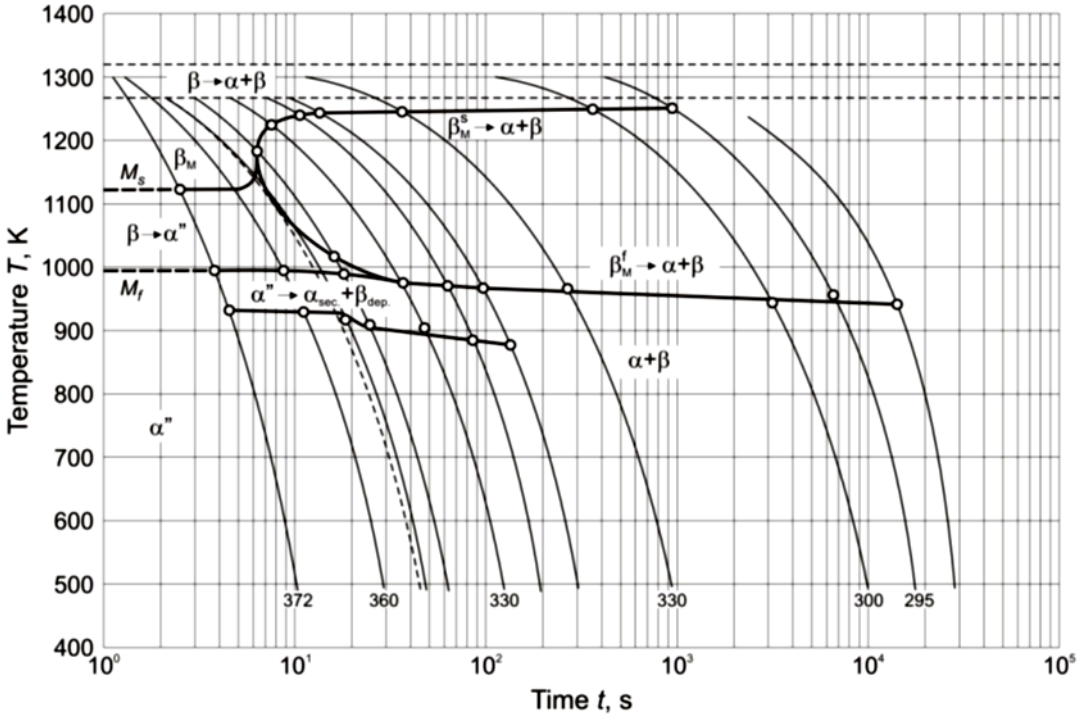

Figure 2.2: Continuous cooling transformation diagram of Ti-6Al-4V alloy [22]

Solution treatment above the beta transus, followed by water-quenching, produces a fully martensitic microstructure (Figure 2.3)[23][4][5][8] [9] [23][15][25][26]. The microstructure consists of the hexagonal martensite (α′-phase) and β-phases. Youssef et al. [7] produced a fine lamellar structure when quenching from about 1050 °C. The hexagonal martensite (α′) is formed during quenching of Ti-6Al-4V alloy from a temperature above the β-transus temperature [4], [5], [8], [9], [24][15]. The α′-phase is a nonequilibrium structure produced by diffusionless transformation of the β-phase. The shape of α′-phase shown in Figure 2.3 is a fine and needle-like [24]. The α′-phase then transforms to a fine β-phase during ageing [24]. The β-phase is found on the grain boundaries [24].

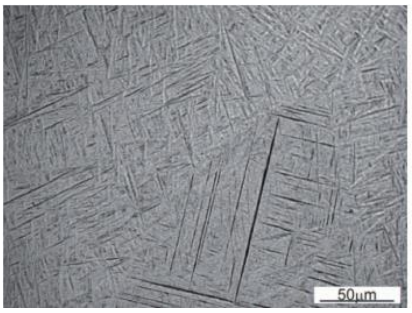

Figure 2.3: Martensitic microstructure[15], showing fine acicular and needle-like shape of α′-phase

As the solution treatment temperature increases, the volume fraction of the β-phase increases, leading to the increase in the volume fraction of the α′-phase after quenching, as shown in Figure 2.4 [8] [20] [8][27]. Heating alpha and beta (α+β) alloy to the solution treatment

temperatures above the beta transus produces a greater ratio of the beta (β) phase, which is transformed to α′ by quenching, leaving a residual β-phase.

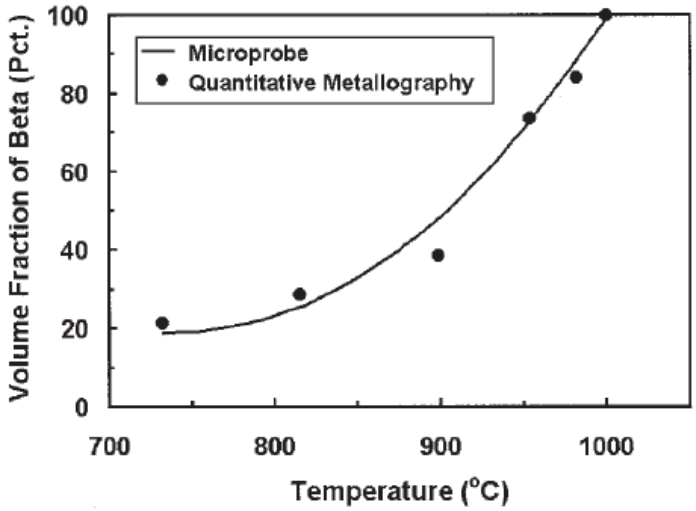

Figure 2.4: The increase in the volume fraction of the β-phase as the temperature increases for the Ti-6Al-4V alloy [20]

The β-grain size increases with the increasing solution treatment temperature (Figure 2.5) [28] [29]. Gil et al. [29] studied the growth of grain size by solution treating the Ti-6Al-4V alloy at various temperatures, soaking times and cooling times and found grains to grow larger as the temperature increased (Figure 2.5). The β-grain sizes of about 300 to 2000 μm result when the Ti-6Al-4V alloy is solution-treated above the β-transus temperature [13] [29].

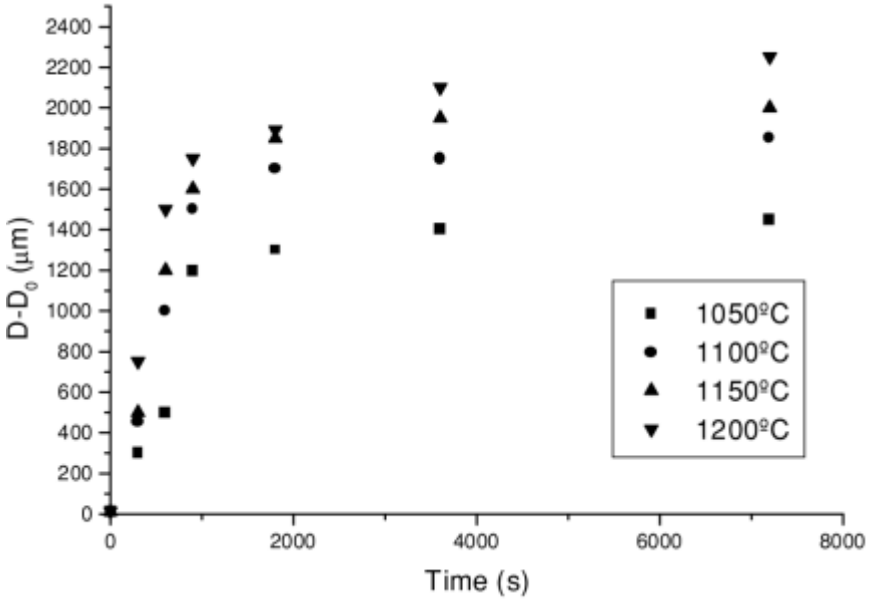

Figure 2.5: The increase in grain size of the Ti-6Al-4V alloy as a function of temperature and time (D_o is the initial grain size, while D is the final grain size) [29]

Air-cooling after solution treatment above the beta transus temperature produces a partial martensitic morphology shown in Figure 2.6 [23] [25][30][15] [31]. The grain boundaries consist of a mixture of α and β-phases while the grains consist of α′-phase needles and fine α-laths. As the cooling rate drops, the α-laths become thicker and the α-phase content increases. However, the β-grain sizes remain unchanged.

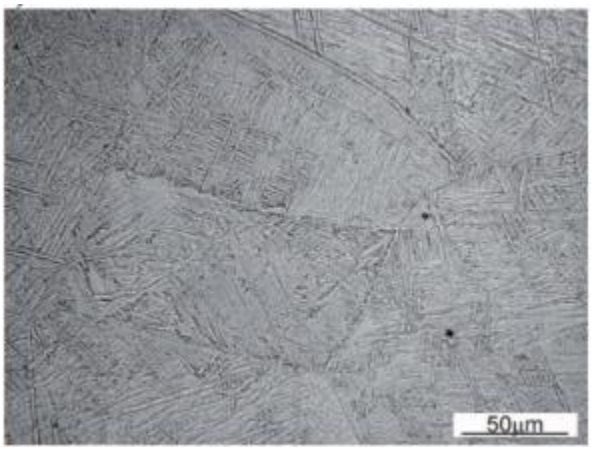

Figure 2.6: Partial martensitic microstructure showing α', α-grain boundaries and α-laths [15]

A coarse colony lamellar microstructural morphology containing the Widmanstätten morphology regions (Figure 2.7) may be produced by solution treatment above the β-transus temperature, followed by furnace-cooling[15] [7], [8], [18]–[23][26] [10]) [30]. The grain boundaries consist of the α-phase, while the grains consist of colonies of the α/β-lamellae. Lamellar structures are characterised by the following microstructural features; β-grain size, α-lamellar size, α/β-colony size and α-phase grain boundary [9][22]. The Widmanstätten microstructure forms when new α-colonies nucleate, not only on the β-phase boundaries, but also on boundaries of other colonies, growing perpendicular to the existing lamellae [22]. Sugahara et al [32] produced a Widmanstätten microstructure by solution heat-treating Ti-6Al-4V alloy at 1050 ºC for 30 minutes and cooling to room temperature at 6 °C/min. Dabrowski [15] produced a Widmanstätten α-phase morphology when cooling the Ti-6Al-4V from 1020 °C at cooling rates of 7.3 to 0.0651 °C/s. For a lamellar microstructure, the cooling rate affects the α lamellar size, α/β-colony size and the extent of the lamellar size at β-grain boundaries [9][12]. Lower cooling rates produce bigger colony sizes and thicker α-plates (Figure 2.8) [9] [29]. The diffusivity of the stable α-phase is increased and promoted by slow cooling, hence the increase in thickness as the cooling rate decreases. As the solution treatment temperature increases, the width of the α-plates increases (Figure 2.8) [29].

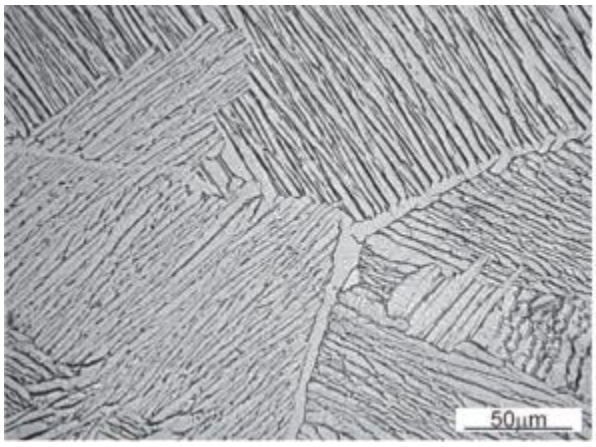

Figure 2.7: The colony lamellar or Widmanstätten microstructure [15]

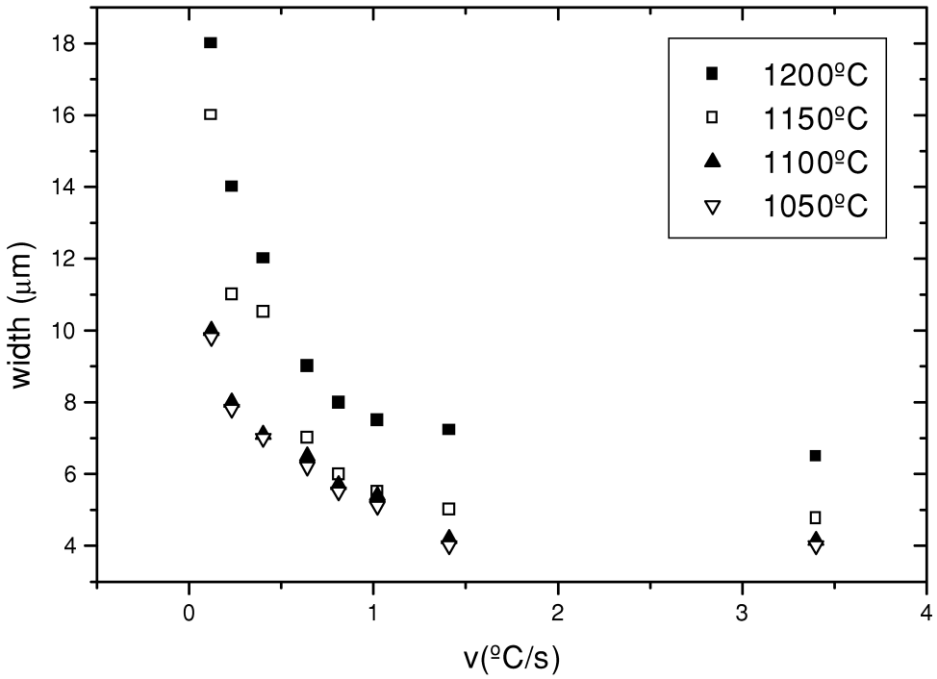

Figure 2.8: The variation of the lamellar plate width as a function of the cooling rate in Ti-6Al-4V alloy [29]

Compared to the fully martensitic morphology, the colony lamellar morphology has bigger β-grains and thicker α-lamellae [15] [31]. The slow cooling rate allows the alloy to experience longer exposure to higher temperatures than when rapid quenching is done. This results in noticeable grain growth in the lamellar morphology.

Longer solution treatment dwelling times lead to excessive grain growth [18] [29]. The grain size increases with increasing soaking times for the same temperature as shown in Figure 2.5. Grain growth occurred rapidly in the first 15 to 20 minutes and slowed down thereafter. The change in slope occurring at around 1000 seconds (16 minutes) is evidence of the decrease in grain growth rate. This was interpreted by the decrease in grain boundary area per unit volume ratio during grain growth, therefore lowering the driving force for grain growth.

Oxidation of titanium alloys readily takes place above 427 °C and heat treatments need to be done in a vacuum or inert atmosphere [17][24][18]. Should oxidation not be prevented, oxygen will react with titanium to form an oxygen-enriched brittle layer called the alpha case, shown in Figure 2.9 [19]. The alpha case, which is a mixture of $Ti0_2$ and Al_30_2 can later be removed by costly machining or chemical milling methods [9][19]. Leyens and Peters [19] showed the alpha case thickness to be below 200 μm at temperatures below 700 °C, while Donachie et al [18] reported that the material stock removal required is about 400 μm after exposure for 1 to 2 hours for temperatures of 1039 °C to 1066 °C. The micro-hardness profile (Figure 2.9) shows that hardness is greater at the sample surface where the oxygen content (presence of α-case) is high and it is lower in the sample where there is little or no dissolved oxygen in the α-phase [19].

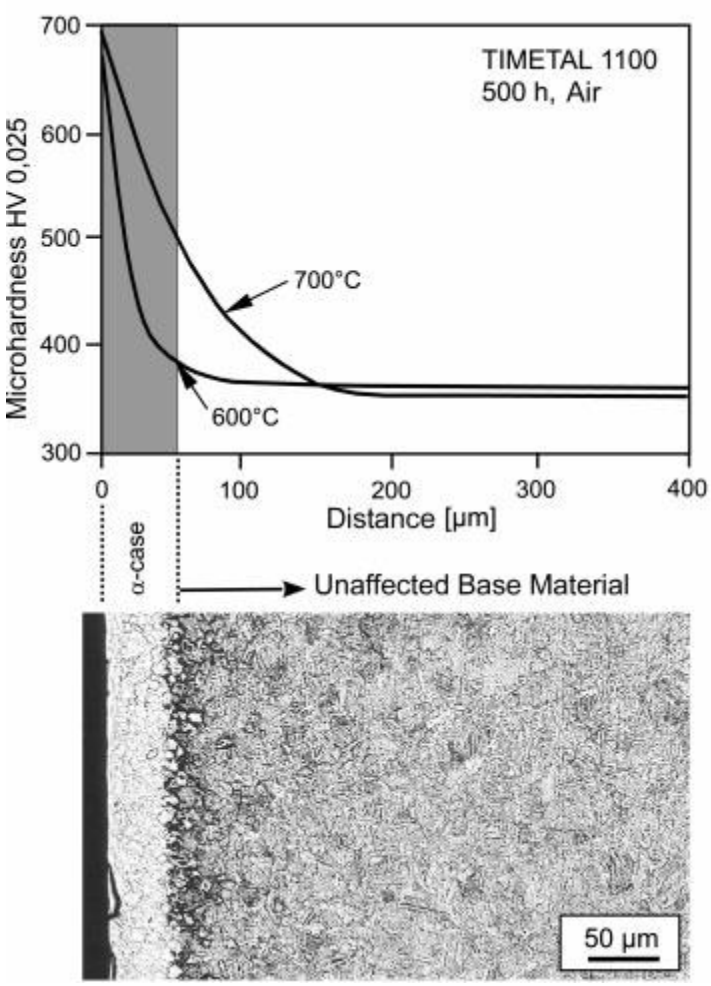

Figure 2.9: Micro-hardness profile after 500 hours of exposure to 600 °C and 700 °C and cross-section showing alpha case [19]

The oxide layer formed on commercially pure titanium shows (Table 2.1) the thickness to be about 360 µm after half an hour of exposure to air at a temperature of 1095 °C.

Table 2.1: Thickness of oxide formed on commercially pure titanium as a function of temperature [18]

Temperature		Measurable thickness	
C	F	mm	in.
315	600	None	None
425	800	None	None
540	1000	None	None
650	1200	<0.005	<0.0002
705	1300	0.005	0.0002
760	1400	0.008	0.0003
815	1500	<0.025	<0.001
870	1600	<0.025	<0.001
925	1700	<0.05	<0.002
980	1800	0.05	0.002
1040	1900	0.10	0.004
1095	2000	0.36	0.014

Heated for ½ h in air

Oxidation rates vary considerably for titanium alloys as shown in Figure 2.10. The Ti-6Al-4V alloy shows the lowest oxidation rate compared to that of the other titanium products shown in Figure 2.10. The presence of both aluminium and titanium protects the bulk of the alloy from further oxidation by the formation of the surface $Ti0_2$ and Al_30_2. This oxidation background implies that the alpha case thickness formed during heat treatment of the Ti-6Al-4V alloy at about 1100 °C for 30 minutes will always be below 500 μm.

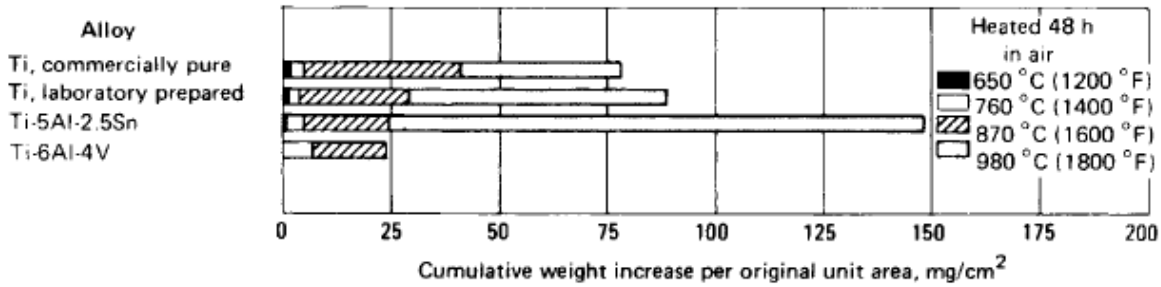

Figure 2.10: Oxidation of titanium and titanium alloys in air at various temperatures [18]

The purpose of solution treatment above the β-transus is to homogenize and transform all the primary α-phase to the β-phase, which during quenching, forms the fine α′-martensitic phase. The presence of α′ during ageing is ideal for manipulation of the microstructure and mechanical properties. There is a difference of opinions in the literature on whether the appropriate temperature for solution treatment is below or above the β-transus. The current project is of a view that where solution treatment is below the β-transus, some of the primary α-phase does not dissolve and can still be visible at the end of the heat treatment. The effect of the rolling texture would still be present in the primary α-phase, leading to heterogeneity the in mechanical properties for different orientations.

2.2 Ageing treatment

Most literature sources suggest that it is costly and time-consuming to solution-treat and age the Ti-6Al-4V alloy. It is preferable to find optimum solution treatment conditions and avoid ageing treatment [4][8][10]. Ageing treatment is carried out to improve the ductility of the alloy after solution treatment and quenching. Reda et al. [8] proposed to solution-treat the Ti-6Al-4V alloy below the β-transus to avoid grain-coarsening and the formation of a high-volume fraction of fine α′-martensite. This temperature to optimise strength, elongation and impact strength was found to be 900 °C. However, ageing has been utilised to further improve the strength of the Ti-6Al-4V alloy. Ageing is primarily affected by the ageing temperature and time, while the cooling rate has a negligible effect. As ageing temperatures approach annealing temperatures (700 to 850 °C), overageing occurs [18][24][22]. Ageing temperatures of about 400 to 650 °C were reported [24][18][7][5][12][24][18] [33][34].

Optimum ageing temperatures for high strength are reported to be about 500 to 550°C [12] [35] [23] [34] [27][18][34]. Ageing temperatures below 500 °C were found to have no effect on the microstructural morphology [12] [36]. The α′-martensite that formed after quenching transformed to the fine α and β-phases during ageing [12][35][18][5]. Ageing treatment of a fully martensitic morphology at temperatures of 360 °C to 600 °C showed the microstructure to coarsen as ageing temperatures reached 600 °C, Ouchi et al. [27]. Wang et al. [37] reported similar results where coarsening of the α-phase occurred after ageing a martensitic morphology at temperatures of 600 °C to 700 °C, while ageing at 500 °C decomposed the α′-phase to form the fine α and β-phases. As the ageing temperature increases, decomposition of

the α′-phase reaches completion and coagulation of the fine α-phase starts, leading to a coarser α-phase [12]. Gil et al. [14] reported on specimens that were solution treated and WQ followed by ageing at 400 °C, 600 °C, 700 °C and 800 °C and the results were contrary to what Ouchi et al. [27] and Wang et al. [37] found. According to Gil et al. [14], the decomposition of martensite to fine α and β-phases continues from ageing temperatures of 400 °C up to 800 °C without any coarsening taking place. Furthermore, the content of the fine α and β-phases increases until precipitation reaches completion at 800 °C. The authors did not consider the stability temperature range for the fine α and β-phases, as well as the possibility of the α-phase coarsening with increasing ageing temperature [14].

Optimum ageing times for the precipitation of the fine α and β-phases have been found to be about 30 minutes, after which either coarsening of the α-phase occurs or no decomposition takes place [12][14][23][27]. According to Gil et al. [14], there is no coarsening of the α-phase as the ageing time increases for all temperatures evaluated (400 to 800 °C). Other authors found ageing times longer than 8 hours to lead to coarsening of the α-phase [23] [27].

Ageing of a lamellar morphology leads to hardening of the α-phase by precipitation of Ti_3Al (α_2) [38][13] [24] [39]. The α_2-phase forms on alloys containing more than 6% Al and is promoted by higher oxygen content [24]. Precipitation occurs at temperatures below 550 °C. The α_2-phase's solvus temperature ranges from 550 °C to 600 °C and is dependent on the alloy composition and oxygen content. Any ageing above this temperature leads to the disappearance of the α_2-phase [38]. Mutombo et al. [21] showed the α_2-phase in the Ti-6Al-4V to exist only up to a temperature of 625 °C and to disappears when the temperature was raised further (Figure 2.11). Figure 2.11 was generated by Mutombo et al. [21] using the thermodynamic software CompuTherm Pandat™.

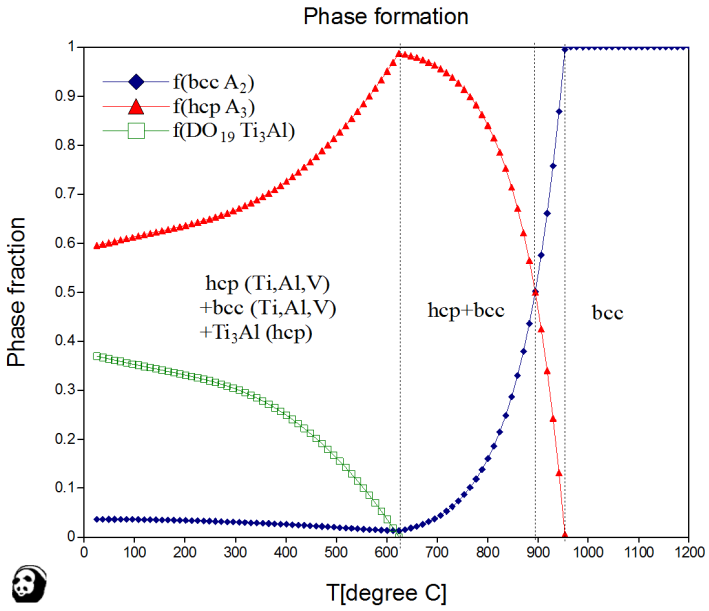

Figure 2.11: Phase stability of α, α_2 and β-phase from room temperature to 1200 °C [21]

Carreon et al. [13] studied the ageing treatment of the colony lamellar Ti-6Al-4V alloy at temperatures of 515 °C, 545 °C and 575 °C for ageing times of up to 576 hours. Nanometer-sized α_2-phase particles were precipitated in the α-phase. The morphology stayed the same for all the ageing times and temperatures as the α-grain boundary, the colony size, the α-platelet size, and the β-grain size were not affected. Increasing the ageing time led to an increase in the content of the α_2-phase due to increased precipitation (Figure 2.12). The

content of the α_2-phase stayed constant after about 150 hours of ageing as the precipitation reached completion. Higher ageing temperature reduced the content of the α_2-phase. Lee et al. [39] reported a different finding to that of Carreon et al. [13] where the content of the α_2-phase continued to increase after 300 hours of ageing a Ti-6Al-4V with a lamellar morphology at 545 °C. According to Lee et al. [39], precipitation of the α_2-phase continued as ageing time increased.

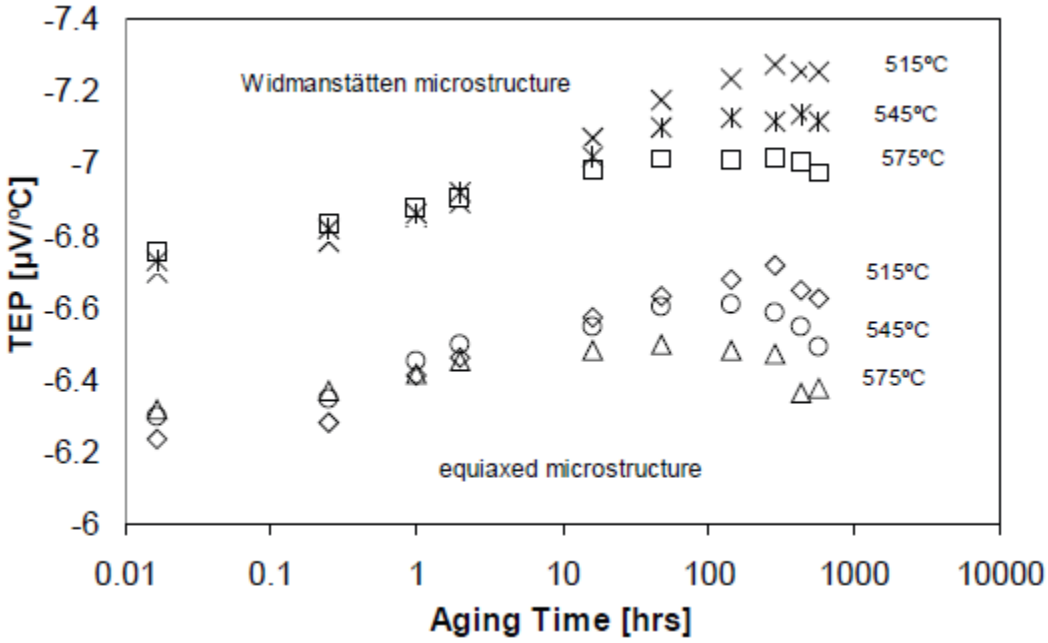

Figure 2.12: Change in the α_2-phase content with ageing temperature and ageing time measured using the Thermo Electric Power method (TEP). Higher TEP means higher α_2-phase precipitates [13]

2.3 Hardness and tensile strength

Microstructural features that improve hardness also improve tensile strength. Hall-Petch-hardening, precipitation-hardening and martensitic transformation are among some of the commonly known strengthening methods of metals. The Hall-Petch equation (Equation (2-1)) shows that the yield strength (σ_y) increases as the grain size (d) decreases. As the grain size decreases, the average number of grain boundaries increases. The grain boundaries become obstacles to the dislocation movement, which leads to delayed deformation and consequently to increased strength. Precipitation-hardening results from the formation of fine precipitates in metal grains during heat treatment. The precipitates act as obstacles to dislocation movement, which leads to increased strength. The greater the content of precipitates, the greater the hardness or yield strength. Martensitic transformation also leads to strengthening of metals [18]. Greater levels of dislocation are known to exist in martensitic microstructures, which promote dislocation interactions and entanglement resulting in increased strength [26] [6]. All these strengthening methods indicate that finer microstructures will have a greater hardness or tensile strength than coarser ones. Titanium alloys have also been strengthened using similar methods[6] [18][26]

$$\sigma_y = \sigma_0 + \frac{K_y}{\sqrt{d}} \tag{2-1}$$

Where σ_y is the yield strength, σ_0 is a material constant, K_y is the strengthening coefficient and *d* is the average grain diameter.

Hardness and strength of the titanium alloys are affected by the relative contents of the α and β-phases, and their morphology [19]. The β-titanium alloy is known to be harder than the α-Ti alloy as shown in Figure 2.13 [40]. The hardness differences are attributed to the ease of deformation of the α-phase as compared to the β-phase [6][19]

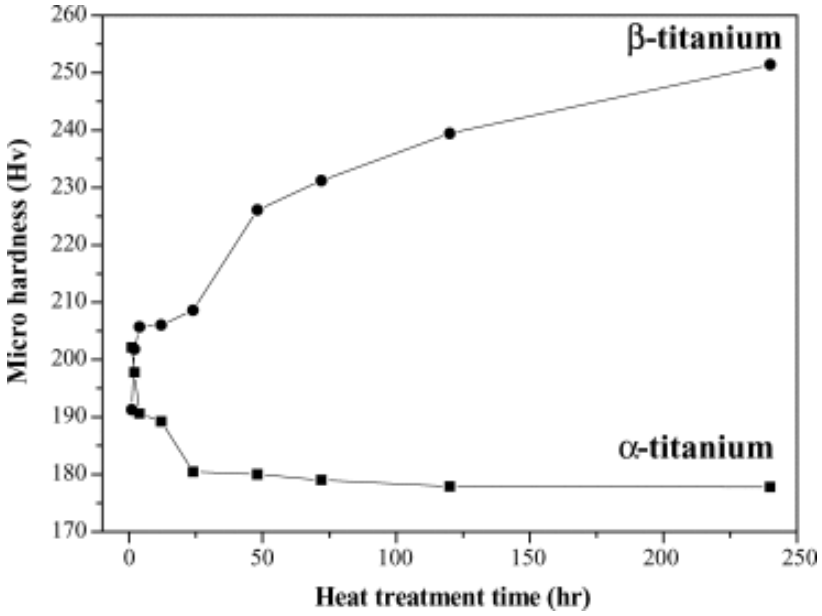

Figure 2.13: Micro-hardness variation of α-Ti and β-Ti specimens after heating at 750 °C and 1000 °C for different times and quenching [40]

The volume fraction of the fine martensitic needles increases when the quenching temperature is increased. This results in increased hardness and tensile strength (Figure 2.14) [4], [7], [8], [29]. However, the ductility decreases when the content of the martensitic needles is increased. As the heat treatment temperature increases, the volume fraction of the β-phase increases, leading to increased martensite during quenching, hence a greater hardness or strength.

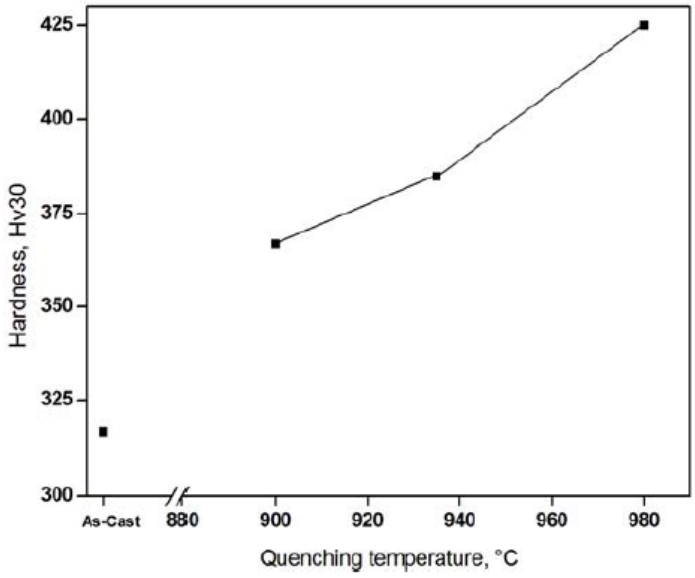

Figure 2.14: Hardness of Ti-6Al-4V alloy as a function of quenching temperature [8]

Water-quenching leads to the formation of fine martensitic needles, yielding greater strength, while slow furnace-cooling produces coarse lamellar structures, resulting in lower strength [18][4]. Other scholars [7][24] [26] [4] [41] [15] [12][42] agree that higher cooling rates produce greater volume fraction of the martensite which causes the tensile strength to increase. The increase in strength with increasing volume fraction of the fine martensitic needles is consistent with the Hall-Petch-strengthening mechanism. The cooling rate can also affect the size of the lamellae, with fine lamellar structures yielding greater hardness values as shown in Figure 2.15 [7]. The as-cast Ti-6Al-4V has the lowest hardness due to the presence of coarse β-grains and coarser α/β-lamellar microstructures. The ductility decreases as the hardness or tensile strength increases. The yield strength is affected by the alpha morphology produced from different heat treatments. The fine martensitic morphologies give a high yield strength while the coarse plate-like alpha gives a low yield strength (Figure 2.16) [26]. The presence of oxygen during heat treatment leads to the formation of a hard and brittle alpha case plus dissolved oxygen, resulting in the greatest yield strength as indicated in Figure 2.16.

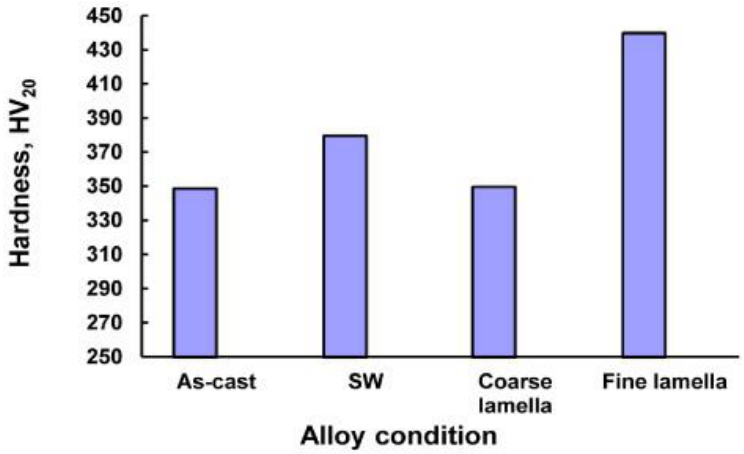

Figure 2.15: Hardness values of the Ti-6Al-4V of different microstructures (SW is swaging) [7]

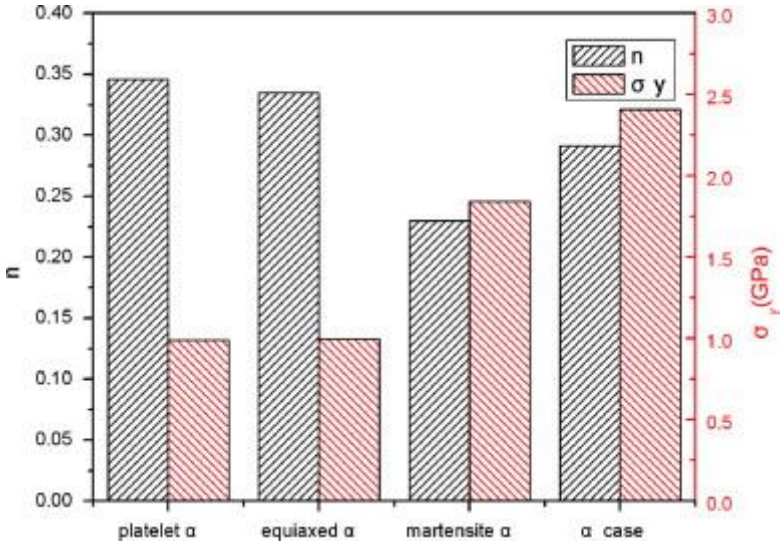

Figure 2.16: Strain-hardening exponent (n) and yield strength (σ_y) of the Ti-6Al-4V alloy of different alpha morphologies [26]

The strength of the Ti-6Al-4V alloy can be increased by solution treatment above the β-transus temperature, followed by ageing [24] [43] [35]. The presence of the martensitic

needles, the formation of fine α or β-phases, and the precipitation of the α_2-phase lead to an increase in strength of the Ti-6Al-4V alloy. The age-hardening response of the martensitic type microstructures is derived from the presence of martensitic needles, which decompose to form the fine β-phase. However, the age-hardening of the lamellar microstructure is mainly due to the precipitation of the α_2-phase.

Ageing of the martensitic morphology leads to increased strength due to the decomposition of the martensitic needles and the formation of the fine α and β-phases [37] [35][43] [27] . As the ageing temperature increases above 650 °C, the fine α and β-phases coarsen, which leads to a reduction in strength (Figure 2.17). The results of Wang et al. [37] and Ouchi et al. [27] are in agreement that as the ageing temperature increases, the hardness drops due to coarsening of the α and β-phases. However, the results of Gil et al. [14] are contrary to those of Wang et al. [37] and Ouchi et al. [27]. According to Gil et al. [14], as the ageing temperature increases, the hardness increases due to the increase in the content of the fine α and β-phases (Figure 2.18).

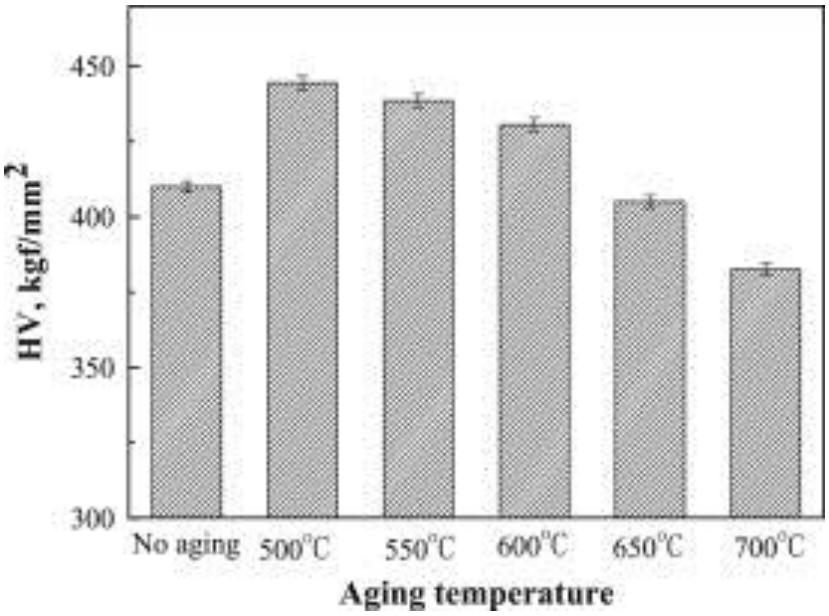

Figure 2.17: Vickers hardness of Ti-6Al-4V/TiBw (95/5 vol. %) composites that were solution-treated at 990 °C and water-quenched, followed by ageing at different temperatures for 6 hours and air cooled [37]

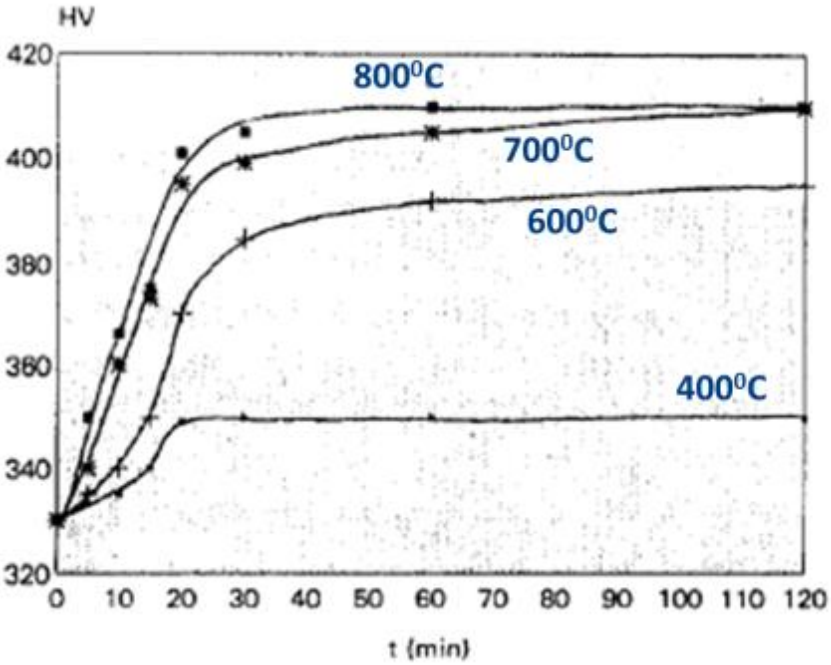

Figure 2.18: Hardness evolution with ageing temperature and time for a fully martensitic Ti-6Al-4V alloy [14]

Longer ageing times promote coarsening of the α-phases, hence a reduction in hardness for ageing temperatures of 480 °C to 600 °C [27]. Gil et al. [14] and Ouchi et al. [27] reported different results with regard to the effect of ageing time in age-hardening of the fully martensitic morphology. According to Gil et al. [14], ageing times above 30 minutes do not affect hardness. This is attributed to the precipitation of the α and β-phases having reached saturation at an ageing time of 30 minutes. However, Ouchi et al. [27] showed longer ageing times to result in overageing and hence a reduction in hardness (Figure 2.19). At higher ageing temperatures, the drop in hardness grows larger as the ageing time increases [27]. However, coarsening of the α-phase was not found at lower ageing temperatures of 360 °C and 420 °C.

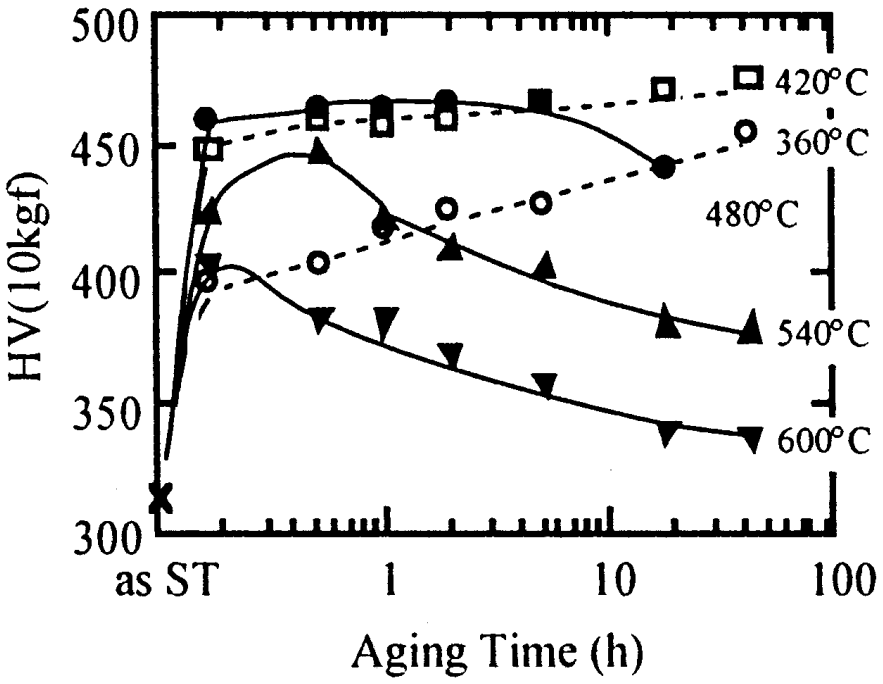

Figure 2.19: The change in hardness with ageing temperature and time [27]

Ageing of the Ti-6Al-4V alloy with a lamellar morphology led to an increase in hardness due to the precipitation of the α_2-phase from the α-phase [13] [39][38]. As the ageing temperature increases, the hardness drops due to the dissolution of the α_2-phase (Figure 2.20) [13]. Carreon et al. [13] found the hardness to stay constant after an ageing treatment for about 140 hours due to the precipitation of the α_2-phase having reached completion. However, Lee et al. [39] found hardness to increase as ageing time increased due to the continuous increase in precipitation of the α_2-phase (Figure 2.21) for an ageing temperature of 545 °C. The results of authors Carreon et al. [13] and Lee et al. [39] contradict each other.

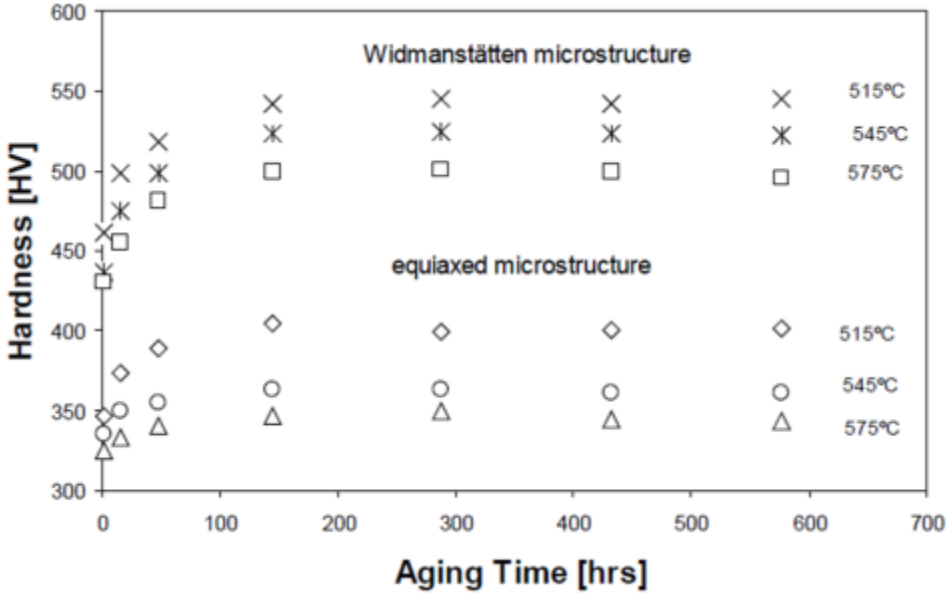

Figure 2.20: Change in hardness with ageing temperature and ageing time for Ti-6Al-4V alloy [13]

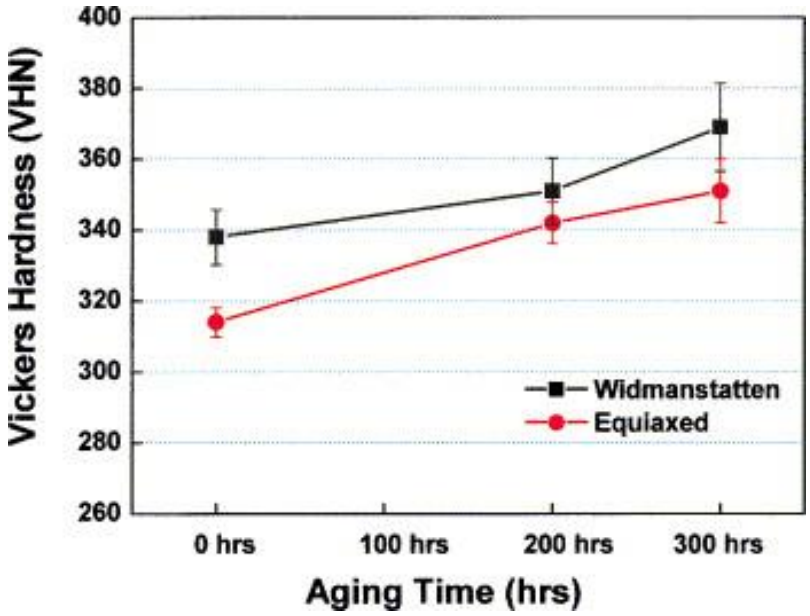

Figure 2.21: The effect of ageing time in hardness of the Ti-6Al-4V alloy aged at 545 °C [39]

The strength-ductility balance is defined as the product of the ultimate tensile strength (UTS) and % elongation (% EL) [44]. The strength-ductility balance is commonly used to rank various titanium alloys for application where high UTS and high ductility are required [27][44]. Chao et al. [44] suggested the use of the strength-ductility balance as an indicator of optimised mechanical properties of the Ti-6Al-4V alloy.

2.4 Strain-hardening (Work-hardening) behaviour

The strain-hardening exponent, n, is an empirical parameter to measure stretch formability of metallic materials [45]. The strain-hardening exponent is also a measure of the increase in strength due to plastic deformation. Gupta et al. [6] define strain-hardening as the use of permanent deformation to increase the strength of a metal. Strain-hardening results from the interactions of dislocations with each other and other features of the microstructure such as grain boundaries, precipitates and solute atoms [6]. The dislocations move during deformation until they are blocked by other dislocations or barriers. The dislocations then pile up and require more energy to move them. The generation, pile-up and movement of dislocations needing more energy lead to strengthening of metals [6].

Gupta et al. [6] reviewed the role of strain-hardening in the selection of materials for aerospace application and reported the interaction of dislocations as the principal strain-hardening mechanism. The strain-hardening exponent of the as-received alloy is lower than in the solution-treated and air-cooled specimens, due to the formation of a fine lamellar structure, which impedes dislocation movement. The solution-treated and WQ specimens lead to a greater strain-hardening rate due to the presence of greater dislocation density than in the ST and AC specimens [41] [46][26]. Ageing of the solution-treated and WQ specimens increases the strain-hardening exponent due to the increase in the number of fine α-phase particles that impede dislocation movement. Increasing the ageing temperature reduces the strain hardening as the α-phase content increases and coarsens.

Strain-hardening of a Ti-30Zr-5Al-3V (wt. %) alloy was determined for solution treated and WQ or AC or FC specimens [47]. It was found that the strain-hardening exponent of the ST and WQ specimen was greater than that of AC and FC specimens, due to an increased content of dislocations in the WQ specimen. The value of the strain-hardening exponent

increases with increasing β-phase and martensitic phase content, but is independent of the average thickness of α-plates [47]. The dislocation movement and multiplication during plastic deformation is faster in the β-phase than in the α-phase, hence greater strain-hardening in the solution treated and WQ specimens is found. The work by Godfrey et al. [48] showed dislocations to be visible in the β-phase but not in the α-phase.

The relative content of the β-phase was found to be the dominant factor in strain-hardening of alpha-beta titanium alloys, while the β-grain size did not have a notable effect [1][6][41][47]. Deformation twinning occurs in high-purity polycrystalline α-titanium and low stacking fault energy face centred cubic metals such as brass 70/30 (Figure 2.22) [1] [49]. The continuous decrease in the strain-hardening rate indicates the absence of twinning as shown for copper. The formation of twins increases the rate of strain-hardening [49] [50]. The presence of aluminium in the Ti-6Al-4V alloy suppresses the occurrence of deformation twinning, hence no twinning is experienced [6] [47][49][50].

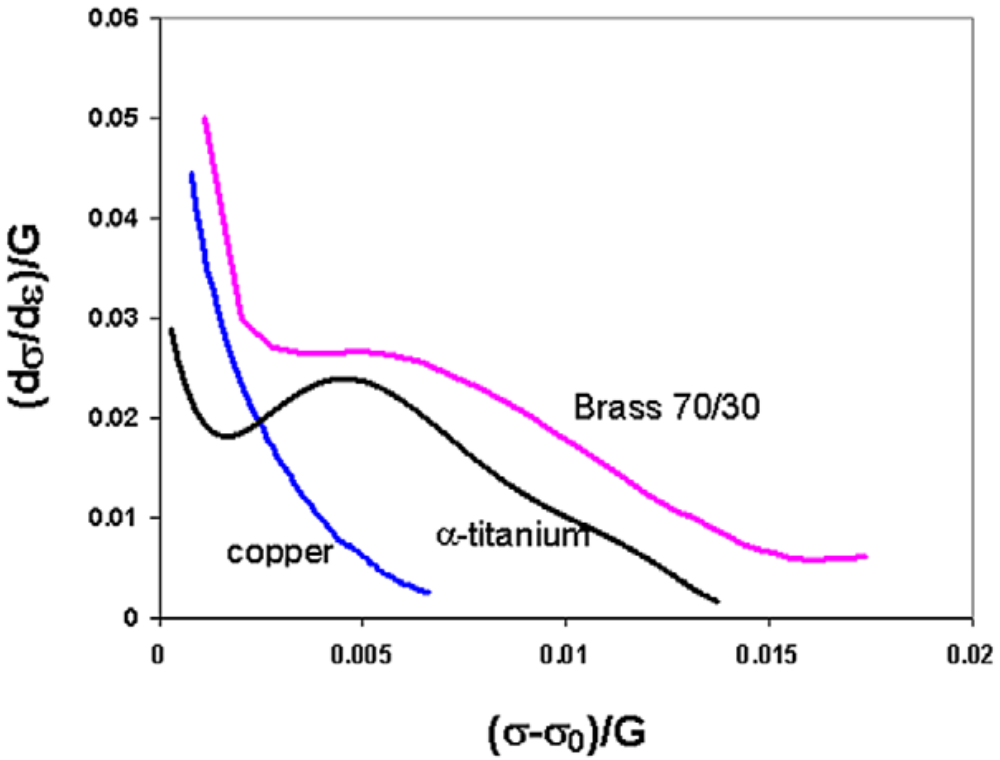

Figure 2.22: Normalised strain-hardening rates for titanium, brass 70/30 and copper [1]

There is a need to use a material with the highest possible strength and still meet the formability requirements in aerospace applications [6]. However, most aerospace alloys are not designed with the benefit of strain-hardening in mind, even though strain-hardening has an important role in the strengthening of alloy systems.

2.5 Fracture mechanics and fracture toughness

Toughness of a material is defined as the ability of a material to absorb impact, or alternatively as a measure of crack resistance [51]. The area under a stress strain curve for an unnotched tension specimen is used to characterise material ductility or the energy required per unit volume to deform the material. A Charpy test is used to determine impact toughness of a material containing a notch [51][52]. The results of a Charpy test and tensile test would not be relevant for a material containing a sharp crack. The application of a fracture mechanics approach has a role to play where the material contains a crack. This approach

takes into account the parameters that affect structural integrity. These parameters are the applied stress, the size and the rate of propagation of the existing crack, and the fracture toughness of the material [52][51].

The fracture toughness is defined as a material's property to resist crack propagation or the ability to withstand fracture in the presence of a crack [51][53][52]. The strength, on the other hand is a measure of resistance to fracture in the absence of a prior crack. It is well known in the literature that where the fracture toughness is high, the tensile strength is low or vice versa. The crack opening mode of fracture toughness is mode 1 and is termed K_{1C}. The K_{1C} is the value of the stress intensity factor (K_1) that causes the existing crack to grow. The underlying principle of fracture mechanics is that an unstable fracture will occur when K_1 reaches a critical value. To obtain valid fracture toughness values, the thickness of the test piece must be such as to allow plane strain conditions. The resultant apparent fracture toughness, K_{1Q}, is then termed plane strain fracture toughness, provided the thickness exceeds the value of Equation (2-2) and is a true material property. Equation (2-2) [51][53][52] indicates the validity conditions for plane strain fracture toughness.

$$B \geq 2.5\left(\frac{K_{1C}}{\sigma_{ys}}\right)^2 \tag{2-2}$$

The plate thickness is denoted by *B*, the fracture toughness by K_{1C} and the yield strength by σ_{ys}. Equation (2-2) indicates that the greater the value of K_{1C}, the bigger the plate thickness required to confirm plane strain conditions. Should the equation not hold after the fracture toughness test has been done, the reported value is an indication only and cannot be taken as the valid plane strain fracture toughness value of the material. At plane strain conditions, the value of K_{1C} is not dependent on specimen thickness as shown in Figure 2.23.

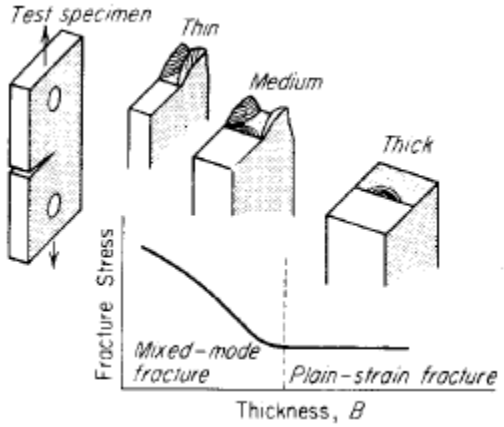

Figure 2.23: Effect of specimen thickness on stress and fracture mode [52]

Where the plate thickness is thinner than required, the measured fracture toughness will always be greater than the real K_{1C} as shown on the left side of Figure 2.23 where the fracture toughness starts to rise. The thinner specimen will give a mixed mode fracture while the thicker specimen will give flat fractures and the fracture toughness will be constant with increasing thickness.

Several specimen geometries shown in Figure 2.24 are commonly used for fracture toughness testing. These are the single-edge V-notch beam (SEVNB) and compact tension (CT) specimen [51][53][52][54][55][56][11]. The CT specimen can either be a disc-shaped or bar type.

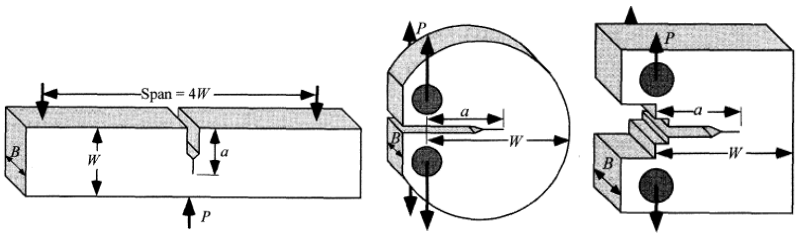

Figure 2.24: Geometries of the fracture toughness specimen (a) SEVNB, (b) disc shaped CT , and (c) bar shaped CT [55]

2.5.1 Titanium fracture toughness

For greater fracture toughness or improved fracture resistance, beta annealing, or beta solution treatment followed by furnace-cooling is recommended as larger α/β-colonies are produced [18][57]. Lütjering and Williams [38] confirm the dominance of the α/β-colonies over the contribution of the ductility in fracture toughness of the α+β titanium alloys. The ELI Ti-6Al-4V grade is known to yield greater fracture toughness values than the standard grades, due to its lower oxygen content [18][58].

Impact toughness of an Ti-6Al-4V alloy is an indirect measure of fracture toughness, and decreases with increasing quenching temperature as shown in Figure 2.25. The decrease is attributed to the greater volume fraction of α′-martensite that increases as the quenching temperature increases. The martensitic needles are known to be a poorer medium for energy absorption [8]. The Charpy impact toughness test is not a standard fracture mechanics method for fracture toughness but can be used as an indicator of the toughness of materials. Fracture mechanics provides a quantitative evaluation of fracture toughness while the Charpy test is qualitative [53]. The Charpy test is performed at greater strain rates while normal fracture toughness tests are done at lower strain rates. The presence of a crack in a fracture mechanics specimen makes it desirable to determine its fracture toughness compared to that of a machined notch in a Charpy specimen.

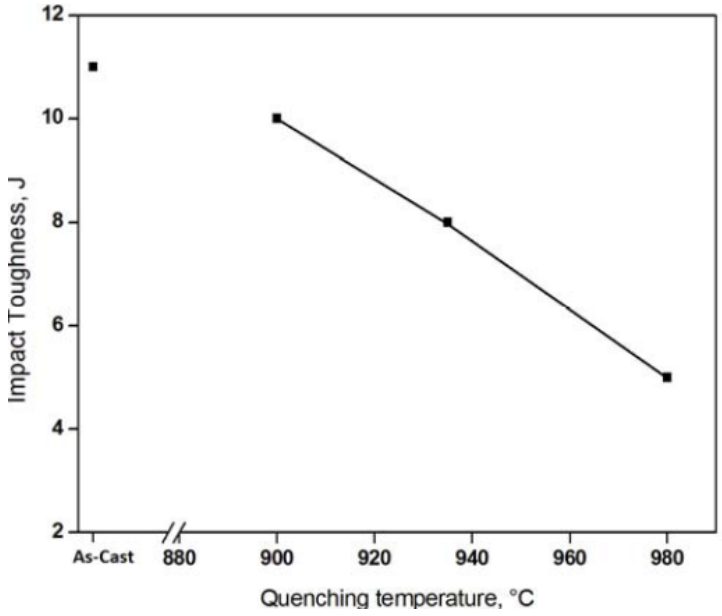

Figure 2.25: Impact toughness of a Ti-6Al-4V alloy as a function of its quenching temperature [8]

Guo et al. [42] measured the fracture toughness of the Ti-6Al-4V alloy that was solution-treated above the beta transus and WQ or AC or FC. The FC specimens (colony lamellar microstructure) gave the highest fracture toughness values while the WQ gave the lowest fracture toughness values. The greater fracture toughness value of the colony lamellar microstructures was due to the larger β-grains, larger α-laths and the presence of randomly oriented α/β-colonies. The colonies cause repeated crack direction changes, leading to reduced crack intensity and hence greater fracture toughness. The martensitic microstructure resulted in less crack branching and consequently a smooth fracture path. The AC specimen gave fracture toughness values in-between the WQ and FC specimens as the colonies were fewer and finer than in the FC specimen. Only one ageing temperature and time were used and the fracture toughness values of the aged specimens were not compared to those of the unaged specimens.

Feng et al. [54] compared the fracture toughness of cast Ti-6Al-4V and the same cast alloy followed by hot isostatic pressing (HiPping). The post HIPped samples gave greater fracture toughness values than those of the as-cast Ti-6AL-4V due to the larger α-lamellar platelets and a larger α/β-colony size. The as-cast samples showed an intergranular fracture indicating weaker grain boundaries while the post HIPped showed a transgranular fracture. The transgranular fracture needed more energy to advance the crack, hence improved ductility and fracture toughness. More crack deflection and branching were found in the post HIPped samples. Feng et al. [54] reported that plane strain fracture toughness validity conditions were not met, hence fracture toughness results reported were considered an estimate but not a true value of fracture toughness.

Shademan et al. [59] investigated the effect of cooling rate on the fracture toughness of Ti-6Al-4V with a colony α/β-microstructure (Table 2.2). Greater cooling rates gave smaller colony sizes, lower α content and thinner α-laths. The fracture toughness increased with decreasing cooling rates due to the increase in the size of the α/β-colonies and α-laths. This finding is consistent with the work of Feng et al [54] and Lütjering and Williams [38], showing the fracture toughness to increase with increasing colony size. The coarse lamellar microstructure shows increased crack branching, resulting in zig-zag crack growth, while the fine lamellar structure gives a smoother crack front (Figure 2.26). True plane strain fracture toughness conditions were not achieved [59].

Table 2.2: Summary of microstructure and properties [59]

Microstructure	β layer continuity (yes/no)	Widmanstatten colony size (μm)	α lath size (μm)	Volume % α	Volume % β	UTS (MPa)	ε_f (%)	Fracture toughness K_{Ic} (MPa $\sqrt{m}$)
A	No	118.20 ± 2.74	3.45 ± 0.61	66.65	33.35	912	7	121
B	No	168.88 ± 5.03	6.59 ± 0.21	78.56	21.44	878	11.9	109[a]
C	Yes	312.50 ± 17.22	14.14 ± 0.88	77.91	22.09	934	7.6	152[a]
D	Yes	19.57 ± 2.22[b]		77.26	22.74	922	15	57[a]

Microstructure A: 1070 °C/30 min/cool @ 25 °C/min to 400 °C/Ar quench to RT.
Microstructure B: 1070 °C/30 min/cool @ 3 °C/min to 400 °C/Ar quench to RT.
Microstructure C: 1070 °C/30 min/cool @ 1 °C/min to 400 °C/Ar quench to RT.
Microstructure D: Mill-annealed (as received).
[a] Not valid according to ASTM.
[b] α grain size (μm).

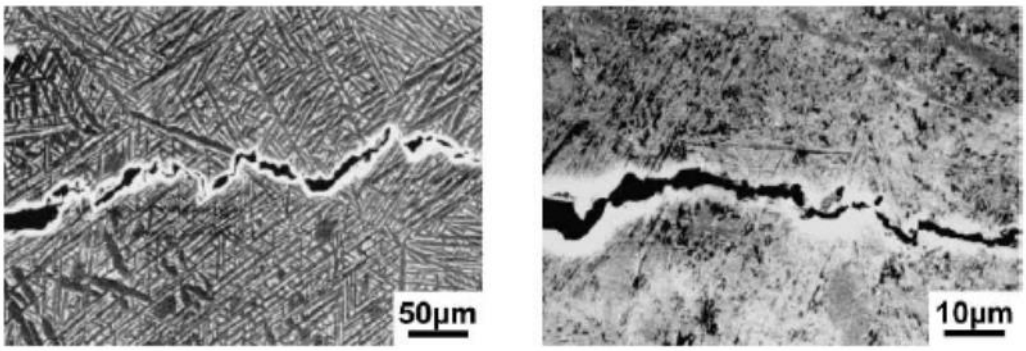

Figure 2.26: SEM micrographs showing a crack path in Ti-6Al-4V alloy specimens after fracture toughness testing for (a) coarse lamellar and (b) fine lamellar structure [38]

The β-grain size in a colony lamellar microstructure has been shown to directly affect the colony size more than it affects the fracture toughness [57]. As the grain size increases, the colony size and the number of colonies increase, leading to an increase in fracture toughness. The crack path is more zigzag in larger colonies, consuming more energy than the straight crack path in smaller colonies (Figure 2.27).

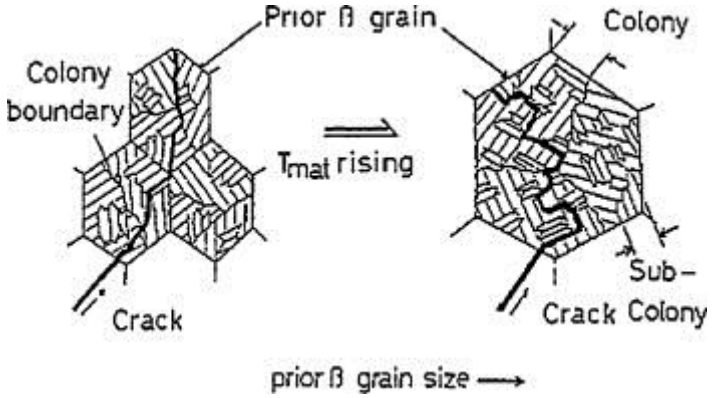

Figure 2.27: Crack propagation path with increasing β-grain size [57]

The effect of ageing treatment in the fracture toughness of the Ti-6Al-4V alloy is not widely reported. However, Lee et al. [60] showed the fracture toughness of the Widmanstätten morphology to decrease after ageing due to the precipitation of the hard and brittle α_2-phase which promoted crack initiation (Figure 2.28).

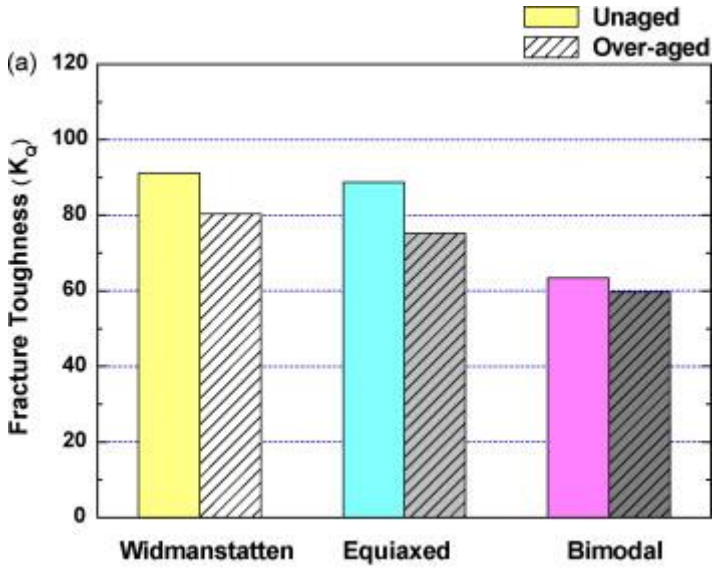

Figure 2.28: Apparent fracture toughness after overageing the Ti-6Al-4V alloy [60]

A review by Banerjee and Williams [61] showed the fracture toughness and tensile properties in Figure 2.29 for various titanium alloys. The α-Ti alloys are shown to have the highest fracture toughness values while the β-Ti alloys have the highest yield strength values. Figure 2.29 shows that for the same levels of yield strength, the fracture toughness of the lath α morphology is greater than for the equiaxed α morphology. The authors highlighted the need to have a material with greater fracture toughness and greater yield strength for aerospace applications. It would also be ideal to improve either the fracture toughness or the yield strength without compromising the other property.

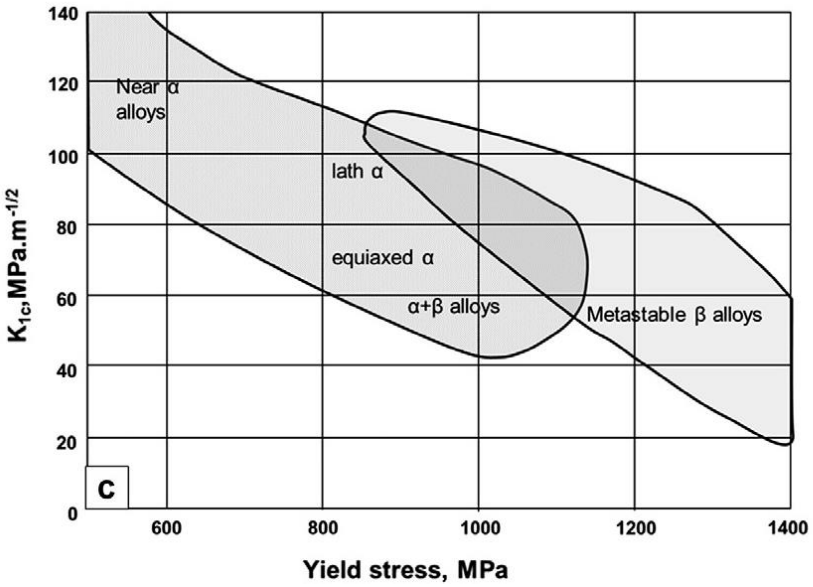

Figure 2.29: Fracture toughness compared to the yield strength of titanium alloys [61]

2.6 Fatigue crack growth

The fatigue crack growth rate as expressed schematically by the Paris curve is shown in Figure 2.30. The curve is generated according to the method described in detail by the fatigue crack growth rate testing standard, ASTM E-647 [62]. Region 2 is of interest to the designer,

where one can calculate the Paris constants of various materials. The constants are used to identify a material that has better fatigue crack growth resistance. Various authors have shown region 2 to be microstructure sensitive for titanium alloys [11][63]. The stress intensity applicable to region 1 will not cause a crack to grow below the threshold stress intensity (ΔK_{th}). Above the ΔK_{th}, the crack will grow at a steady rate as shown in region 2 of the fatigue crack growth curve. Region 3 corresponds to the stress intensity where the crack growth rate is so high that brittle fracture occurs. The literature has shown region 3 not to be microstructure sensitive. The stress intensity where fracture occurs is termed the terminal stress intensity (K_c) and can be used to predict the relative fracture toughness of materials.

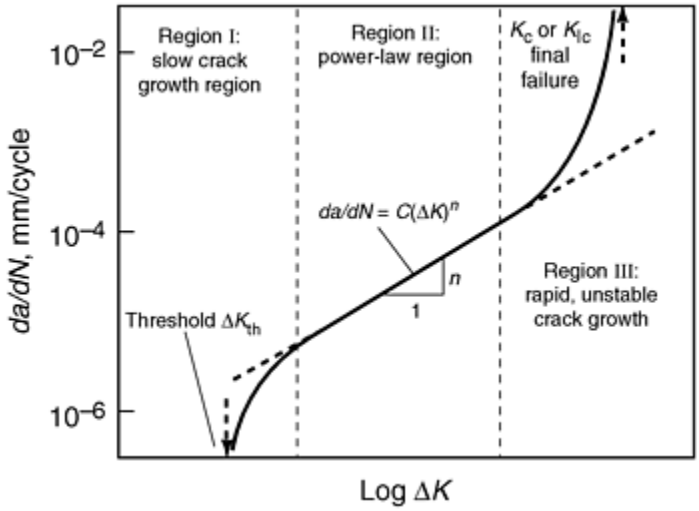

Figure 2.30: Paris curve da/dN compared to delta K [51]

The factors that improve the fracture toughness of the Ti-6Al-4V alloy are similar to those that improve fatigue crack growth resistance [24]. It is well known that beta-annealed and furnace-cooled microstructures resulting in coarse lamellar microstructures have the highest fatigue crack growth resistance [10][11][63]. Benedetti and Fontari [10] showed the lamellar microstructure to have a better fatigue crack growth resistance than the bimodal structure, due to the presence of randomly oriented colonies in the lamellar microstructure. Crack propagation was found to follow a more tortuous path in the lamellar microstructure, leading to slower crack propagation rates. Kruger et al. [63] and Nalla et al. [11] reported similar findings confirming that the lamellar microstructure has a greater fatigue crack growth resistance than the bimodal microstructure. The authors [10][11][63] compared the coarse lamellar colony microstructure to the fine-grained bimodal microstructure and found the appearance of a larger crack deflection in the coarse lamellae. Leyens and Peters [19] showed the coarse lamellar microstructure had a greater fatigue crack growth resistance than the equiaxed microstructure, due to a larger crack deflection.

Li et al. [31] studied fatigue crack propagation of titanium alloys produced from solution treatment followed by water quenching, or air cooling or furnace cooling. Contrary to other reports, the air-cooled titanium alloy was found to give better fatigue crack growth resistance than the furnace-cooled alloy. Li et al. [31] attributed the unusual results to the few colonies formed in the lamellar microstructure even though the colonies were larger. However, the Paris equation determined by Li et al. [31] indicates that the furnace-cooled (colony lamellar microstructure) titanium alloy has a better fatigue crack growth resistance than the air-cooled alloy. The water-quenched titanium alloy gave the lowest crack growth resistance due to the fine martensitic needles and the absence of colonies. As the cooling rate decreased (air-cooled), the α-laths formed and grew in size, and α/β-colonies formed, improving the fatigue crack growth resistance of the air-cooled microstructure. Peters and Lütjering [64] attributed

the superior fatigue crack growth resistance of the colony lamellar microstructure to the extrinsic toughening mechanism resulting from larger colonies. These mechanisms are large crack deflection and branching that are non-existent in finer martensitic microstructures. Figure 2.31 confirms the superior role of coarse lamellar microstructures during fatigue crack growth of macrocracks in the Ti-6Al-4V alloy [38].

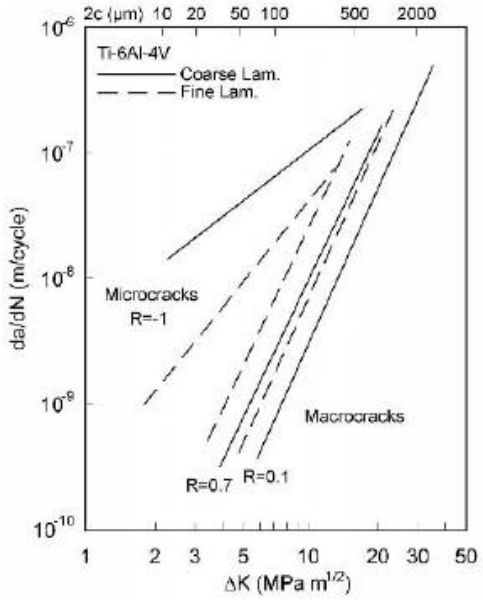

Figure 2.31: Fatigue crack propagation in Ti-6Al-4V alloy with coarse and fine lamellar microstructures [38]

The effect of ageing in fatigue crack growth resistance of the Ti-6Al-4V alloy is not widely covered in the literature.

Fractographic studies of the Ti-6Al-4V alloy specimens that showed better resistance to crack propagation showed rougher fracture surfaces [11] [65] [66] [42][63]. The surface would show a dimple-like ductile fracture. The colony lamellar microstructures with coarse α/β-laths are preferred for high fracture toughness and high resistance to fatigue crack growth. Crack propagation is slowed down by the formation of secondary cracks and crack branching at colonies. Crack propagation follows the boundary between α and β-laths. The crack will propagate in a straight line until it meets a differently oriented α/β-colony, forcing a change in direction and consequently leading to a reduction in the crack propagation rate. High-strength materials have smoother and flatter fracture surfaces due to a reduced crack deflection. Crack propagation is faster in the microstructure with few obstacles which cause crack branching or crack zigzagging. The presence of fine microstructural features such as fine α-laths and sub-grains (colonies) leads to small crack deflection, hence easy crack propagation.

In summary, the literature survey conducted indicates that the solution heat treatment done above the beta transus temperature of the Ti-6Al-4V is at a temperature range of 1000 to 1070 °C, while the ageing temperatures are between 500 °C to 750 °C. The presence of colony lamellar structures and a low-volume fraction of α′-martensite is proposed to lead to both high fracture toughness and high fatigue crack growth resistance, while the higher-volume fraction of the martensitic needles leads to a high tensile strength.

Even though extensive literature on the heat treatment of the Ti-6Al-4V alloy exists, there is still limited data available on the effect of ageing treatment. The microstructural evolution during the ageing treatment of the Ti-6Al-4V alloy has not been sufficiently explored. There

are contradictions about the effect of ageing treatment in some of the reported results on ageing treatment of the Ti-6Al-4V alloy. It has also been found that there is limited data available on the effect that an ageing treatment has in the resulting mechanical properties. Most published literature on mechanical properties of the Ti-6Al-4V alloy uses hardness as a method to evaluate the response to ageing treatment. Even though hardness is an inexpensive method to understand the response to heat treatment, its correlation with yield strength is relatively poor. Due to the fundamental relationship of hardness to the tensile strength which is closely related to the fatigue strength, the hardness and the fatigue strength do, however, also have a close relationship.

Other mechanical properties, such as yield strength, fracture toughness and fatigue crack growth rate need to be determined to effectively understand the response of the Ti-6Al-4V alloy to heat treatment. These results are crucial for accurate design of metallic structures. It is generally assumed that the fracture toughness, or loosely termed toughness of metals can be derived direct from ductility results obtained from the tensile testing. The continued use of structures containing cracks need information about the real fracture toughness, which cannot be calculated from ductility results alone. For this reason, it is essential to use fracture mechanics when determining fracture toughness or fatigue crack growth resistance.

CHAPTER 3 Methodology

The methodology followed to generate results for this project and to answer the questions posed in the introduction is outlined in this chapter. The material used, heat treatment conditions complied with, and the details of the methods for microstructural analysis are described. The procedure includes mechanical testing, fractography analysis and determination of mechanical properties. The chapter is divided into sections which are materials, heat treatment, microstructural characterisation, hardness measurements, tensile testing, fracture toughness testing and fatigue crack growth testing.

3.1 Materials

The titanium alloy used was wrought commercial grade 23 Ti-6Al-4V ELI, (Extra Low Interstitial) produced by BAOJI Titanium industry in China. The material's chemical composition is shown in Table 3.1. The alloy was received as forged rods of 74 mm diameter and 200 mm length.

Table 3.1: Chemical composition of the as-received Ti-6Al-4V ELI alloy

Alloying elements (weight %)								
Ti	Al	V	Fe	C	N	O	H	Residual elements
balance	6.38	4.23	0.15	<0.01	0.01	0.1	0.002	<0.40

3.2 Heat treatment

The solution treatment temperature (1050 °C) above the beta (β) transus temperature was chosen to convert the Ti-6Al-4V's initial phases to the single β-phase before cooling. The effects of crystallographic texture from rolling or forging on mechanical properties were also eliminated by solution treatment above the beta transus temperature. This heat treatment ensures that the mechanical properties are not affected by the orientation of the specimen during testing [67][38][19]. The thickness of the oxidation layer was expected to be below 1 mm, as indicated in the literature [18][19].

3.2.1 Solution heat treatment

The as-received Ti-6Al-4V wrought alloy was cut into 10 mm thick discs and solution-treated (ST) at 1050 °C for 30 minutes in air in a Naber N150 muffle furnace. The flow diagram of the specimen preparation is shown in Figure 3.1. The solution-treated specimens were either water-quenched (WQ), or air-cooled (AC) or furnace-cooled (FC). The WQ cooling rate was estimated to be 1000 °C/minute while the AC rate was estimated to be about 100 °C/minute [38]. The FC rate was measured to be about 400 °C/hour. Microstructural analysis and hardness measurements were carried out.

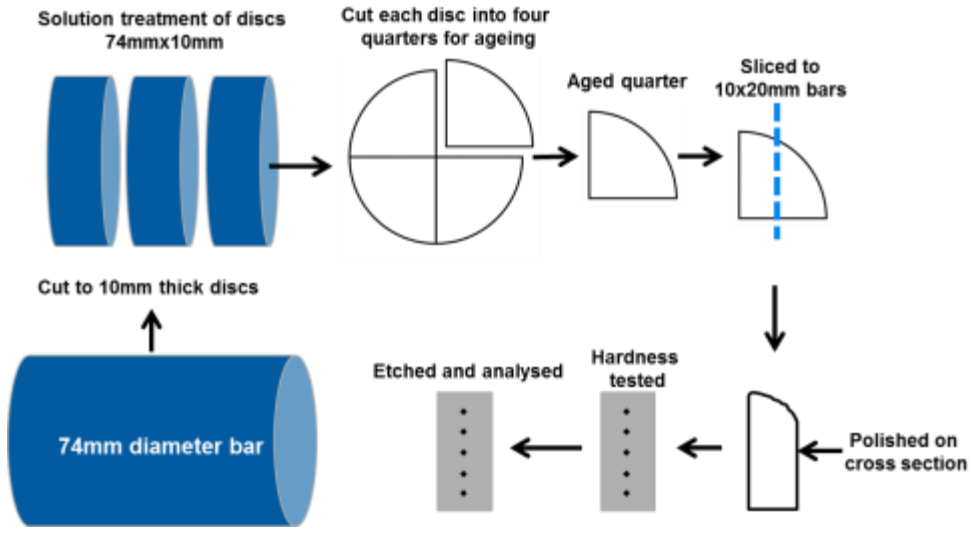

Figure 3.1: Specimen preparation for heat treatment, microstructural analysis and hardness measurements

The alpha case that formed during solution treatment was removed during machining before mechanical properties were measured.

3.2.2 Ageing treatment

In order to evaluate the influence of ageing and the subsequent cooling rate and temperature on the microstructural evolution, the experimental matrix shown in Table 3.2 was used. All the specimens were ST at 1050 °C for 30 minutes and WQ. The ageing time was kept constant at 0.5 hours, while the ageing cooling rate was either WQ or FC for each specimen. The microstructural analysis and hardness measurements were carried out on all the specimens.

Table 3.2: Experimental ageing cooling rate and temperature

Ageing temperature (°C)	Ageing cooling rate	
	FC	WQ
500	✓	✓
600	✓	✓
700	✓	✓
800	✓	✓
900	✓	✓

The solution treated and WQ Ti-6Al-4V specimens were aged according to the experimental matrix indicated in Table 3.3 to evaluate the effect of ageing time on the microstructural evolution. The same cooling rate of FC was used for all the specimens after ageing for different times. The ageing times of 0.5, 2, 24 and 48 hours were used. All the specimens were prepared for microstructural analysis and hardness measurements.

Table 3.3: The matrix of experiments to investigate the effect of ageing time followed by FC

Ageing temperature (°C)	Ageing time (hours)			
	0.5	2	24	48
500	✓	✓	✓	✓
650	✓	✓	✓	✓
750	✓	✓	✓	✓
800	✓	✓	✓	✓
900	✓	✓	✓	✓

The ageing response of the lamellar morphology was also included in the current study, as the lamellar morphology is widely reported in the literature. The as-received Ti-6Al-4V alloy specimens were solution-treated at 1050 °C for 30 minutes and FC as before, followed by ageing at temperatures of 750 °C, 800 °C and 900 °C, and the ageing cooling rate was WQ. Ageing times of 0.5, 2, 24, and 48 hours were selected. Compared to ageing of the fully martensitic microstructure, higher temperatures were chosen for ageing of the lamellar microstructure as it is known to be stable at temperatures of 800 °C and below. Table 3.4 shows the experimental matrix used to evaluate the influence of ageing time and temperature on the microstructure of the Ti-6Al-4V with a colony lamellar structure. Microstructural analysis and hardness measurements were carried out.

Table 3.4: Experimental conditions to evaluate ageing of ST and FC specimens

Ageing temperature (°C)	Ageing time (hours)			
	0.5	2	24	48
750	✓	✓	✓	✓
800	✓	✓	✓	✓
900	✓	✓	✓	✓

3.3 Microstructural characterization

All heat-treated specimens were sectioned to remove the alpha case. The specimens were ground and polished to obtain scratch-free and mirror-finished surfaces. The polished specimens were cleaned in the ultrasonic bath using ethanol for about 10 minutes and then dried. Kroll's reagent (1 ml HF + 2 ml HNO_3 + 333 ml water) was used to etch the specimens for about 20 to 30 seconds.

A Leica DMI5000M inverted Optical Microscope (OM) equipped with image analysis software (Image Pro Plus) and a Jeol JSM-6510 Scanning Electron Microscope (SEM) equipped with X-ray Electron Diffraction Spectrometry (EDS) were used to investigate the microstructural changes after the solution treatment and ageing. Heat-treated specimens were analysed by using the OM and SEM. The beta (β) grain size, α′-needle width, α-lath width, size of α/β-colonies and α/β-content were quantified.

A Leica MZ 16A stereo microscope was used to measure the beta (β) grain size using the linear intercept method according to the ASTM standard E-112 [68]. ImageJ 1.50b software was used to determine the β-grain size. Five images were acquired at 18x and ten lines drawn per image for grain size measurements. The average linear intercept grain size was determined from equation (3-1) as follows:

$$Average \text{ intercept } grain\ size = \frac{Length\ of\ line}{No.\ of\ intercepts} \quad (3\text{-}1)$$

The median linear intercept grain size, standard deviation, and coefficient of variation were determined for each specimen. It should be pointed out that the determination of grain size becomes challenging where the grain boundaries are not clear. The challenge was evident in the ST and WQ (fully martensitic) specimens while the ST and FC (colony lamellar) specimens consisting of α-phase grain boundaries were easier to measure.

Ten SEM micrographs taken at 1000x were used to determine the thickness of the α-laths with five lines drawn per micrograph perpendicular to the laths. The orientation of the α-laths was not taken into consideration during the measurements. The thickness of the α-laths was determined as for grain size determination. Median intercept lath thickness, standard deviation, and coefficient of variation were computed for each specimen.

The measurement of the α′-lath thickness required high-resolution SEM micrographs, ten images taken at 3000x were used. Five individual α′-laths from each image were identified and their widths measured manually. Median lath width, standard deviation, and coefficient of variation were determined.

The colony size was quantified by the linear intercept method similar to determining the grain size. The stereo microscope was used to obtain ten images at 30x magnification. Five lines were drawn per image and the intercepts were counted. Median colony size, standard deviation, and coefficient of variation were computed for each specimen.

The volume fraction of the α and β-phases was measured only on the basketweave and colony lamellar microstructures where the α and β-laths were clearly visible. Prediction of the volume fraction of the α-phase could not be achieved using the lever rule from the available phase diagrams of the Ti-6Al-4V alloy. The same ten SEM images used for the α-lath width measurements were used. ImageJ 1.50b software was used to establish the fractions of the α and β-phases. Median α/β volume fraction, standard deviation, and coefficient of variation were computed.

3.4 Hardness measurements

Micro-hardness was selected to evaluate microstructural homogeneity, which was essential to understand in this work. Homogeneity of the microstructure is an important consideration in determining the consistency of the mechanical properties further on. Macro-hardness was also performed to obtain bulk relative hardness values of different heat treatments.

Vickers micro-hardness was measured in accordance with the ASTM standard E384 [69]. The automatic Vickers micro-hardness tester FM-700 equipped with Future–Tech software was used to measure the hardness change and microstructural homogeneity. A specimen of about 10 mm by 20 mm was cut from the heat-treated specimen as shown in Figure 3.1. Each polished specimen, not etched, was indented with a 500 gram force for 15 seconds. Forty five hardness indentations were made at the centre of the specimen to avoid the alpha-case. Median average, standard deviation, and coefficient of variation were calculated for each hardness results of the specimen.

Macro-hardness results were obtained for selected variants for comparison with the micro-hardness according to the ASTM standard E384 [69]. A load of 10 kg was applied for 15 seconds using the Vickers hardness tester FV-700. The ST/WQ, ST/AC and ST/FC specimens were selected for the macro-hardness measurements.

3.5 Tensile testing

The test was chosen to compare the results of the current project with published data. It was also essential to understand the influence of ageing treatment on microstructural evolution and on the tensile properties.

The specimens for tensile property measurements are indicated in Table 3.5 and designated as variant 1 (V1) up to variant 7 (V7). The variants were selected to have microstructural morphologies ranging from a fully martensitic morphology, partially martensitic, basketweave to a lamellar morphology.

Table 3.5: Tensile testing matrix

Heat treatment conditions	V1	V2	V3	V4	V5	V6	V7
ST temperature (°C)	1050	1050	1050	1050	1050	1050	1050
ST soaking time (hours)	0.5	0.5	0.5	0.5	0.5	0.5	0.5
ST cooling rate	WQ	WQ	WQ	WQ	WQ	FC	FC
Ageing temperature (°C)	-	500	800	900	900	-	900
Ageing time (hours)	-	0.5	0.5	0.5	24	-	0.5
Ageing cooling rate	-	FC	FC	FC	FC	-	WQ

Even though crystallographic texture was not expected to influence tensile properties, the specimen orientation relative to rolling direction is shown in Figure 3.2. Tensile testing was performed perpendicular to the bar rolling direction. Final machining of tensile test specimens was carried out after all the heat treatments had been completed to remove the oxidation layer formed during solution treatment. Sub-size tensile test specimens were prepared according to the standard ASTM E8M [70]. The details of the tensile specimen preparation are shown in Figure 3.3 while the specimen drawing is included in Appendix I. Room temperature tensile testing was performed at a constant crosshead speed of 0.5 mm/min on an Instron™ 1342 tensile tester. The strain was measured by using an extensometer attached to the gauge section of the test specimen. The extensometer was then removed at a strain of 5% to prevent damage during specimen fracture. Tensile testing was continued until the specimen fractured. The tensile extension was also recorded from the start of the test to the end by using a Linear Variable Differential Transformer (LVDT) gauge. Three specimens were tested for each variant.

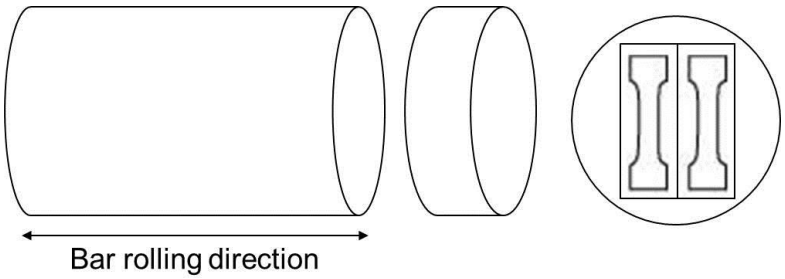

Figure 3.2: The schematic diagram showing the tensile specimen orientation from the bar

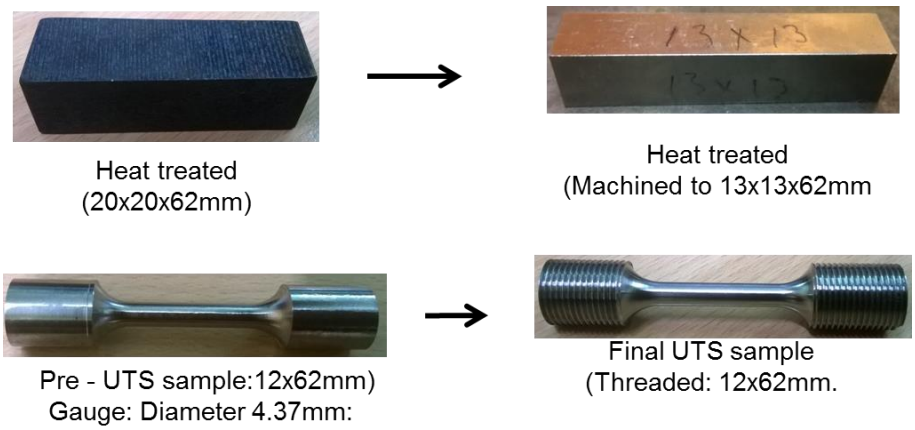

Figure 3.3: The specimen preparation flow details for tensile testing

The 0.2% proof strength (YS), Ultimate Tensile Strength (UTS), percentage Elongation (% EL) and percentage Reduction in Area (% RA) were determined. Median average, standard deviation, and coefficient of variation were computed from three specimens. The strength ductility balance (UTS x % EL) was calculated and compared for different variants [44].

The strain-hardening exponent *(n)* and the strain-hardening rate ($\frac{d\sigma}{d\varepsilon}$) were determined from a true stress true strain plot from the yield point up to the point necking according to the Hollomon equation (Equation (3-2)) as detailed in ASTM standard E647-00 [45]. The strain-hardening exponent was determined from the slope of the log true stress log true strain plot as shown in Equation (3-3).

$$\sigma = K(\varepsilon)^n \tag{3-2}$$

Where σ is the true stress, K is the strength coefficient, ε is the true strain and *n* is the strain (work) hardening exponent.

$$\log\sigma = \log K + n\log\varepsilon \tag{3-3}$$

The strain-hardening rate ($\frac{d\sigma}{d\varepsilon}$) was determined from the local slope of the true stress-true strain plot by fitting a power curve and finding the derivative of the curve's equation at every true strain value. The plots of the strain-hardening rate versus the true strain, and the strain-hardening rate versus the true stress were generated and analysed.

Fractography studies of the tensile tested specimens were performed on the polished cross-sectional view and also on the fractured surface. A Leica DMI5000M inverted OM and a Jeol JSM-6510 SEM were used as before for failure and microstructural analysis.

3.6 Fracture toughness testing

The determination of fracture toughness for metals is an important consideration in the design of structures, as cracks cannot be completely avoided in design or in service [52]. Knowledge of fracture toughness is useful where a structure has an existing crack and one is not sure whether the structure will fail or not when loaded. Ductility results from a tensile test are often used to indicate the relevant toughness of materials. The ductility method, however, is not sufficient to determine whether failure will occur or not when a crack is present in a structure. This section emphasises the need to determine the plane strain fracture toughness of the material where the structure thickness would not influence the results. Accurate

determination of plane strain fracture toughness requires a specimen of a critical thickness [52]. The method selected in this section was a fracture mechanics method where the test was carried out on a specimen with a pre-existing sharp crack. A compact tension (CT) specimen was used to determine the fracture toughness.

The Ti-6Al-4V alloy specimens selected for fracture toughness testing are shown in Table 3.6 and identified as specimen 1 (S1), specimen 2 (S2) and specimen 3 (S3). The specimens were chosen to have a variety of microstructural morphologies ranging from a fully martensitic to a lamellar microstructural morphology. The influence of ageing on the microstructural morphology (S2) was also included.

Table 3.6: Fracture toughness testing matrix

Heat treatment conditions	S1	S2	S3
ST temperature (°C)	1050	1050	1050
ST soaking time (hours)	0.5	0.5	0.5
ST cooling rate	WQ	WQ	FC
Ageing temperature (°C)	-	900	-
Ageing time (hours)	-	24	-
Ageing cooling rate	-	FC	-

Final machining of the fracture toughness test samples was performed after all the heat treatments had been completed. Figure 3.4 shows the details of the preparation of the fracture toughness specimen.

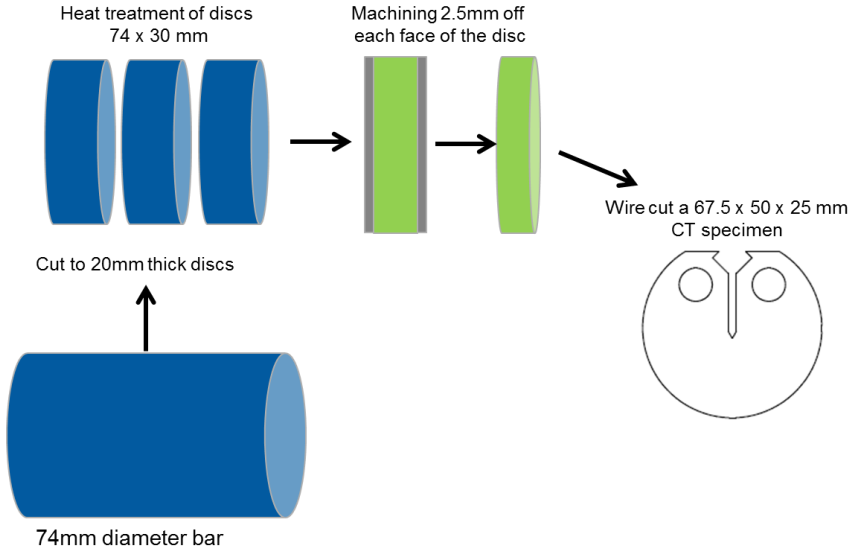

Figure 3.4: Details of specimen preparation for fracture toughness measurements

Single-edge disc type CT specimens with a thickness (B), width (W), height (H) and crack length (*a*) were prepared according to the ASTM standard E399 [56]. The schematic of the specimen used is shown in Figure 3.5 and the full details of the drawing are shown in Appendix I. Final machining of fracture toughness test samples was done after all the heat treatments had been completed. A 2.5 mm thick layer was machined on both sides of the sample to remove any oxidation layer and dissolved oxygen.

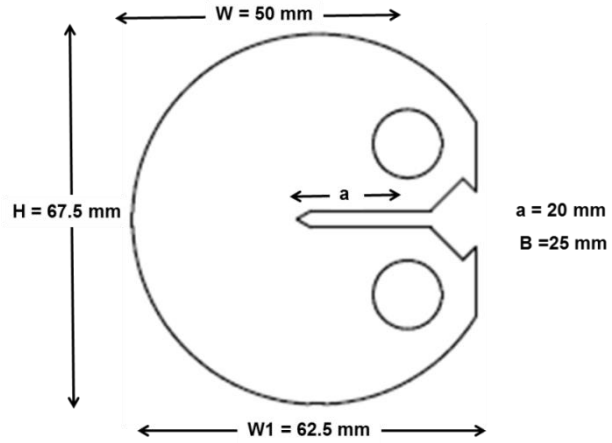

Figure 3.5: A schematic drawing of a 25 mm thick disc shape CT specimen

The CT specimens were polished on both sides to a mirror finish. The polishing was required to aid in crack observation during pre-cracking [11]. An Instron^{TM} 1342 tensile tester was used to introduce a fatigue pre-crack of about 5 mm before the fracture toughness testing was carried out. The stress intensity factor range of 15 to 18 MPa.m$^{0.5}$ with a frequency of 15 Hz and a load ratio R, ($R = P_{min}/P_{max}$) of 0.1 was used. In order to monitor fatigue crack growth rate, the compliance method using a Crack Mouth Opening Displacement (CMOD) gauge was used. Having pre-cracked the specimens, the room temperature fracture toughness testing was performed at a constant crosshead speed of 0.5 mm/min. The orientation of the samples for fracture toughness testing is shown in Figure 3.6 with the notch aligned perpendicular to the bar rolling direction.

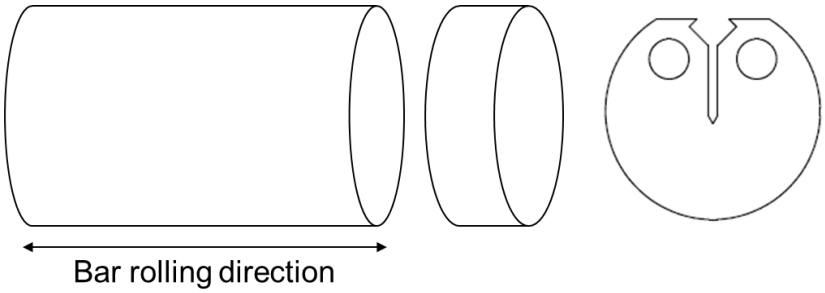

Figure 3.6: The CT specimen orientation relative to the bar rolling direction

Fracture toughness testing was carried out until the maximum load was reached and testing continued, leading to a drop in load. The tested specimen was still intact after testing and rapid loading was performed to split it into two parts for accurate measurement of pre-crack length. The pre-crack length was measured at mid-thickness and at two-quarter thickness points according to the ASTM standard E399 [56]. The average of the three measurements was added to the wire-cut notch length to get the final crack length used for fracture toughness calculations. The crack length measurements were determined on an image of a fractured surface by using ImageJ software.

The conditional fracture toughness, K_Q, was calculated by using equation (3-4).

$$K_Q = \mathrm{f}\left(\frac{a}{W}\right) * \left(\frac{P_Q}{B\sqrt{W}}\right) \tag{3-4}$$

where P_Q is the conditional load, $\mathrm{f}\left(\frac{a}{W}\right)$ is the crack length to width factor, B is the specimen thickness, W is the specimen width and a the average crack length. The value of P_Q is

determined at the 95% slope of the load displacement curve. The process to determine P_Q is described in the ASTM standard E399 [56]. The maximum load (P_{max}) was also recorded and compared to P_Q.

For a disc type CT specimen, $f\left(\frac{a}{W}\right)$ was calculated according to equation (3-5) as follows:

$$f\left(\frac{a}{W}\right) = \frac{\left(2+\frac{a}{W}\right)[0.76 + 4.8\frac{a}{W} - 11.58\ \left(\frac{a}{W}\right)^2 + 11.43\left(\frac{a}{W}\right)^3 - 4.08(\frac{a}{W})^4\ ]}{\left(1-\frac{a}{W}\right)^{3/2}} \quad (3\text{-}5)$$

For plane strain fracture toughness, thickness (B) and remaining ligament (W-a) must all be equal to or greater than $2.5(K_{1Q}/YS)^2$ as shown in Equations (3-6) and (3-7).

$$B \geq 2.5\left(\frac{K_{1c}}{\sigma_{ys}}\right)^2 \quad (3\text{-}6)$$

$$W - a \geq 2.5\left(\frac{K_{1c}}{\sigma_{ys}}\right)^2 \quad (3\text{-}7)$$

The conditional fracture toughness values (K_Q) obtained were evaluated for plane strain conditions according to Equations (3-6) and (3-7). Three samples were tested for each variant and the median average, standard deviation, and the coefficient of variation determined. The OM and the SEM were used for fractography studies on tested specimens.

3.7 Fatigue crack growth rate testing

The fatigue life of a part containing a sharp crack is determined by the number of cycles to propagate a crack to a critical condition [51]. A CT specimen is a commonly used method to determine the Fatigue Crack Growth Rate (FCGR) and was selected for this project. The method has been extensively used and understood [10][11] [51] [63].

The same variants used for fracture toughness testing were also selected for FCGR testing. Sample preparation and orientation for FCGR were similar to those used for fracture toughness testing in Figure 3.4 and Figure 3.6. Single-edge bar type CT specimens with a thickness (B), width (W), crack length (a) and height (H) were prepared according to the ASTM standard E399 [56]. The schematic of a specimen used is shown in Figure 3.7, while the full details are included in Appendix I.

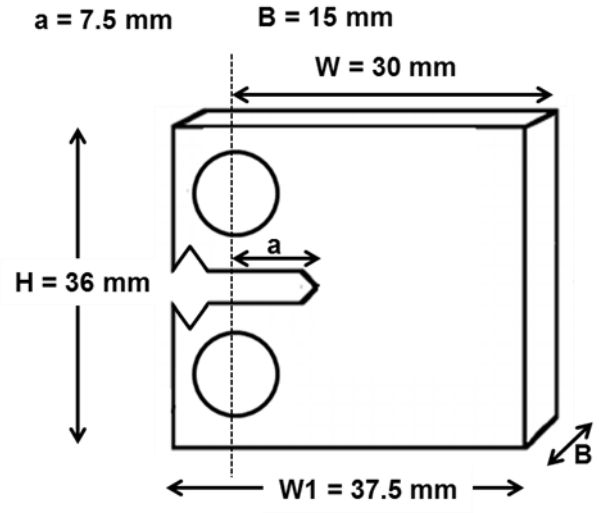

Figure 3.7: A schematic drawing of a 15 mm thick bar type CT specimen used for FCGR

The test was performed according to the fatigue crack growth ASTM standard E647 [62]. A 7.5 mm starter notch was introduced by using wire cutting. A CMOD gauge was used to monitor the fatigue crack growth. Room temperature FCGR testing was carried out by using an Instron™ 1342 tensile tester at a constant delta load amplitude (ΔP) of 8000 N, which had a sine wave form with a cyclic load ratio ($R = P_{min}/P_{max}$) of 0.1 and a frequency of 10 Hz. Three samples were tested for each variant.

The crack length (a) was measured by using the compliance method while the number of cycles (*N*) and the load amplitude (*ΔP*) were recorded. The fatigue crack growth rate, $\frac{da}{dN}$ was determined by using the secant method shown in equation (3-8) according to the ASTM standard E647. From a set of (a_i, N_i) data points, $\frac{da}{dN}$ was calculated by finding the slope of the straight line between two adjacent points, as follows:

$$\left(\frac{da}{dN}\right)_{\overline{a}} = \frac{a_{i+1} - a_i}{N_{i+1} - N_i} \tag{3-8}$$

The average crack size ($\overline{a}$) between two adjacent points was determined as shown in equation (3-9) and used to calculate the change in the stress intensity factor (ΔK).

$$\overline{a} = 1/2(a_{i+1} + a_i) \tag{3-9}$$

The change in the stress intensity factor (ΔK) was calculated according to equation (3-10).

$$\Delta K = \left(\frac{\Delta P}{B\sqrt{W}}\right) \frac{\left(2 + \frac{a}{W}\right)\left[0.866 + 4.64\,\frac{a}{W} - 13.32\,\left(\frac{a}{W}\right)^2 + 14.72\left(\frac{a}{W}\right)^3 - 5.6\left(\frac{a}{W}\right)^4\right]}{\left(1 - \frac{a}{W}\right)^{3/2}} \tag{3-10}$$

where ΔP is the load amplitude, *B* is the thickness of the sample; *W* is the width of the sample and $\frac{a}{W}$ is the ratio of average crack length ($\overline{a}$) to width (*W*).

A plot of crack length (a) versus the number of cycles (N) was produced. A Paris curve showing the fatigue crack growth rate (da/dN) versus ΔK was also generated by plotting da/dN versus ΔK on logarithmic scale as in equation (3-11). The Paris constants, *C*, and *m*,

which are related to specimen size, material variables and test conditions, were determined from the straight line region of the Paris curve by plotting $\log\frac{da}{dN}$ against $\log(\Delta K)$ according to equation (3-12). The slope of the curve gave the value of *m* while the intercept was log *C*.

$$\frac{da}{dN} = C(\Delta K)^m \tag{3-11}$$

$$\log\frac{da}{dN} = \log C + m\log(\Delta K) \tag{3-12}$$

The value of the threshold stress intensity (ΔK_{th}) needed to be determined at the da/dN values of 10^{-10} to 10^{-8} m/cycle according to the ASTM standard E647 [62]. However, the da/dN values of the Ti-6Al-4V alloy of this study were greater than 10^{-8} m/cycle. The ΔK_{th} values were then reported as the lowest ΔK values recorded where the crack started to propagate. The critical stress intensity (K_c) was read off from the raw data as the highest recorded ΔK values during the test. The OM and the SEM were used to perform fractography studies on the polished cross-section and on the fractured surface.

The results obtained from this chapter are presented in the results chapter (Chapter 4).

CHAPTER 4 Research results

This chapter presents all the results of the influence of ageing treatment parameters on the microstructural evolution. Microstructural analysis results from Optical Microscopy (OM), Scanning Electron Microscopy (SEM), as well as hardness measurements, are presented. The chapter further presents results of the influence of microstructural morphology on the mechanical properties (tensile, fracture toughness and fatigue crack growth rate) of the Ti-6Al-4V alloy. The fractography results are also reported.

4.1 Microstructure and hardness

The SEM microstructure of the as-received Ti-6Al-4V alloy is shown in Figure 4.1. The microstructure consisted of the globular primary α-phase shown as the dark phase surrounded by the bright β-phase. The average grain size of the as-received alloy was about 8 μm and its hardness was 310 ±5.6 $HV_{0.5}$.

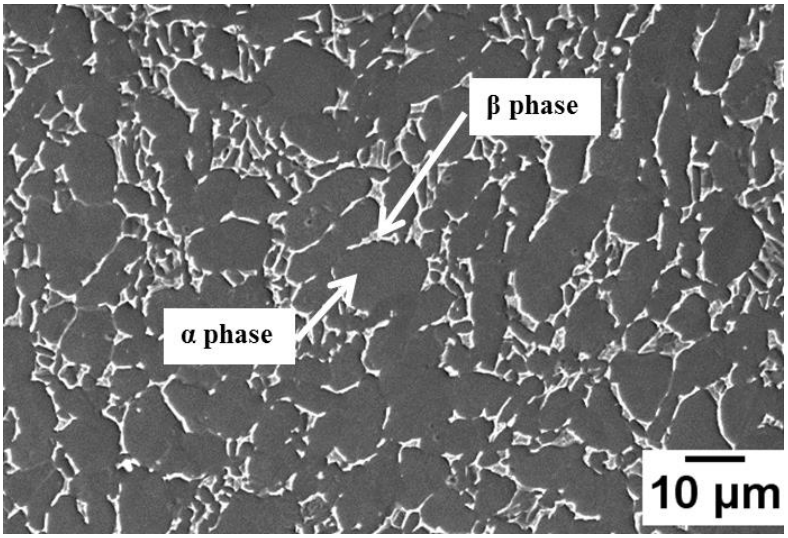

Figure 4.1: SEM micrograph of the as-received Ti-6Al-4V alloy

The Ti-6Al-4V specimens that were solution-treated and water-quenched (WQ) produced a fully martensitic microstructural morphology, as shown in Figure 4.2 (a), which consisted of fine acicular α′-martensitic needle-like phases while the grain boundaries (GB) comprised the β-phase. The specimens of Ti-6Al-4V alloy that were solution-treated (ST) followed by air-cooling (AC), produced a partially martensitic microstructure shown in Figure 4.2(b). The microstructure was identified by the partial transformation of β-phase to α-phase on the grain boundaries and shown as dark-coloured phases. The grain boundaries are a mixture of dark (α-phase) and bright-coloured phases (β-phase). Fine α and β-lamellar structures are visible within the grains. A colony lamellar microstructure is shown in Figure 4.2 (c), which was produced from solution treatment followed by furnace cooling (FC). The colony microstructure has GB of α-phase resulting from the complete transformation of β-phase to α-phase. The grains consist of colonies of α and β-lamellar structures in which α-laths are parallel plate-like structures with thin β-regions sandwiched between them.

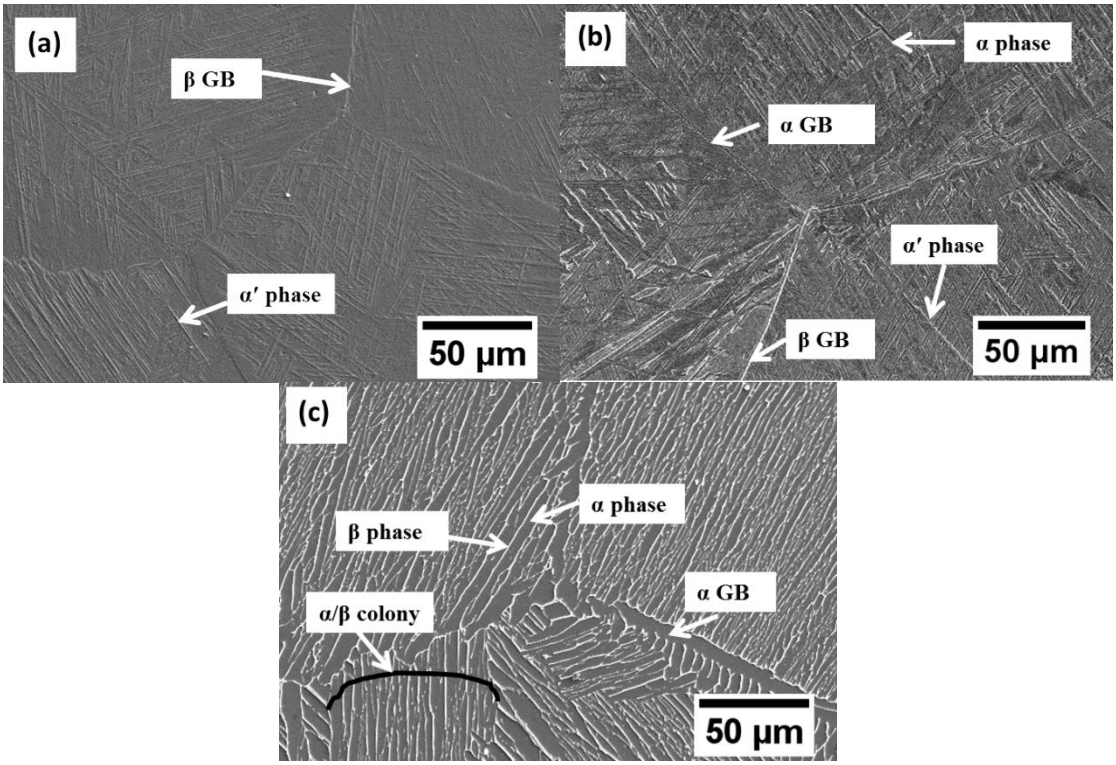

Figure 4.2: SEM micrographs of the Ti-6Al-4V alloy specimens that were (a) ST/WQ, (b) ST/AC and (c) ST/FC

The Vickers micro-hardness results are presented in Figure 4.3. The fully martensitic microstructure showed a slightly greater hardness value than the partially martensitic microstructure, but a significantly greater hardness than the colony lamellar microstructure. Hardness variability was greater in a colony morphology and lower in a fully martensitic morphology.

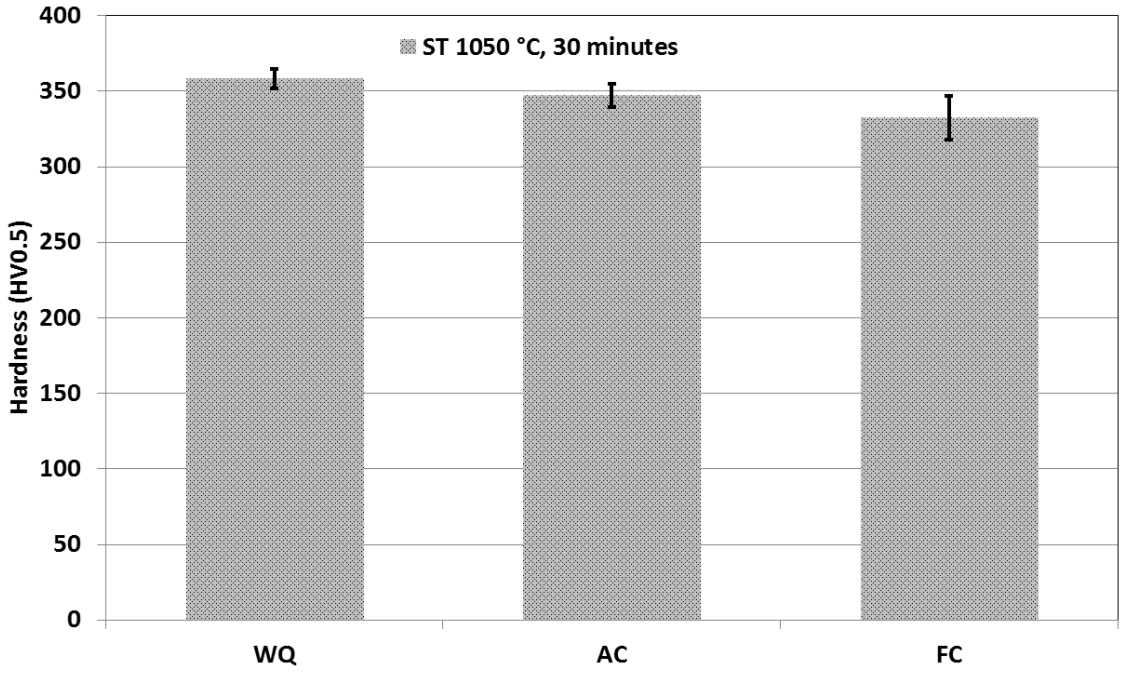

Figure 4.3: Vickers micro-hardness results of specimens ST followed by WQ or AC or FC (Standard Deviation (SD) error bars)

Optical micrographs showing hardness indentations for various solution treatment conditions are shown in Figure 4.4(a) to (c). It is observed that the fully martensitic microstructural morphology (ST/WQ) has finer martensitic needles while the lamellar microstructural morphology (ST/FC) has thicker α-laths. The partial martensitic morphology (ST/AC) shown in Figure 4.4(b) shows in-between hardness values as the α-laths are thinner than in the colony lamellar microstructure but thicker than in the fully martensitic microstructure.

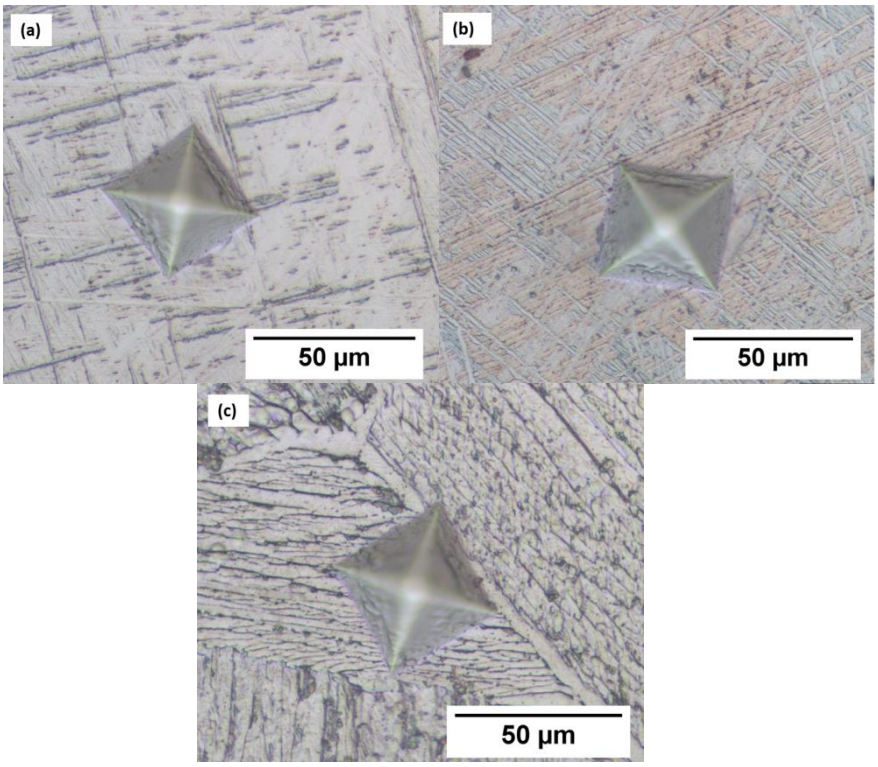

Figure 4.4: Optical micrographs showing micro-hardness indentations in (a) ST/WQ or (b) ST/AC or (c) ST/FC

The hardness profiles of various solution-treated Ti-6Al-4V alloy specimens are shown in Figure 4.5. The solution treatment and WQ specimen showed less variable hardness values than both the ST/AC and ST/FC specimens as indicated in the hardness profiles (Figure 4.5). The ST/FC specimen showed the most variable hardness values.

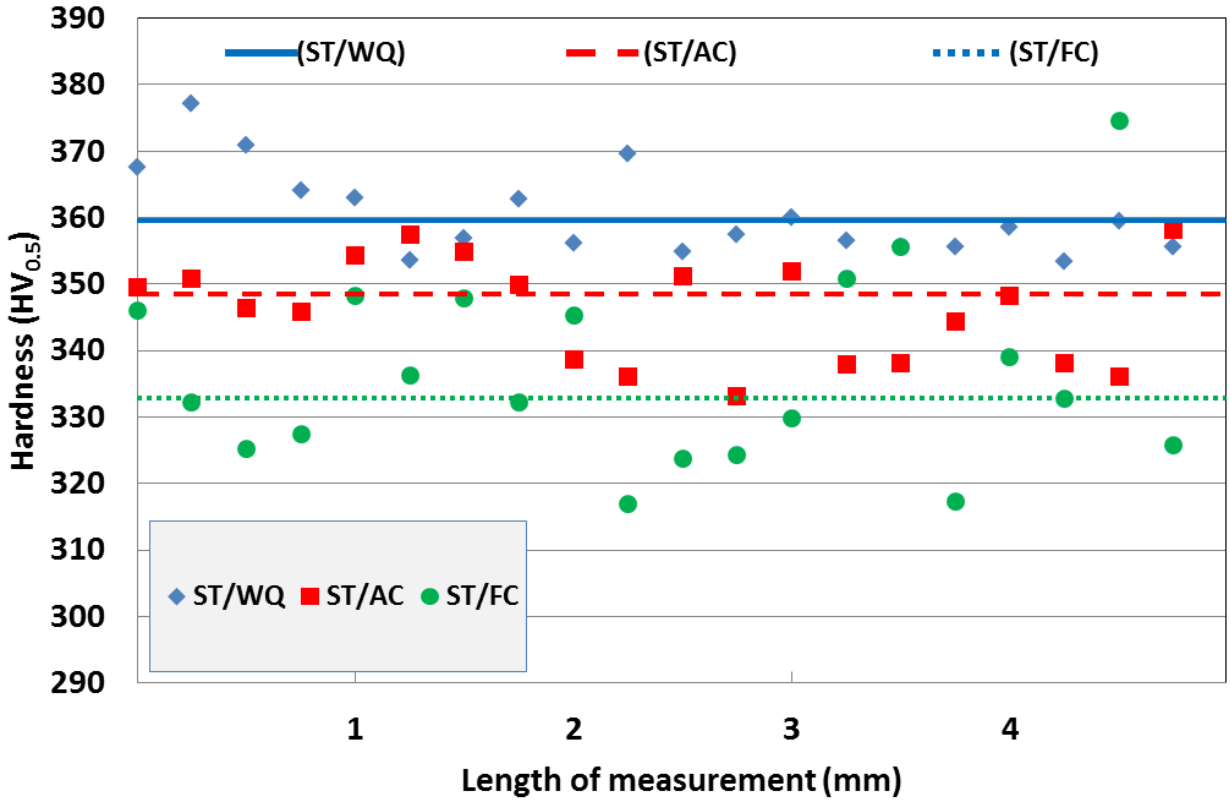

Figure 4.5: Hardness profiles showing variability in the microstructure of the solution treated Ti-6Al-4V alloy, cooled by WQ, AC and FC

The Vickers macro-hardness results are presented in Figure 4.6. The fully martensitic microstructure showed a greater hardness value than both the partially martensitic and the colony lamellar microstructures. The partially martensitic microstructure showed similar hardness results to the colony lamellar microstructure. The variability in the ST/FC specimen was more pronounced in the macro-hardness results.

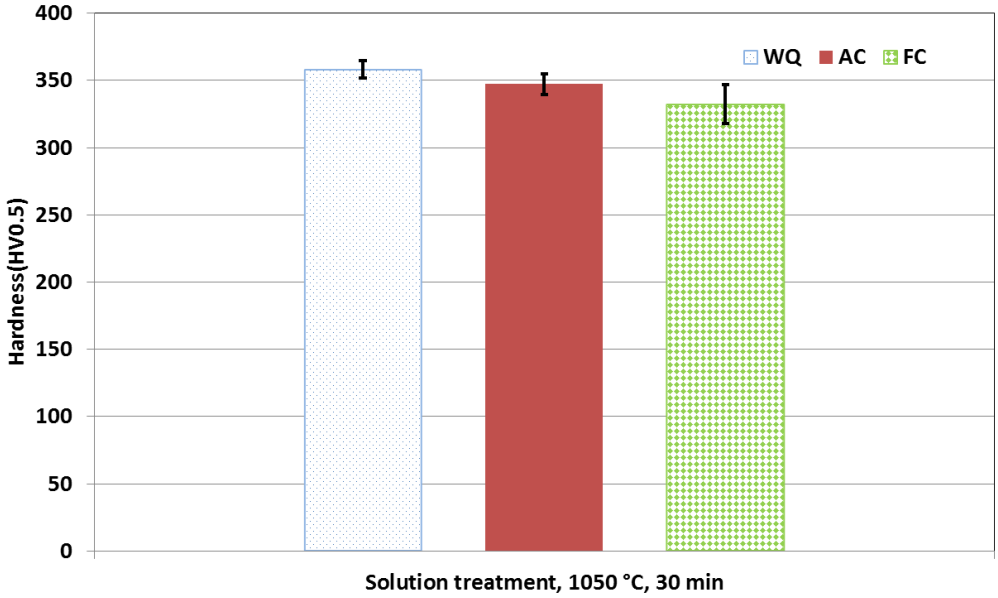

Figure 4.6: Vickers Macro-hardness results of the Ti-6Al-4V alloy specimens after ST/WQ, ST/AC and ST/FC (SD error bars)

Table 4.1 shows the results of microstructural quantification of the solution-treated specimens. The β-grain sizes of the ST/WQ and ST/AC specimens were similar, but smaller than the ST/FC grains. The martensitic needles in the ST/WQ specimens were notably thinner compared to the α-phase laths found in the ST/FC specimens. The α-contents in the ST/WQ and ST/AC specimens were not measured as the difference between the α-phase and the β-phase could not be clearly resolved.

Table 4.1: The β-grain size, lath thickness, α-content and α/β-colony size of ST/WQ, ST/AC and ST/WQ specimens (SD errors)

Specimen details	β-grain size (μm)	α content (%)	lath thickness (μm)	α/β-colony size (μm)
ST/WQ	713±104	*	0.8±0.2	*
ST/AC	649±75	*	*	*
ST/FC	1027±196	83	2.9±1.4	328±64

* could not be measured

Ageing at temperatures of 500, 600 and 700 °C did not alter the microstructural morphology of solution-treated and WQ samples (Figure 4.7, Figure 4.8 and Figure 4.9). The results were the same for both WQ and FC rates after ageing for 30 minutes. The fully martensitic morphology from solution treatment remained unchanged. However, it was observed visually that the content of martensitic needles seemed to reduce as the ageing temperature increased. These results are expanded below.

Ageing at a temperature of 500 °C for 30 minutes did not alter the microstructural morphology of solution-treated and WQ specimens, as shown in Figure 4.7. The fully martensitic microstructural morphology remained unchanged. The results were the same whether the ageing cooling rate was WQ or FC. The martensitic needles of the sample that was ST/WQ, aged, followed by FC (Figure 4.7 (b)) were less visible and shorter than those in the sample that was ST/WQ, aged, followed by WQ (Figure 4.7 (a)).

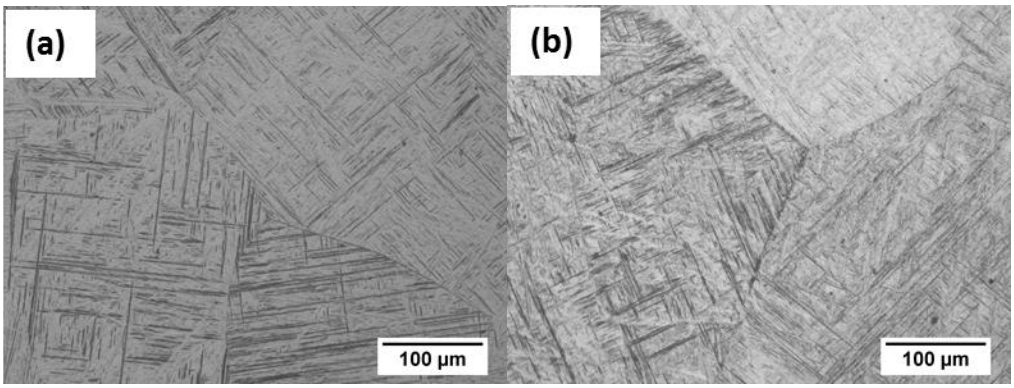

Figure 4.7: Optical images of the Ti-6Al-4V alloy specimens that were ST/WQ, aged at 500 °C for 30 minutes and (a) WQ, (b) FC

The fully martensitic microstructural morphology did not change after ageing at a temperature of 600 °C for 30 minutes for both ageing cooling rates of WQ and FC (Figure 4.8). The specimen that was aged followed by FC (Figure 4.8(b)), showed a reduced volume fraction of martensitic needles than the specimen that was WQ after ageing (Figure 4.8 (a)). It was also evident from Figure 4.8 (b) that the martensitic needles appeared to be shorter.

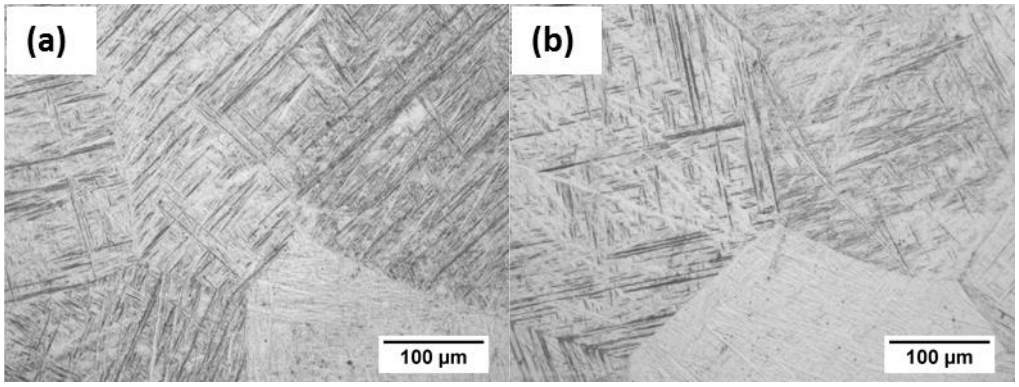

Figure 4.8: Optical images of the Ti-6Al-4V alloy specimens that were ST/WQ, aged at 600 °C for 30 minutes and (a) WQ, (b) FC

The solution-treated and WQ resulting microstructural morphology did not substantially change at an ageing temperature of 700 °C for 30 minutes as shown in Figure 4.9. The morphology remained fully martensitic after ageing and subsequent water-quenching or furnace-cooling. The furnace-cooling after ageing showed more reduced content of martensitic needles (Figure 4.9 (b)) than in the WQ specimen (Figure 4.9(a)).

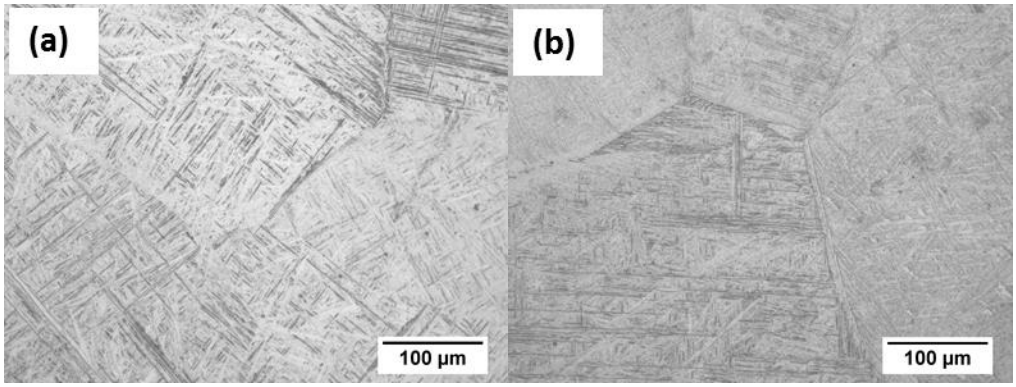

Figure 4.9: Optical images of the Ti-6Al-4V alloy specimens that were ST/WQ, aged at 700 °C for 30 minutes and (a) WQ, (b) FC

Ageing the ST/WQ specimen at temperatures of about 800 and 900 °C for 30 minutes, followed by WQ, changed the microstructural morphology from a fully martensitic to a partially martensitic morphology as shown in Figure 4.10 (a) and (b). The grain boundaries started to change from the β-phase to the α-phase.

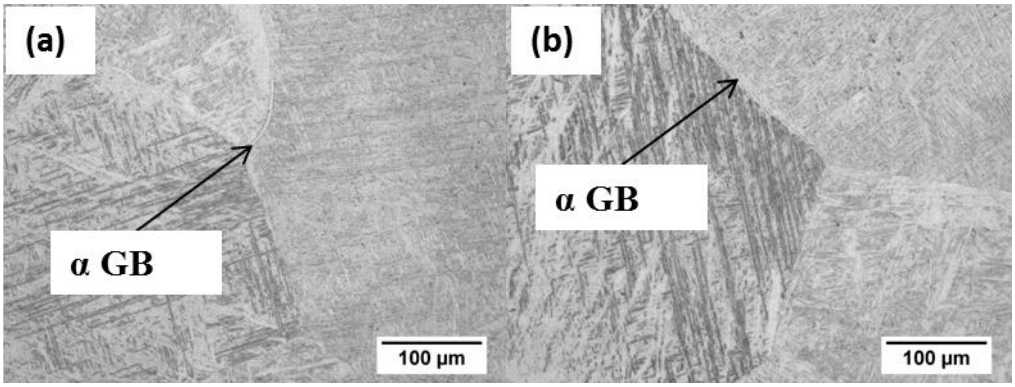

Figure 4.10: Optical images of the Ti-6Al-4V alloy specimens that were ST/WQ and aged at (a) 800 °C for 30 minutes and WQ, (b) 900 °C for 30 minutes and WQ

Ageing Ti-6Al-4V with an initial martensitic structure at 800 and 900 °C for 30 minutes followed by furnace-cooling also led to a partial martensitic morphology as shown in Figure 4.11 (a) and (b). The formation of α-laths within the β-grains was evident in these microstructures.

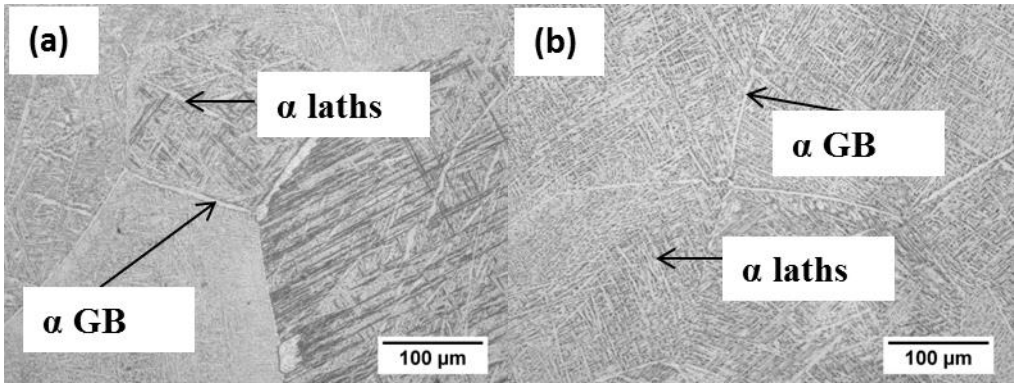

Figure 4.11: Optical micrographs of Ti-6Al-4V alloy specimens that were ST/WQ and aged at (a) 800 °C for 30 minutes and FC, (b) 900 °C for 30 minutes and FC

There was some indication that the Ti-6Al-4V furnace-cooled after ageing gave greater hardness values than the water-quenched Ti-6Al-4V at temperatures of 500 °C to 800 °C as shown in the ageing curve in Figure 4.12. At an ageing temperature of 900 °C, there was no significant difference in the hardness values between the water-quenched and furnace-cooled Ti-6Al-4V.

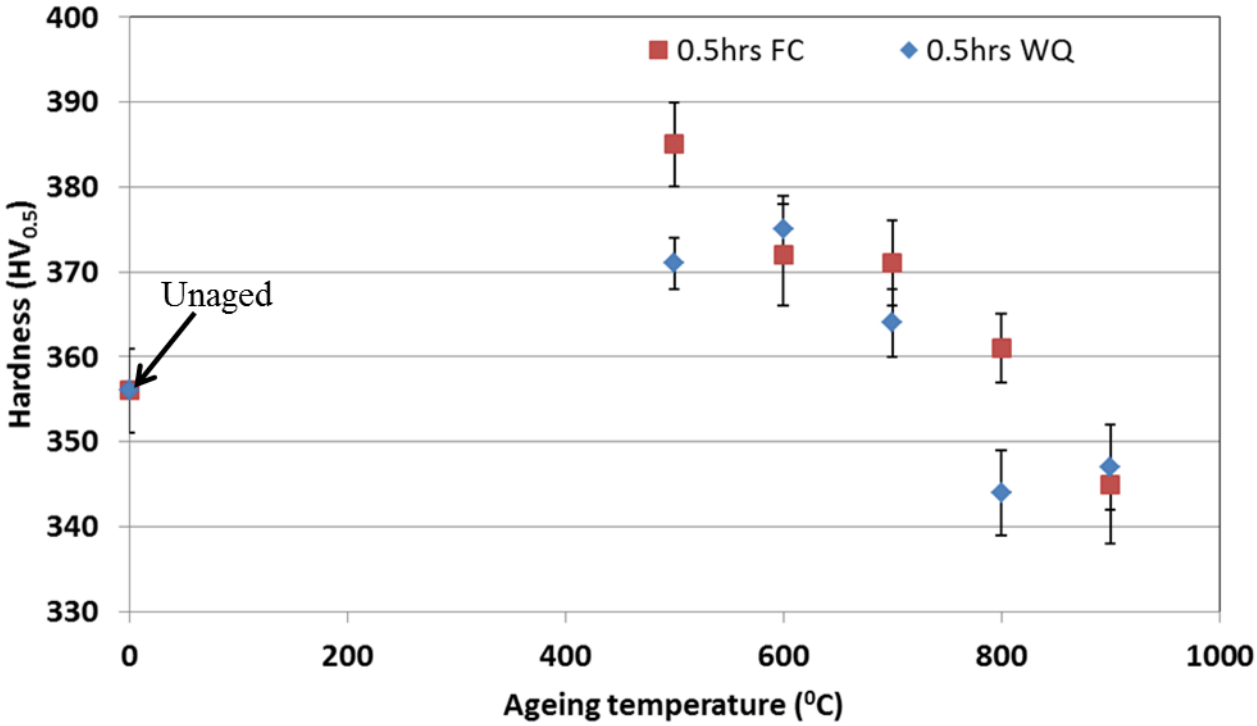

Figure 4.12: Ageing curve showing micro-hardness results of Ti-6Al-4V specimens that were ST/WQ, aged in the temperature range of 500 to 900 °C, followed by either WQ or FC (SD error bars)

The hardness decreased as the ageing temperature increased from 500 to 900 °C, relative to the unaged ST/WQ specimens as shown in Figure 4.12. The graph in Figure 4.12 showed an

initial increase in hardness at an ageing temperature of 500 °C and a continuous drop in hardness resulted as the ageing temperature increased beyond 500 °C.

The effect of ageing times of 0.5 hours and 48 hours on the microstructural morphology at an ageing temperature of 500 °C is shown in Figure 4.13 (a) and (b). The microstructural morphology remained fully martensitic. Evidently, the content of martensitic needles reduced as the ageing time increased. A denuded zone is also observed at the grain boundaries at longer ageing times (Figure 4.13 (b)).

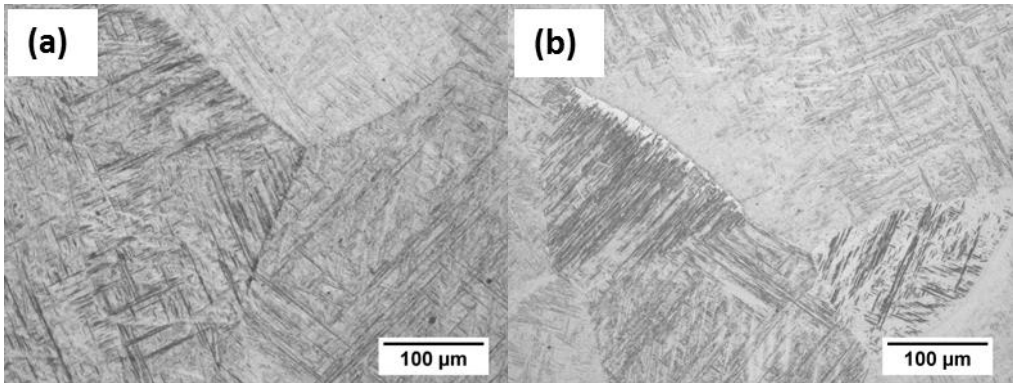

Figure 4.13: Optical micrographs of Ti-6Al-4V alloy specimens that were ST/WQ and aged at 500 °C for (a) 0.5 hours and FC, (b) 48 hours and FC

The effect of ageing times of 0.5 hours and 48 hours on the microstructural morphology at an ageing temperature of 650 °C is shown in Figure 4.14 (a) and (b). The microstructural morphology remained fully martensitic at all ageing times. The denuded zone is observed, as well at the grain boundaries, at longer ageing times, especially at an ageing time of 48 hours (Figure 4.14(b)). Fine α-phase needles started to show within the grains at an ageing temperature of 650 °C and ageing time of 48 hours.

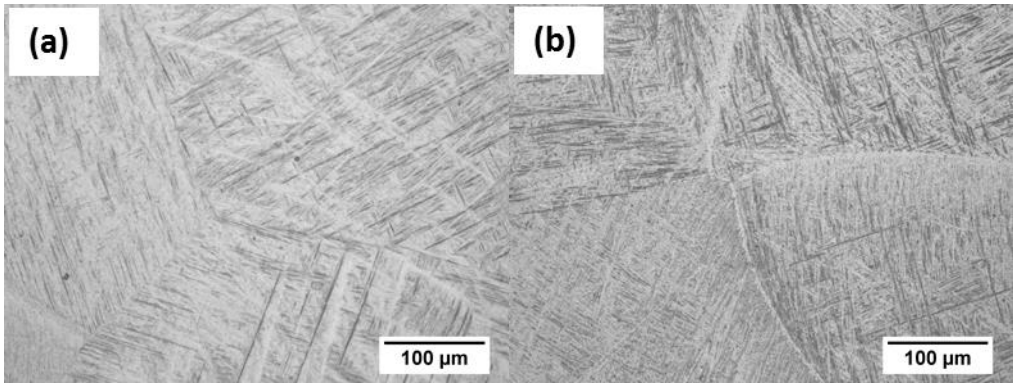

Figure 4.14: Optical micrographs of Ti-6Al-4V alloy specimens that were ST/WQ and aged at 650 °C for (a) 0.5 hours and FC, (b) 48 hours and FC

The effect of ageing times of 0.5 hours and 2 hours on the microstructural morphology at an ageing temperature of 750 °C is shown in Figure 4.15 (a) and (b). The microstructural morphology remained fully martensitic at an ageing time of 0.5 hours (Figure 4.15 (a)), but changed to partially martensitic from an ageing time of 2 hours onwards (Figure 4.15 (b)). The prevalence of the denuded zone at grain boundaries increased, while the formation of α-phase needles was evident. As the ageing time increased to 48 hours, the volume fraction of the α-phase increased (Figure 4.15 (c)).

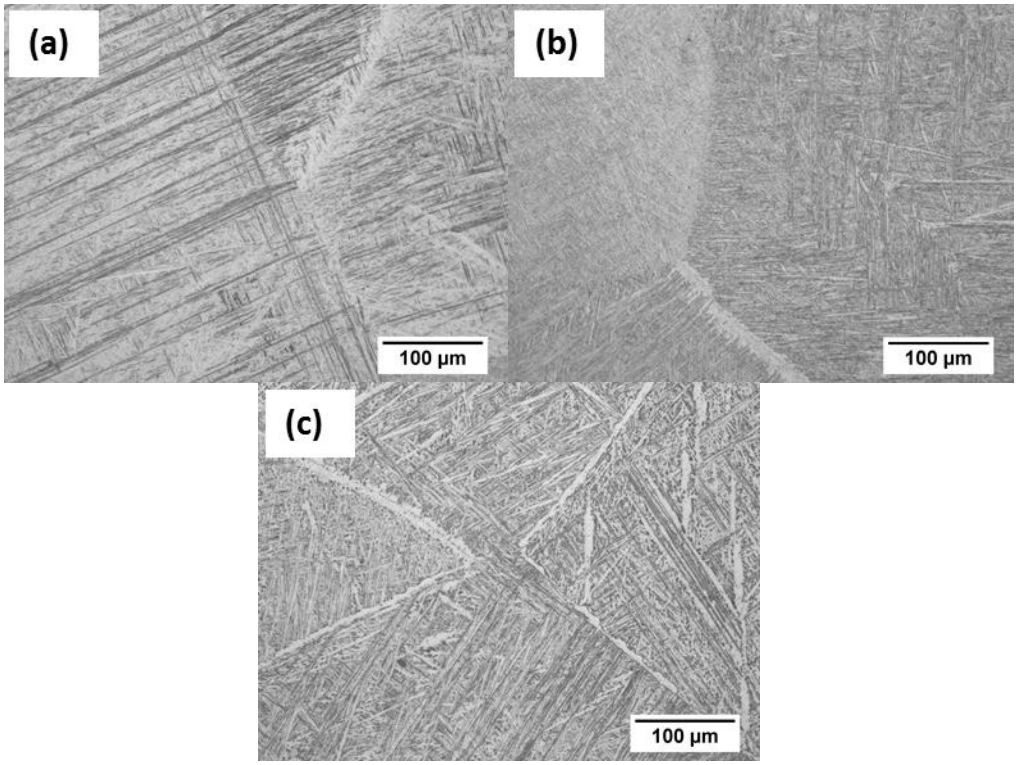

Figure 4.15: Optical micrographs of Ti-6Al-4V alloy specimens that were ST/WQ and aged at 750 °C for (a) 0.5 hours and FC, (b) 2 hours and FC, and (c) 48 hours and FC

The microstructures of specimens aged at 800 °C for 0.5 hours and 48 hours are shown in Figure 4.16. The morphology changed from a fully martensitic to a partially martensitic morphology. As the ageing time increased, coarsening of the α-phase was evident. More α-pools were formed within the grains (Figure 4.16 (b)).

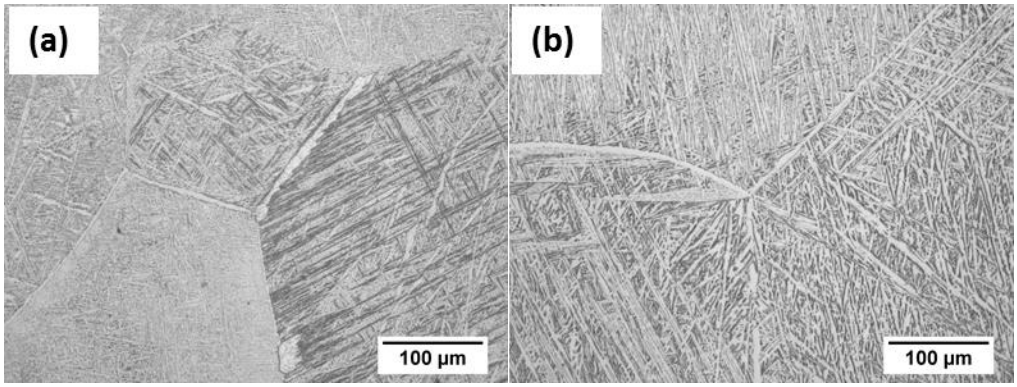

Figure 4.16: Optical micrographs of Ti-6Al-4V alloy specimens that were ST/WQ and aged at 800 °C for (a) 0.5 hours and FC, (b) 48 hours and FC

Ageing at 900 °C for 0.5 hours followed by FC, produced a partially martensitic morphology (Figure 4.17 (a)), but as the ageing time increased to 24 hours and 48 hours respectively, the basketweave morphology formed as shown in Figure 4.17 (b) and (c). It is evident from Figure 4.17 (b) and (c) that the thickness of the α-laths increased compared to that of the specimen aged for 0.5 hours.

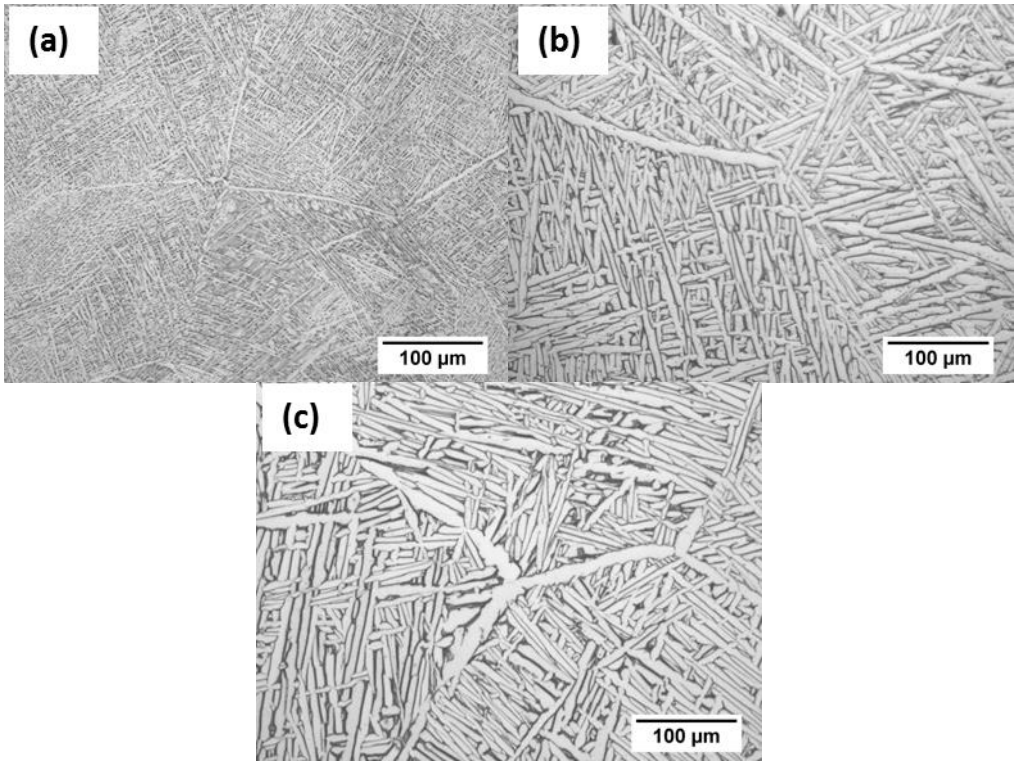

Figure 4.17: Optical micrographs of Ti-6Al-4V alloy specimens that were ST/WQ and aged at 900 °C for (a) 0.5 hours and FC, (b) 24 hours and FC, (c) 48 hours and FC

The influence of ageing time on the hardness for ageing temperatures of 500 °C, 650 °C, 750 °C, 800 °C and 900 °C is shown in Figure 4.18 to Figure 4.22. At these ageing temperatures, as the ageing time increased, the hardness tended to decrease. The variability in hardness values also increased with increasing ageing time.

Figure 4.18 shows micro-hardness results after ageing at 500 °C for 0.5 to 48 hours, followed by FC. Hardness values after ageing for 0.5 hours are greater than the unaged values. The hardness tended to decrease as the ageing time increased.

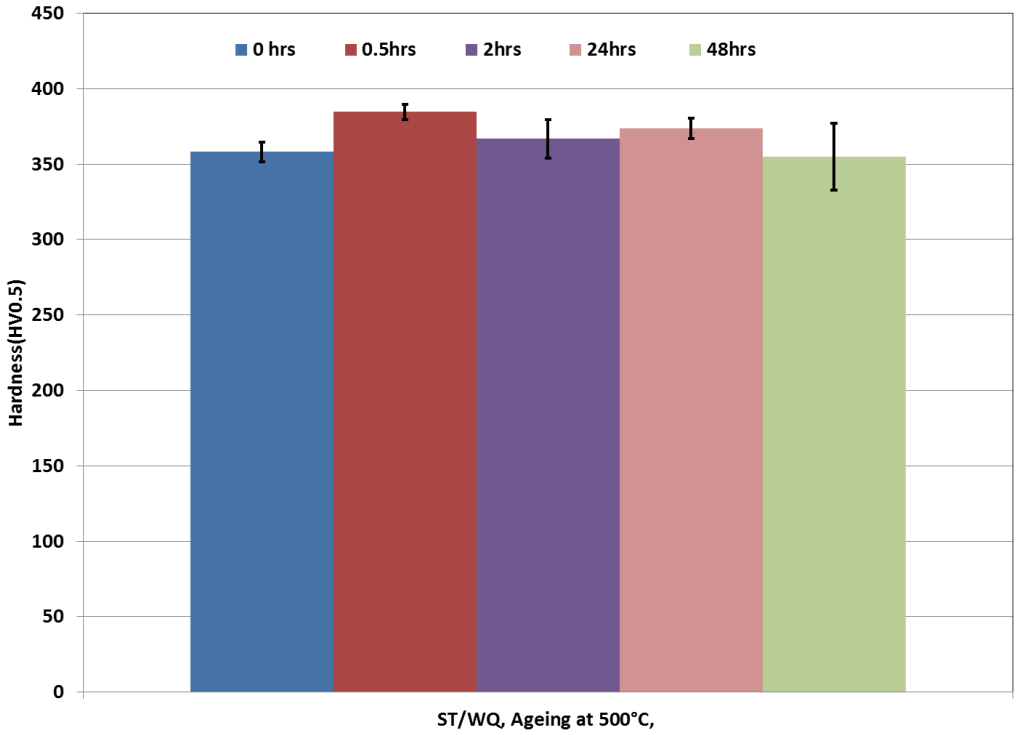

Figure 4.18: Micro-hardness values of ST/WQ specimens, aged at 500 °C for 0.5 hours to 48 hours and FC (SD error bars)

The hardness after ageing at 650 °C for 0.5 hours was also greater than that of the unaged samples (Figure 4.19). Hardness results were similar for the unaged, and ageing times of 2 and 24 hours. As the ageing time increased to 48 hours, the hardness dropped significantly to below the unaged results.

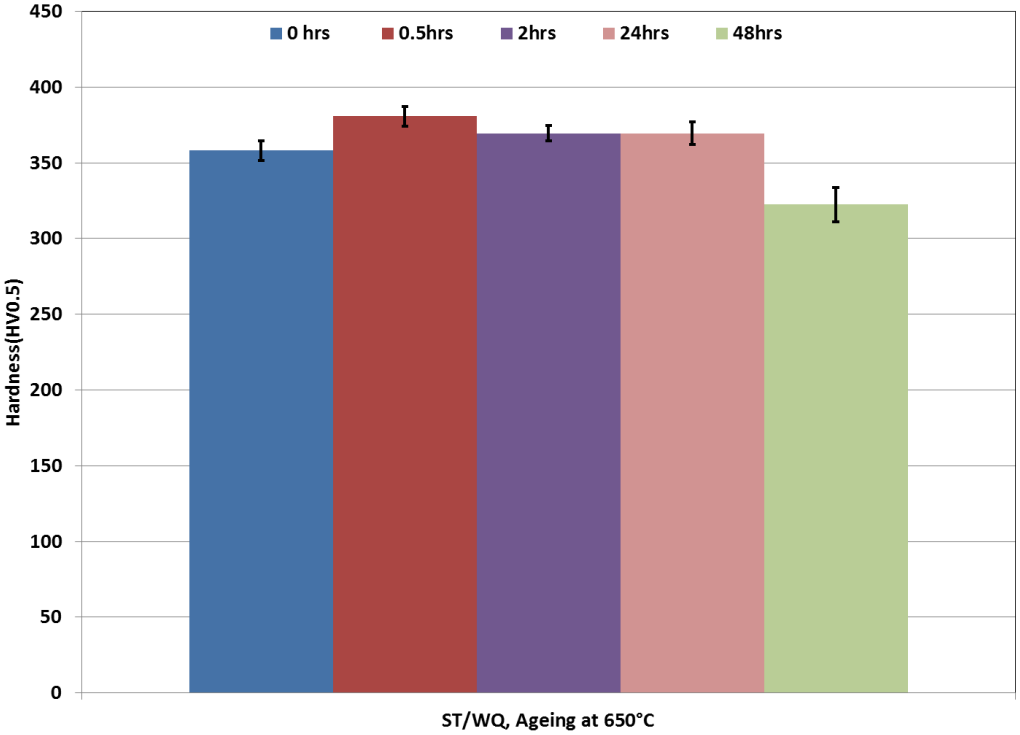

Figure 4.19: Micro-hardness values of ST/WQ specimens, aged at 650 °C for 0.5 hours to 48 hours and FC (SD error bars)

Ageing at 750 °C led to hardness values similar to the hardness of unaged samples (Figure 4.20), however, the hardness tended to decrease as the ageing time increased for ageing temperatures of 800 and 900 °C (Figure 4.21 and Figure 4.22).

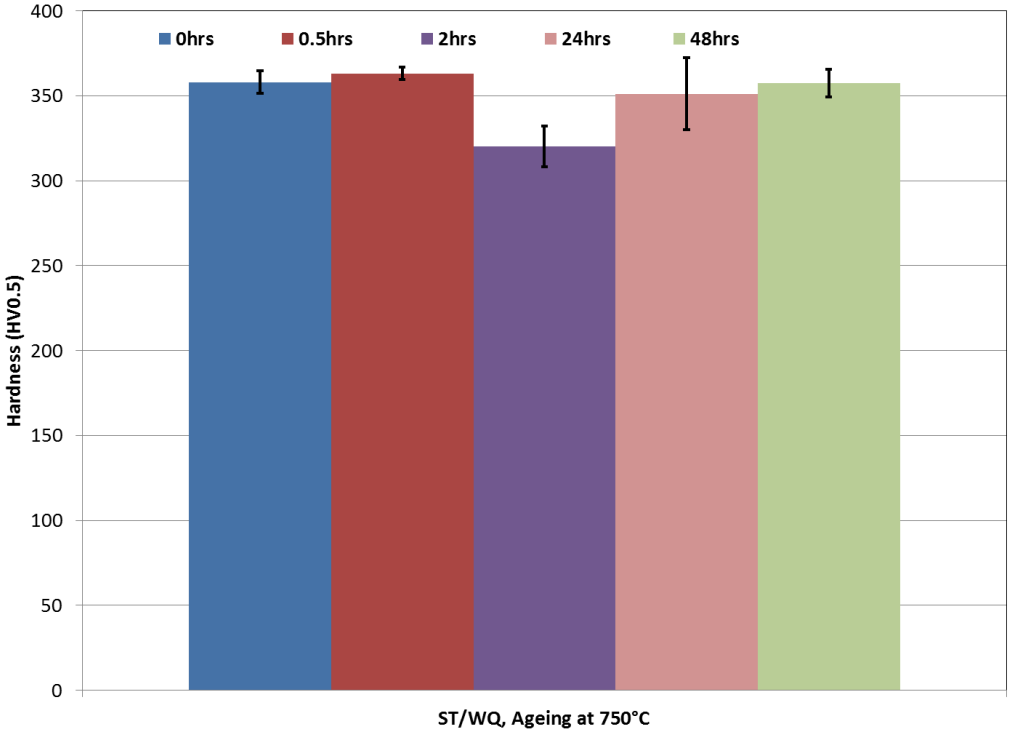

Figure 4.20: Micro-hardness values of ST/WQ specimens, aged at 750 °C for 0.5 hours to 48 hours and FC (SD error bars)

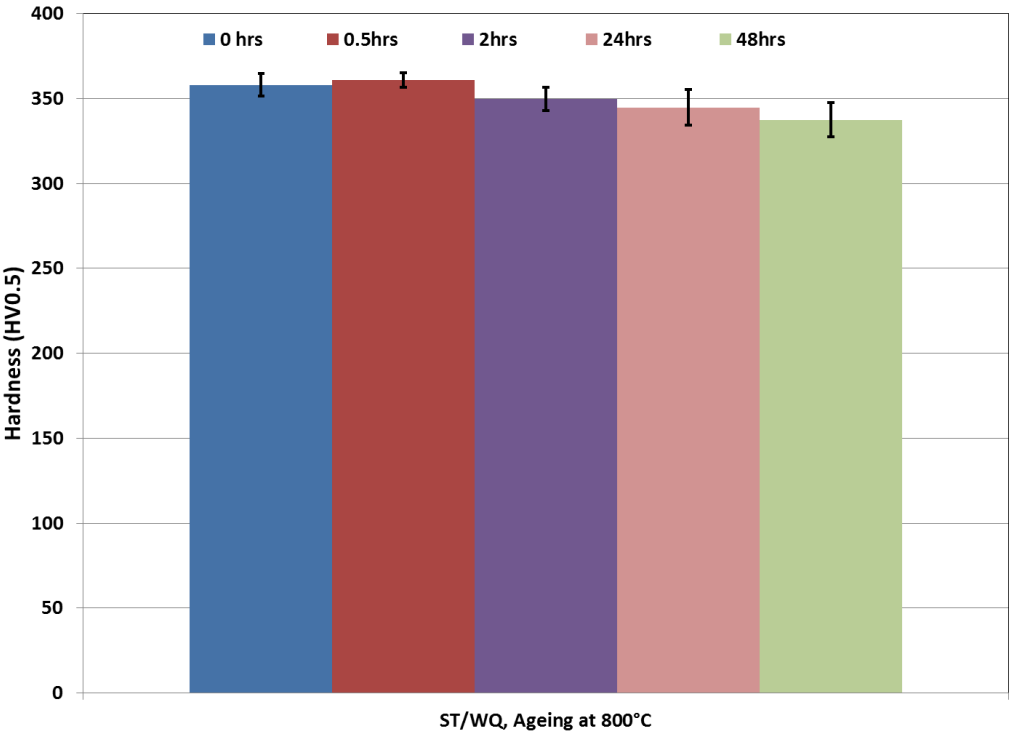

Figure 4.21: Micro-hardness values of ST/WQ specimens, aged at 800 °C for 0.5 hours to 48 hours and FC (SD error bars)

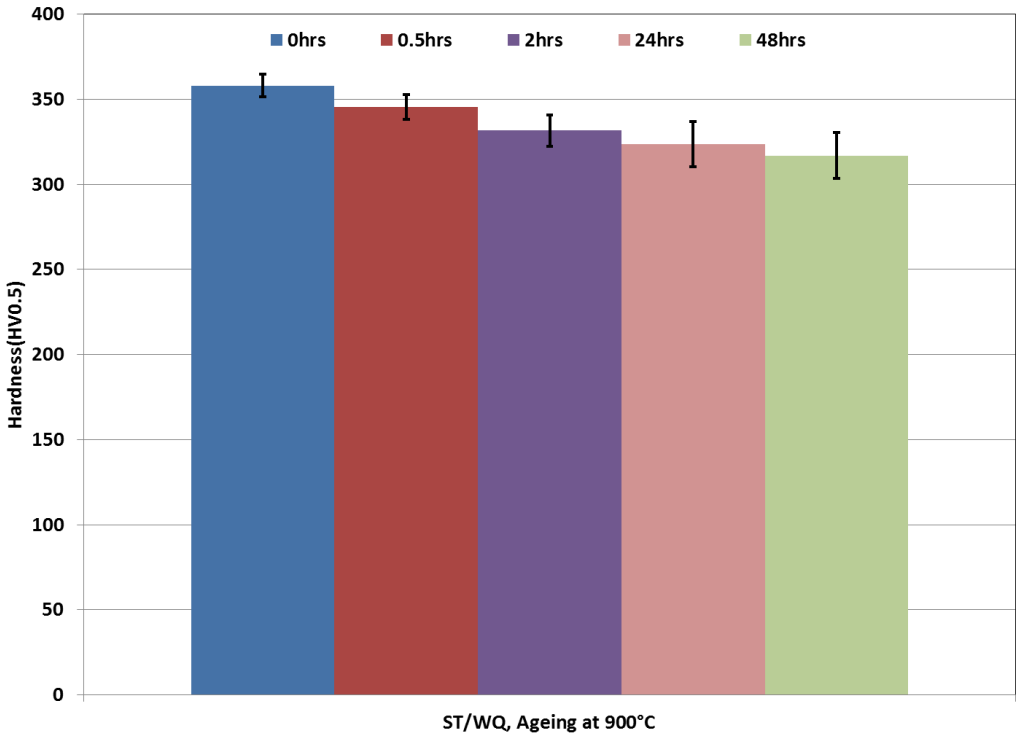

Figure 4.22: Micro-hardness values of ST/WQ specimens, aged at 900 °C for 0.5 hours to 48 hours and FC (SD error bar)

Quantification of the microstructure of selected specimens was carried out and the results are presented in Table 4.2. The entries with a star (*) could not be measured. The results showed that the ageing conditions used did not change the β-grain size of the ST/WQ specimens. The α-laths were thinner at lower ageing temperatures, but increased in thickness as ageing temperatures reached about 800 °C and 900 °C. For ageing temperature of 900 °C, increasing the ageing time from 0.5 hours to 24 hours led to an increase in the α-lath thickness. The α-lath thickness of the unaged and specimens aged at 500 °C was similar. However, the α-content tended to increase with increasing ageing temperature and time.

Table 4.2: The β-grain size, α thickness and α-content of ST/WQ and ST/WQ followed by ageing and furnace-cooling (SD errors)

Specimen details	β-grain size (μm)	α content (%)	α thickness (μm)
ST/WQ	713±104	*	0.8±0.2
ST/WQ-500 °C-0.5 hrs-FC	646±104	*	0.9±0.2
ST/WQ-500 °C-48 hrs-FC	613±96	*	0.8±0.2
ST/WQ-800 °C-0.5 hrs-FC	570±82	*	*
ST/WQ-800 °C-48 hrs-FC	608±90	92±0.9	2.8±0.6
ST/WQ-900 °C-0.5 hrs-FC	642±89	89±0.9	2.0±0.3
ST/WQ-900 °C-24 hrs-FC	720±116	89±0.7	6.1±1
ST/WQ-900 °C-48 hrs-FC	707±102	92±0.9	5.8±1.1

* could not be measured

Figure 4.23 (a) to (g) show SEM micrographs summarising the microstructural evolution during the ageing of the ST/WQ specimens. The unaged ST/WQ microstructure consists of fine and long α′-needles (Figure 4.23 (a)). The microstructure is made up of the α′, α and β-phases, with the β-phase on grain boundaries (GB). The specimen aged at 500 °C for 0.5 hours still showed similar morphology to that of the ST and WQ specimens (Figure 4.23 (b)). As the ageing time increased to 48 hours, the martensitic needles clearly reduced in content

and were shorter (Figure 4.23 (c)). The phases were still the α′ , α and β-phases, with the β-phase on GBs. The ageing temperature of 800 °C for 0.5 hours led to a partial martensitic morphology with the α′-needles having broken down into finer features (Figure 4.23 (d)). The content of the martensitic needles was substantially reduced. The α-phase content had increased due to β into α-phase transformation that also resulted in α-phase on GBs. At an ageing temperature of 800 °C for 48 hours, the longer martensitic needles disappeared (Figure 4.23 (e)). The structure had thicker and shorter α-laths. The microstructure produced by ageing at 900 °C for 30 minutes was similar to the microstructure produced at 800 °C for 48 hours (Figure 4.23 (f)). At an ageing temperature of 900 °C for 24 hours, a different microstructural morphology was produced, and termed basketweave morphology (Figure 4.23 (g)). The microstructure consisted of α and β-phases, with the grain boundaries consisting of the α-phase. The α-laths were substantially thicker than at 0.5-hour ageing time. Some colonies were observed within the microstructure.

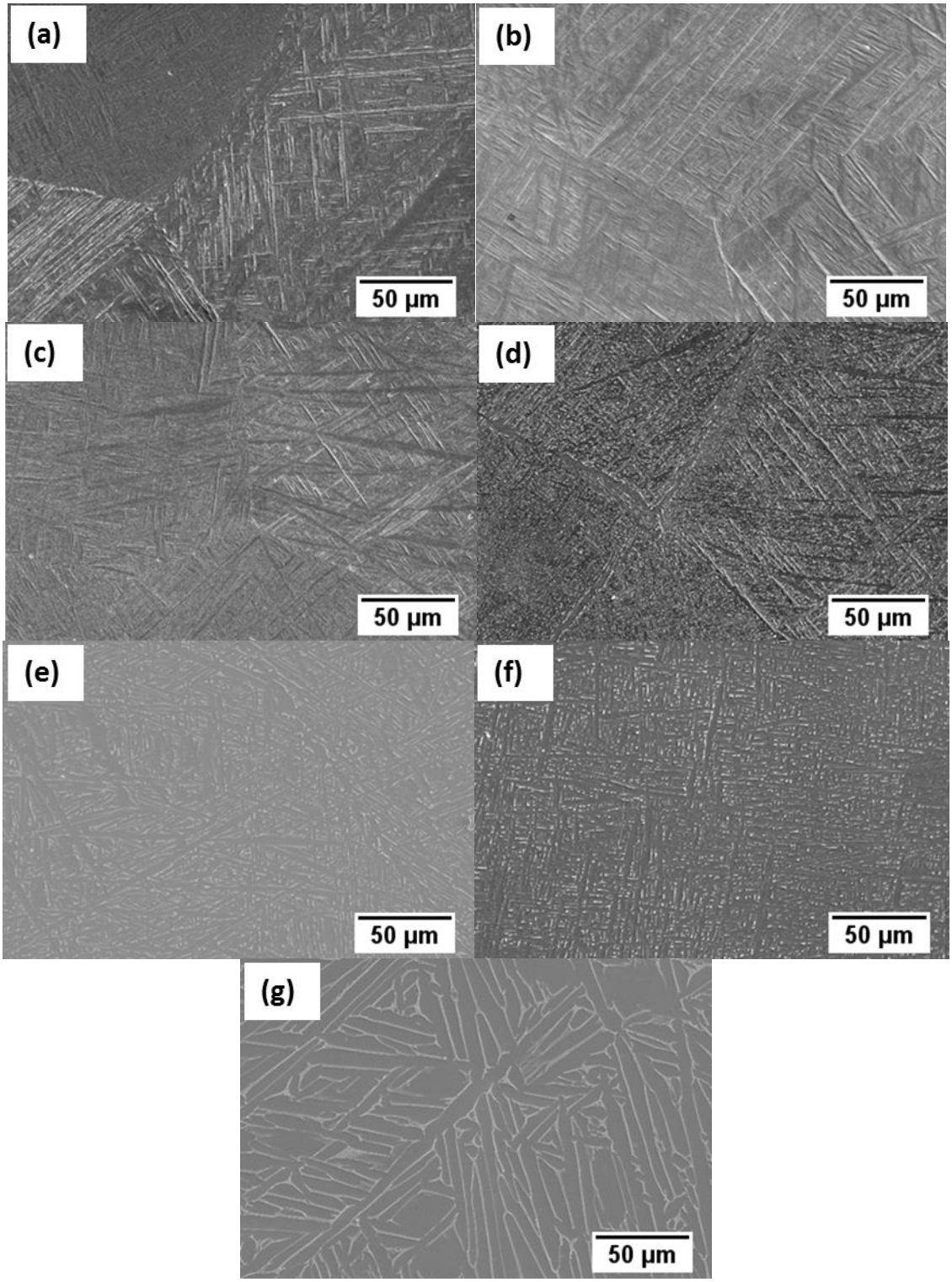

Figure 4.23: SEM micrographs of Ti-6Al-4V alloy specimens that were (a) ST/WQ, (b) ST/WQ-500 °C-30min-FC, (c) ST/WQ-500 °C-48 hrs-FC (d) ST/WQ-800 °C-30min-FC, (e) ST/WQ-800 °C-48 hrs-FC, (f) ST/WQ-900 °C-30min-FC, (g) ST/WQ-900 °C-48hrs-FC

A lamellar microstructural morphology was produced by solution treatment and FC (Figure 4.24). The grain boundaries consisted of α-phase and the colonies of α/β-lamellar were observed within the grains.

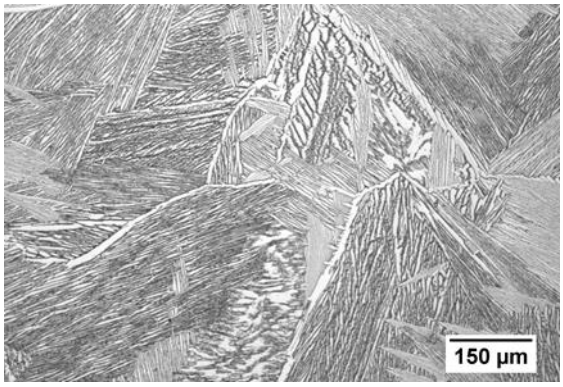

Figure 4.24: Optical micrograph of the ST/FC specimen

The specimens with an initial colony lamellar structure (ST/FC) that were aged at 750 °C, 800 °C and 900 °C for 0.5, 2, 24 and 48 hours, followed by WQ did not show an observable microstructural change (Figure 4.25 to Figure 4.27).

The microstructures after ageing of specimens with a colony lamellar structure at 750 °C for 0.5, 2, 24 and 48 hours, followed by WQ are shown in Figure 4.25 (a) to (d)). Grain boundaries still contain α-phase and no microstructural change is observed.

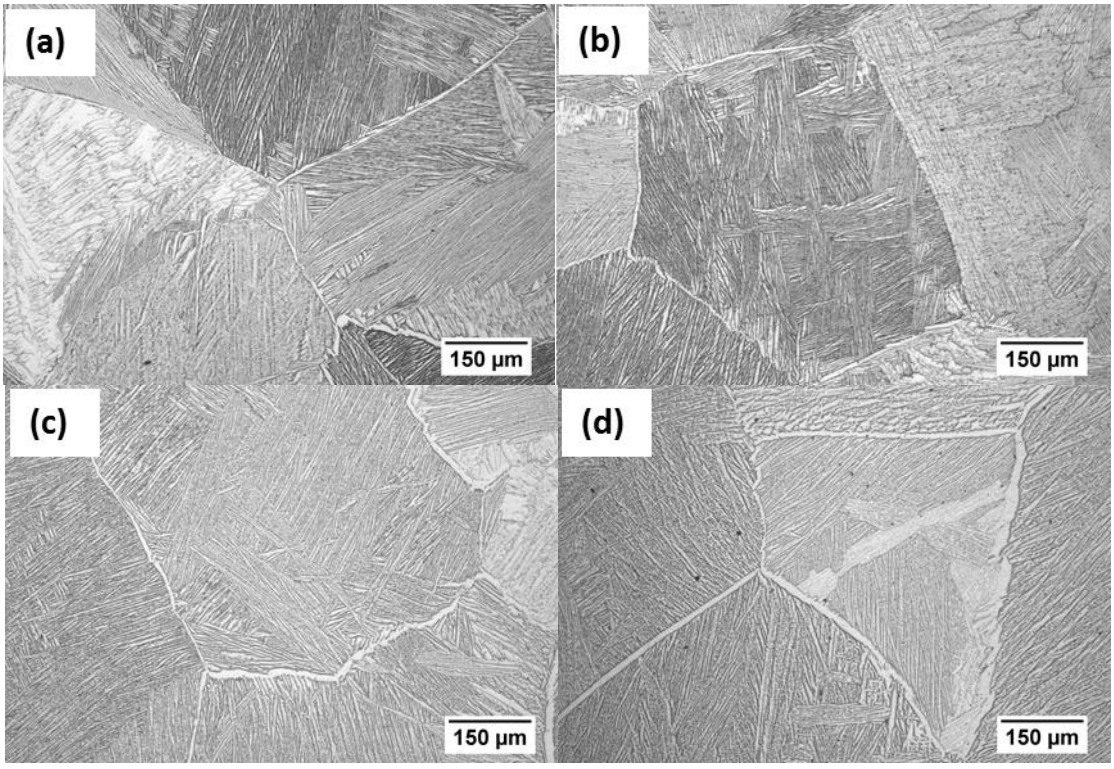

Figure 4.25: Optical micrographs of the ST/FC, aged at 750 °C for (a) 0.5 hours and WQ, (b) 2 hours and WQ, (c) 24 hours and WQ, (d) 48 hours and WQ

Ageing of specimens with a colony lamellar microstructure at 800 °C for 0.5, 2, 24 and 48 hours followed by WQ, did not change the microstructural morphology. The size of the α-laths seemed to be getting thinner after ageing for 48 hours, and the volume fraction of the β-phase (dark phase) seemed to increase as evidenced by the increase in the dark phase (Figure 4.26 (d)).

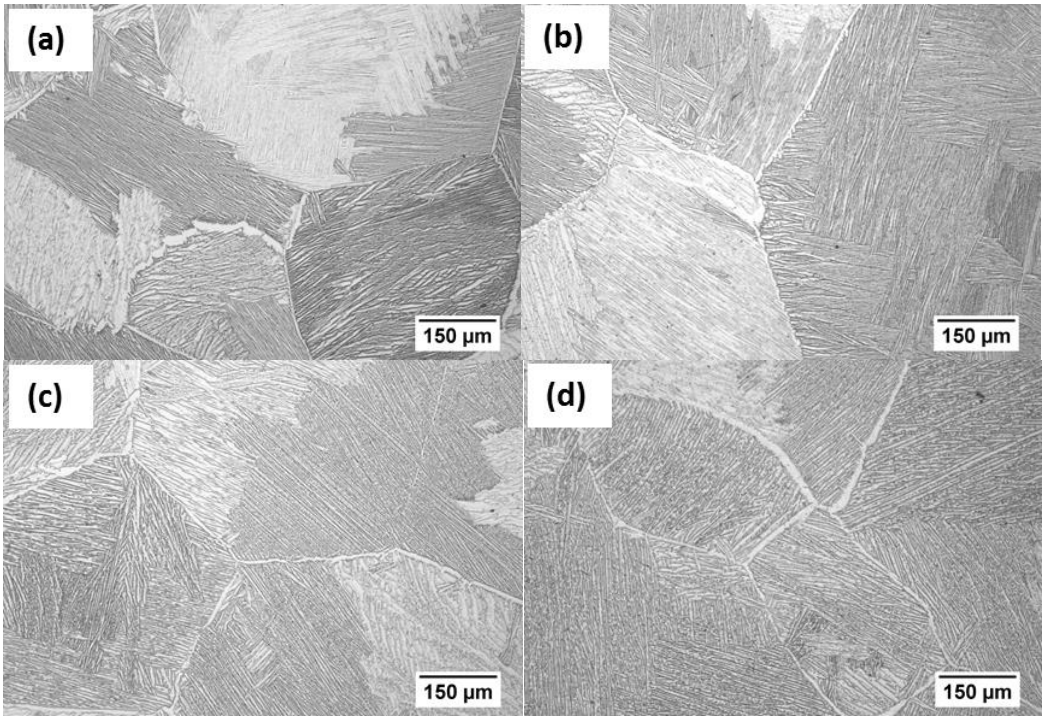

Figure 4.26: Optical micrographs of ST/FC, aged at 800 °C for (a) 0.5 hours and WQ, (b) 2 hours and WQ, (c) 24 hours and WQ, (d) 48 hours and WQ

The microstructural morphology did not change after ageing at 900 °C for 0.5, 2, 24 and 48 hours, followed by WQ (Figure 4.27 (a) to (d)). The α-laths were getting thinner from the ageing time of 0.5 hours and were not easily observed. Grain boundaries still consisted of the α-phase, even after ageing for 48 hours. The content of the β-phase increased from 35% after ageing for 0.5 hours, to 44% after ageing for 48 hours (Figure 4.27 (d)).

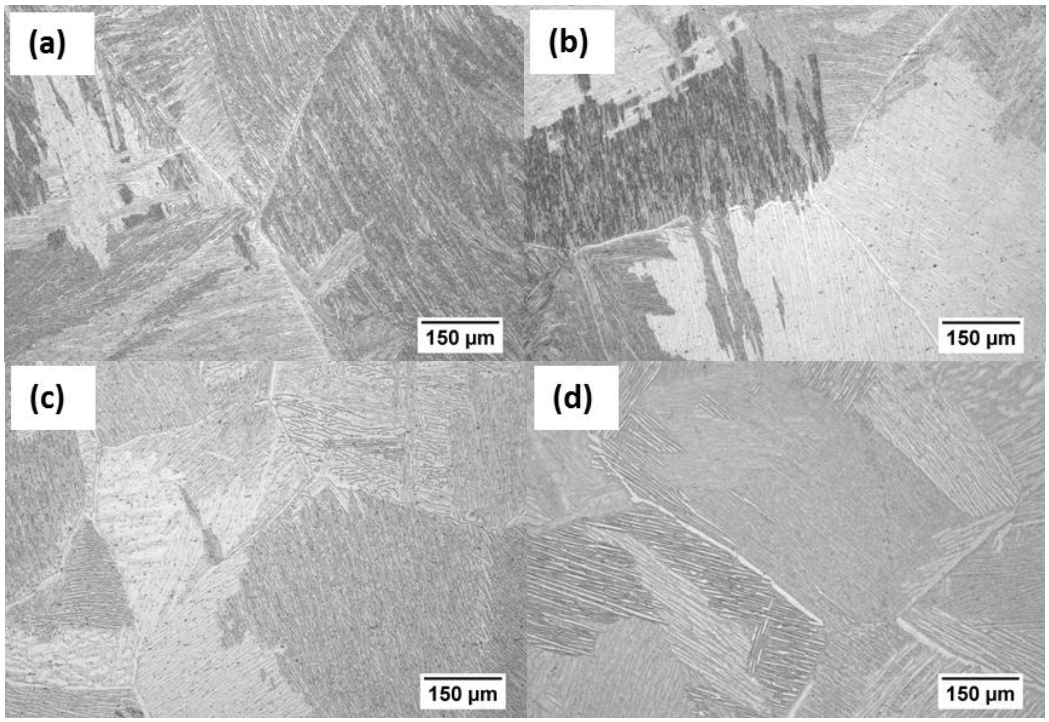

Figure 4.27: Optical micrographs of ST/FC, aged at 900 °C for (a) 0.5 hours and WQ, (b) 2 hours and WQ, (c) 24 hours and WQ, (d) 48 hours and WQ

The micro-hardness results of the ST/FC and aged specimens are shown in Figure 4.28. It can be observed from the graph that the ageing treatments up to 800 °C for 24 hours, followed by WQ, resulted in similar hardness results. Overlapping error bars showed that there were no significant differences between hardness results of the unaged ST/FC specimens and specimens aged up to 800 °C for 24 hours. Ageing at 800 °C for 48 hours, followed by WQ produced a notable increase in hardness compared to the unaged ST/FC specimens. An ageing temperature of 900 °C for 0.5 to 48 hours resulted in comparable hardness values. The hardness values of specimens aged at 900 °C were also not considerably different to the specimen aged at 800 °C for 48 hours. The consistency in hardness results improved at an ageing temperature of 900 °C as the standard deviation error bars were smaller than for all other specimens.

The hardness of the aged Ti-6Al-4V with an initial colony lamellar microstructure increased mainly with increasing ageing temperature.

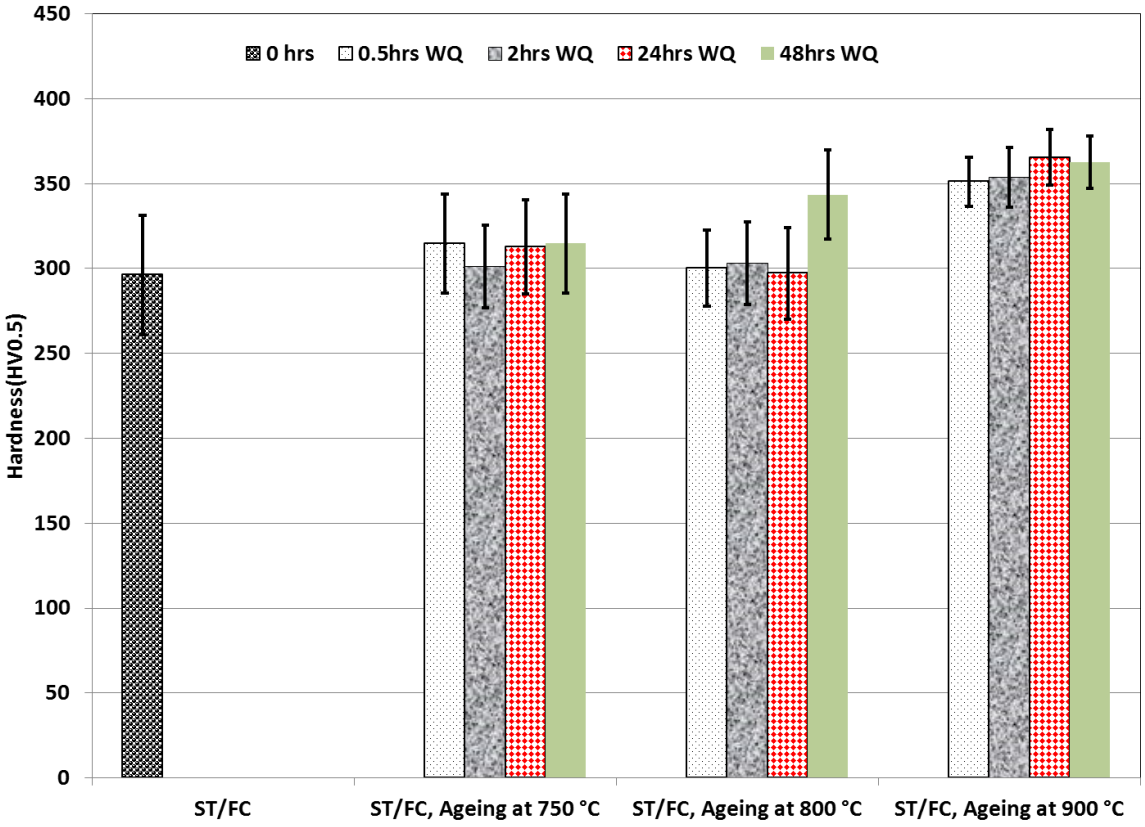

Figure 4.28: The micro-hardness results of the ST/FC specimen, and ST/FC specimens aged at 750 °C, 800 °C, and 900 °C for 0.5 hours to 48 hours, followed by WQ

Table 4.3 shows the quantification of the microstructural features for various heat treatment conditions of the ST/FC specimens. The β-grain size of the ST/FC specimens remained the same after ageing at a temperature range of 750 °C to 900 °C, for ageing times of up to 48 hours. The α-lath thickness and α-phase content of the ST/FC specimen and the ST/FC specimen aged at 750 °C for 0.5 hours were similar. The α and β-phases were not easily differentiable as the ageing temperature increased from 800 °C to 900 °C. This challenge led to the α-phase thickness and α-phase content not being easily quantified at ageing times of 48 hours and ageing temperatures of 800 °C to 900 °C. However, the α-phase content decreased as the ageing temperature increased and at ageing times of 48 hours. The size of the α/β-colonies did not change after ageing within a temperature range of 750 °C to 900 °C.

Table 4.3: The β-grain size, α/β colony size, α-thickness and α-content of ST/FC and ST/FC followed by ageing and WQ (SD errors)

Specimen details	β-grain size (μm)	α/β-colony size (μm)	α thickness (μm)	α content (%)
ST/FC	1027±196	328±64	2.9±1.4	83±3.9
ST/FC-750 °C-0.5 hrs-WQ	864±155	293±51	3.5±1	82±2.8
ST/FC-750 °C-48 hrs-WQ	805±130	318±63	*	70±7#
ST/FC-800 °C-0.5 hrs-WQ	815±138	305±49	*	82±2.7
ST/FC-800 °C-48 hrs-WQ	795±146	347±76	*	68±3.9#
ST/FC-900 °C-0.5 hrs-WQ	865±158	281±47	*	65±4#
ST/FC-900 °C-48 hrs-WQ	816±122	281±47	*	56±1.6#

* could not be measured

the α and β-phases were not easily differentiable.

The SEM images in Figure 4.29 show the change in the α-phase and β-phase contents after ageing of a colony lamellar microstructure. The micrographs show indirectly that as the ageing temperature and time increased, the β-phase content increased (light-coloured phase increased). However, the thickness of the α-laths decreased as can be clearly seen in Figure 4.29 (e) to (f). At ageing times of 48 hours, and an ageing temperature of 900 °C, the α-phase and β-phase started to contain a mixture of the two, and the α/β-laths were not easily differentiable (Figure 4.29 (f) and (g)). At an ageing temperature of 900 °C for 48 hours, the β-laths were thicker than the α-laths. Each α-lath contained some β-phase, while the β-phase contained some α-phase ((Figure 4.29 (g)).

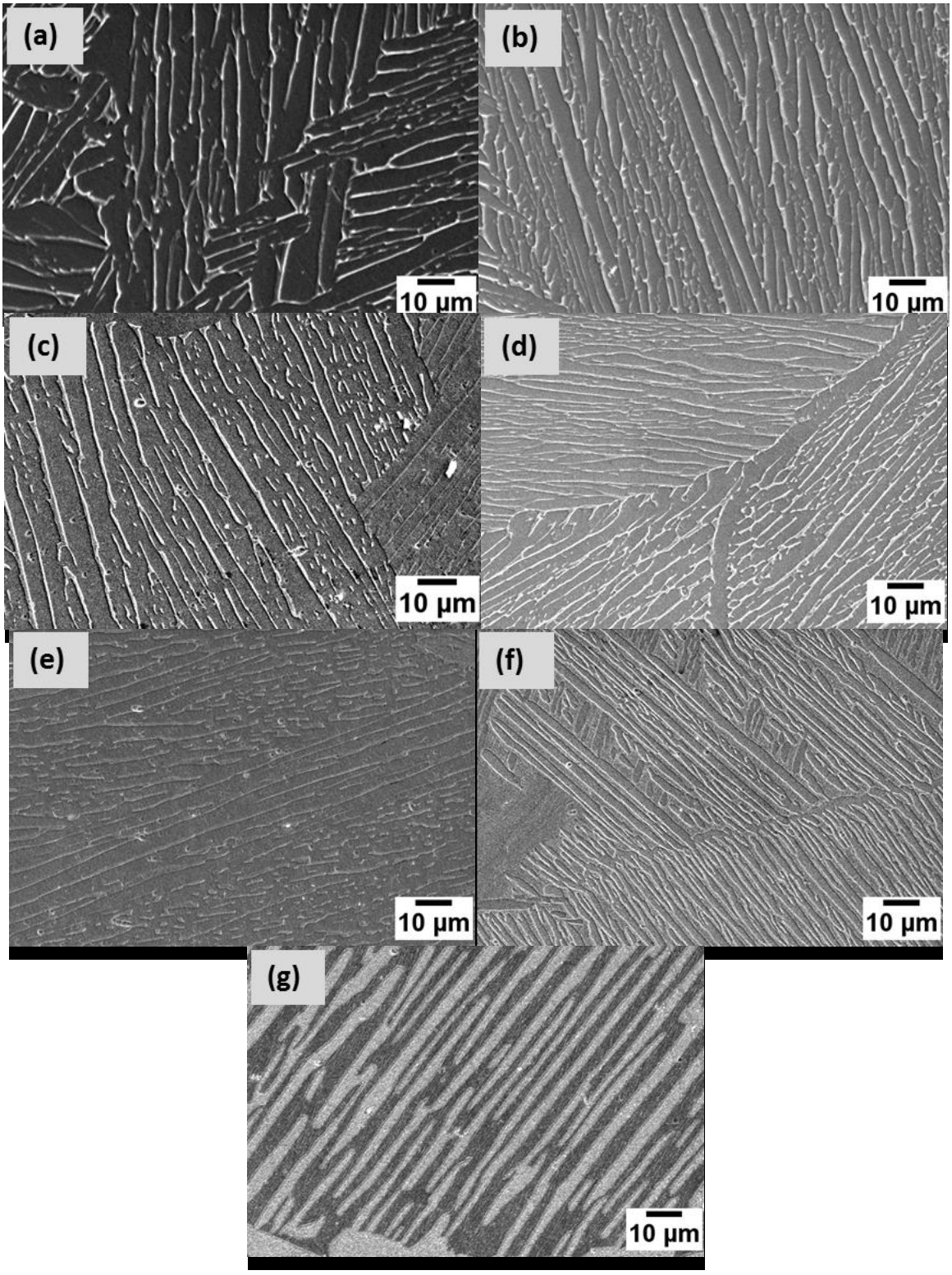

Figure 4.29: SEM micrographs to highlight the contents of α-phase (dark) and β-phase (light) for Ti-6Al-4V specimens that were (a) ST/FC, and ST/FC followed by ageing at (b) 750 °C for 0.5 hours and WQ (c) 750 °C for 48 hours and WQ, (d) 800 °C for 0.5 hours and WQ, (e) 800 °C for 48 hours and WQ, (f) 900 °C for 0.5 hours and WQ, (g) 900 °C for 48 hours and WQ

4.2 Tensile properties

Microstructural quantification of tensile tested variants is shown in Table 4.4. As indicated in Section 4.1 (Microstructure and hardness), the β-grain size of the ST/WQ specimens was smaller than that of the ST/FC specimens. The α-laths were also getting thicker as the ageing temperature increased for the ST/WQ specimens. The α-laths of the ST/FC specimens were thicker than those of the ST/WQ specimens.

Table 4.4: Quantification of the microstructural features of variants tensile tested (SD errors)

Specimen details	β-grain size (μm)	α/β colony size (μm)	α thickness (μm)	α content (%)
ST/WQ	713±104	*	0.8±0.2	*
ST/WQ-500 °C-0.5 hrs-FC	646±104	*	0.9±0.2	*
ST/WQ-800 °C-0.5 hrs-FC	570±82	*	*	*
ST/WQ-900 °C-0.5 hrs-FC	642±89	*	2.0±0.3	89±0.9
ST/WQ-900 °C-24 hrs-FC	720±116	*	6.1±1	89±0.7
ST/FC	1027±196	328±64	2.9±1.4	83±3.9
ST/FC-900 °C-0.5 hrs-WQ	865±158	*	*	*

* could not be measured

The Yield Strength (YS) and the Ultimate Tensile Strength (UTS) results of the ST/WQ specimens followed by ageing, are shown in Figure 4.30. The highest UTS values were obtained from the specimen that was ST/WQ, then aged at 500 °C for 30 minutes, followed by FC. The Yield Strength (YS) of the specimens that were aged at 500 °C and 800 °C were similar to that of the unaged ST/WQ specimens. Specimens aged at 800 °C for 30 minutes and 900 °C for 30 minutes gave UTS values lower than those of the unaged specimens (ST/WQ). The UTS and YS of aged specimens decreased with increasing ageing temperature.

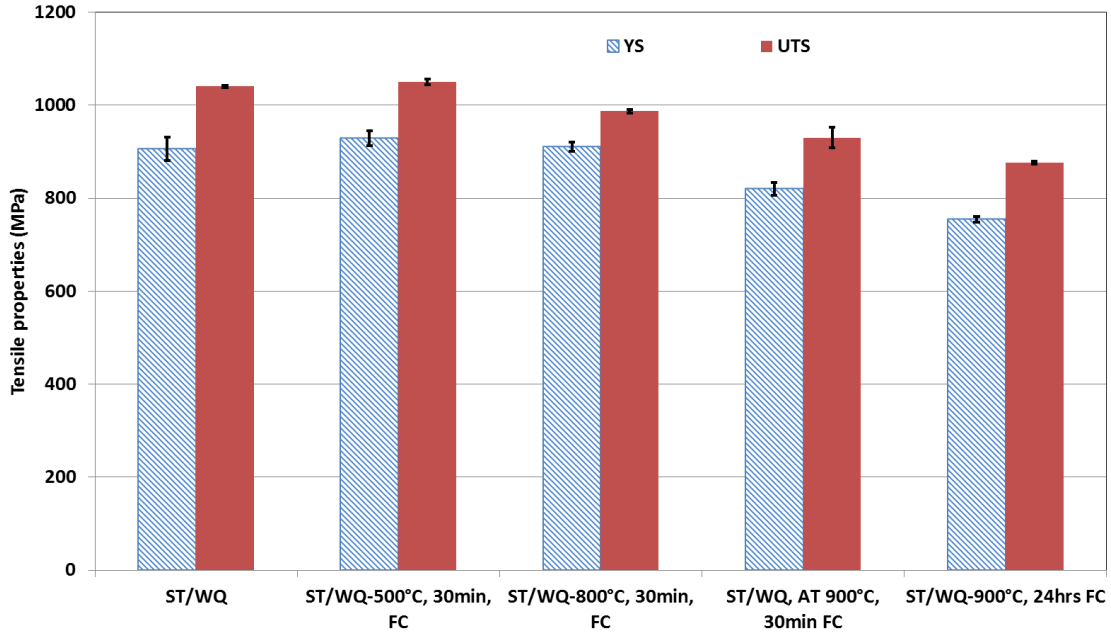

Figure 4.30: Tensile properties (YS and UTS) of the Ti-6Al-4V alloy that were simply ST/WQ, and ST/WQ, then aged, followed by FC

The tensile properties (YS and UTS) of the colony lamellar morphology (ST/FC) and aged colony lamellar are indicated in Figure 4.31. The YS of the aged and unaged specimens was

similar, while the UTS of the aged specimen was slightly greater than that of the unaged specimen.

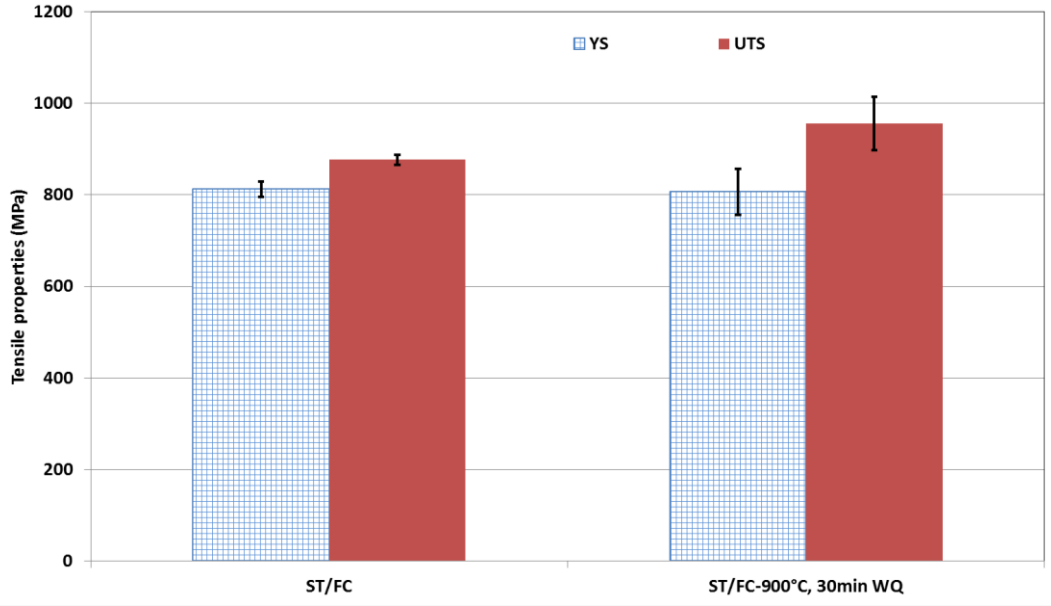

Figure 4.31: Tensile properties (YS and UTS) of the Ti-6Al-4V alloy specimens that were simply ST/FC, and ST/FC followed by ageing

The graph (Figure 4.32) shows the percentage elongation (% EL) and the percentage reduction in area (% RA) of the specimens that were simply ST/WQ, and ST/WQ, followed by ageing. The specimens that were simply ST/WQ and ST/WQ then aged at 500 °C for 30 minutes or aged at 800 °C for 30 minutes, showed similar and lower ductility. However, the specimens that were ST/WQ and then aged at 900 °C for 0.5 hours and 24 hours showed greater ductility. The specimen that was ST/WQ and aged at 900 °C for 24 hours and FC produced considerably greater ductility (high % RA) results. The ductility of the aged specimens increased with increasing ageing temperature.

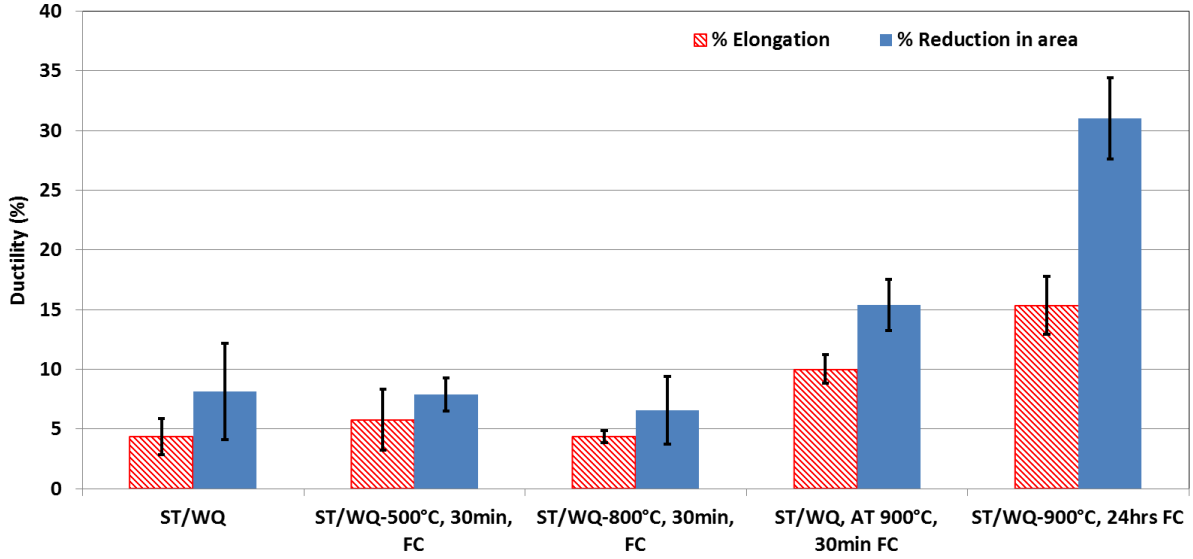

Figure 4.32: Ductility results of the Ti-6Al-4V alloy specimens that were ST/WQ, and ST/WQ then aged, followed by FC

The ductility results of the specimens that were simply ST/FC and ST/FC, followed by ageing, are indicated in Figure 4.33. The % EL of the aged ST/FC specimen was considerably

lower than that of the unaged specimen. The % RA were similar. The results show that ageing reduced % EL.

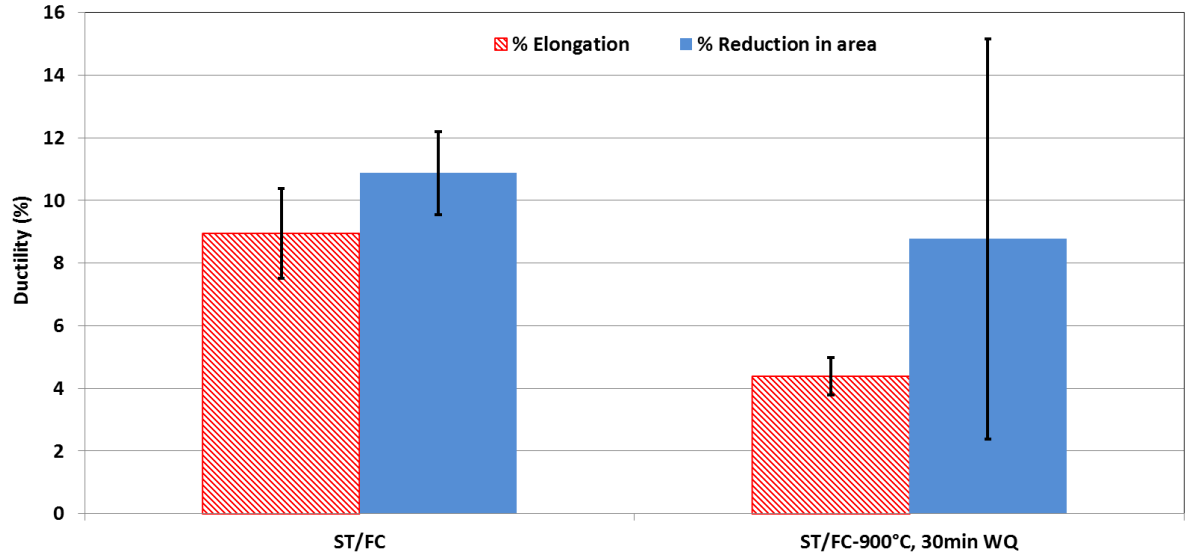

Figure 4.33: Ductility results of the Ti-6Al-4V alloy specimens that were simply ST/FC, and ST/FC then aged followed by WQ

Figure 4.34 shows engineering stress-strain curves of the specimens that were simply ST/WQ and ST/WQ, followed by ageing. The simply ST/WQ specimen, and the ST/WQ specimen followed by ageing at 500 °C showed similar YS, UTS and % EL. Similar elongation results were obtained from the simply ST/WQ specimen, and the specimens that were ST/WQ, followed by aging at 500 °C and 800 °C. The specimen that was ST/WQ, then aged at 900 °C for 24 hours, followed by FC, produced the highest % EL and the lowest YS and UTS, while the specimen that was ST/WQ, then aged at 900 °C for 0.5 hours, also showed considerably greater % EL results. Increasing the ageing temperature and time increased the % EL and reduced the YS and UTS.

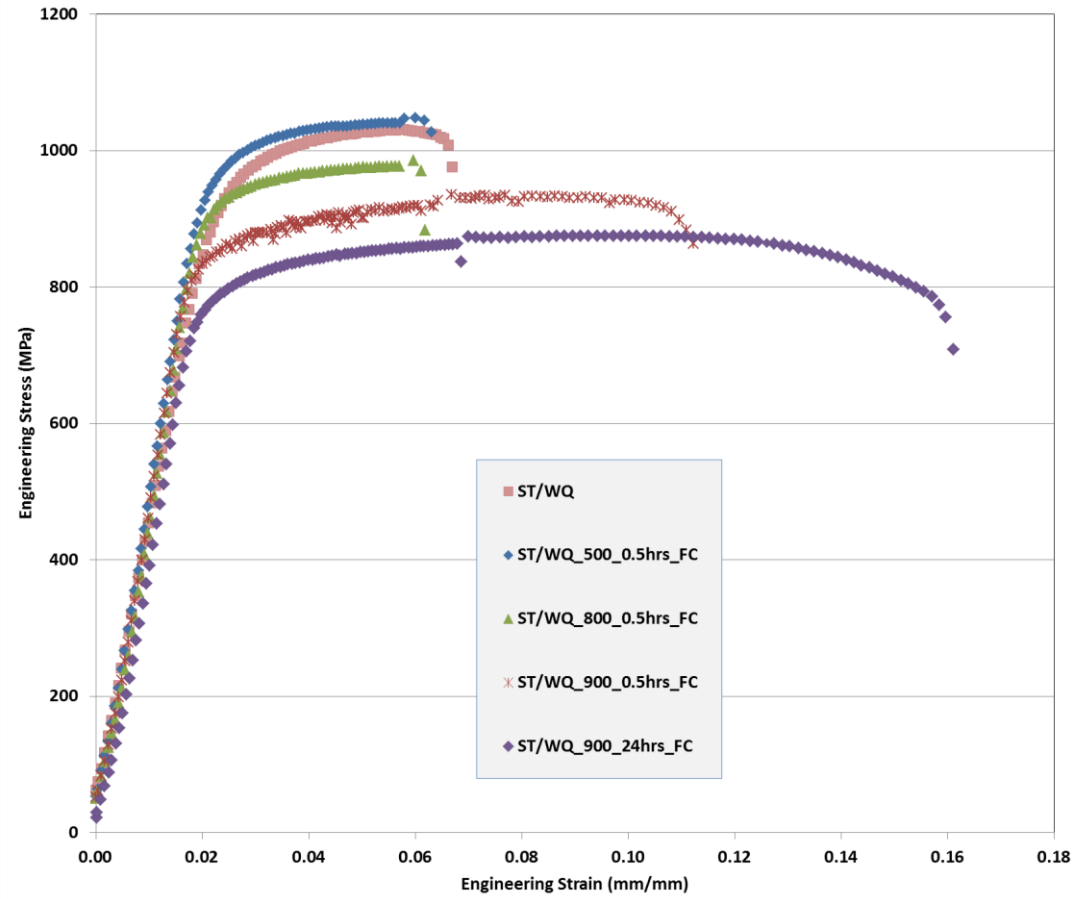

Figure 4.34: Engineering stress-strain plots of specimens of the Ti-6Al-4V alloy that were ST/WQ and ST/WQ followed by ageing

The tensile flow behaviours of the simply ST/FC specimen and the ST/FC specimen aged at 900 °C are shown in Figure 4.35. The aged ST/FC specimen showed a greater YS and UTS than those of the unaged specimen. The % EL of the aged specimen was lower than that of the unaged specimen.

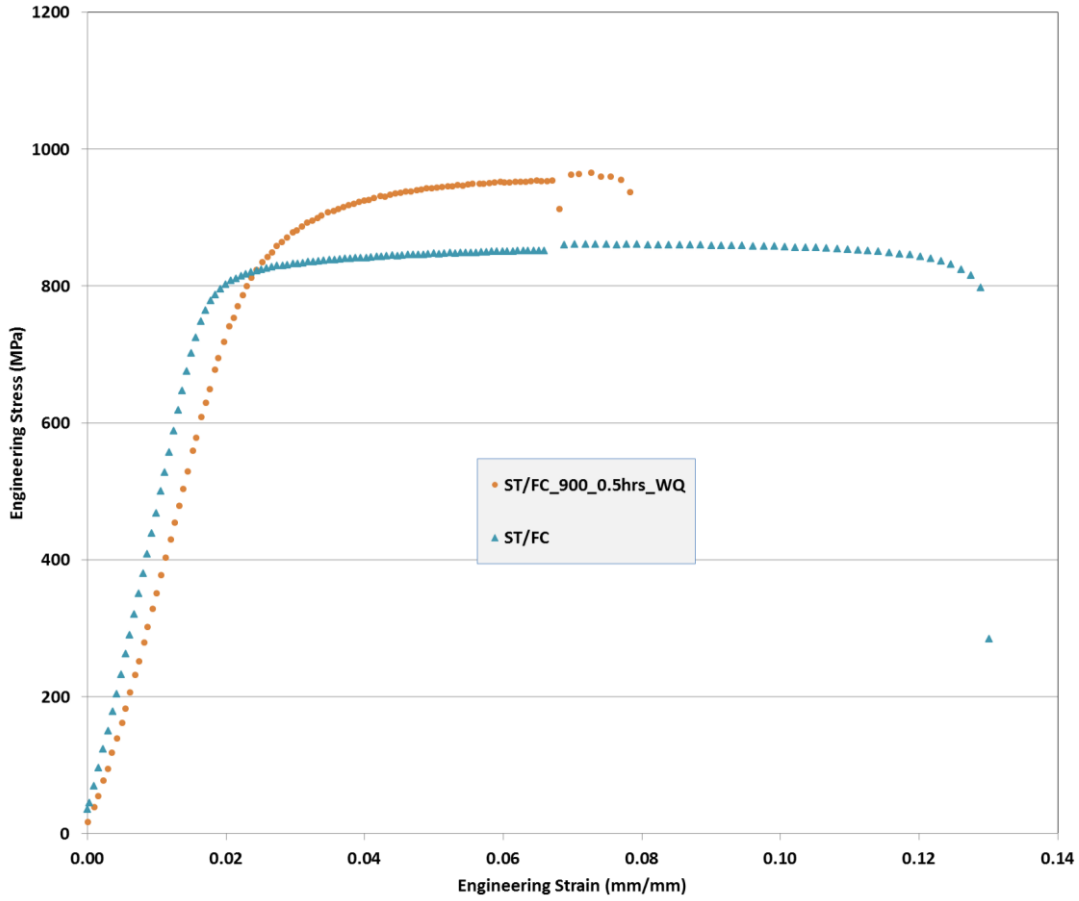

Figure 4.35: Engineering stress-strain plots of the ST/FC and the ST/FC-900°C-0.5hours_FC specimens

The strain-hardening exponents of the Ti-6Al-4V alloy with various microstructures are shown in Table 4.5. The strain-hardening exponent (n) of the fully martensitic specimen (ST/WQ) was greater than that of the lamellar (ST/FC) specimen. Ageing of Ti-6Al-4V with a fully martensitic morphology (ST/WQ) did not show a notable change in the strain-hardening exponent. A considerable increase in the strain-hardening exponent was observed during ageing of Ti-6Al-4V with a lamellar morphology (ST/FC). The specimens that were ST/WQ followed by ageing at 900 °C for either 0.5 hours or 24 hours gave similar strain-hardening exponents. The aged lamellar specimen (ST/FC, 900 °C, 30 min WQ) gave the highest strain-hardening exponent while the ST/FC specimen showed the lowest strain-hardening exponent.

Table 4.5: Strain-hardening exponents and strength coefficients of the Ti-6Al-4V alloy

Specimen details	Strain-hardening Exponent, n ± SD	Strength coefficient , K ± SD (MPa)
ST/WQ	0.12± 0.01	1526± 38
ST/WQ-500°C-30 min-FC	0.11± 0.03	1544± 147
ST/WQ-800°C-30 min-FC	0.08± 0.01	1316± 43
ST/WQ-900°C-30 min-FC	0.11± 0.01	1311± 13
ST/WQ-900°C-24 hrs-FC	0.11± 0.01	1260± 27
ST/FC	0.07± 0	1111± 14
ST/FC-900°C-30 min-WQ	0.16±0.02	1620±163

The strength coefficient (K) of all the tensile tested Ti-6Al-4V specimens indicated in Table 4.5, shows a similar trend to the yield strength reported already. However, the aged colony lamellar specimen (ST/FC-900 °C-30min-WQ), showed the highest K value consistent with a high strain-hardening exponent.

Figure 4.36 shows the strain-hardening rate versus the true strain for the ST/WQ specimen and aged ST/WQ specimens. The fully martensitic morphology (ST/WQ) produced a greater strain-hardening rate, while the basketweave morphology (ST/WQ-900 °C-24 hrs-FC) had the lowest. All the specimens resulted in a similar and continuous drop in the strain-hardening rate as the true strain increased. The strain-hardening rate tended to decrease with increasing ageing time and temperature.

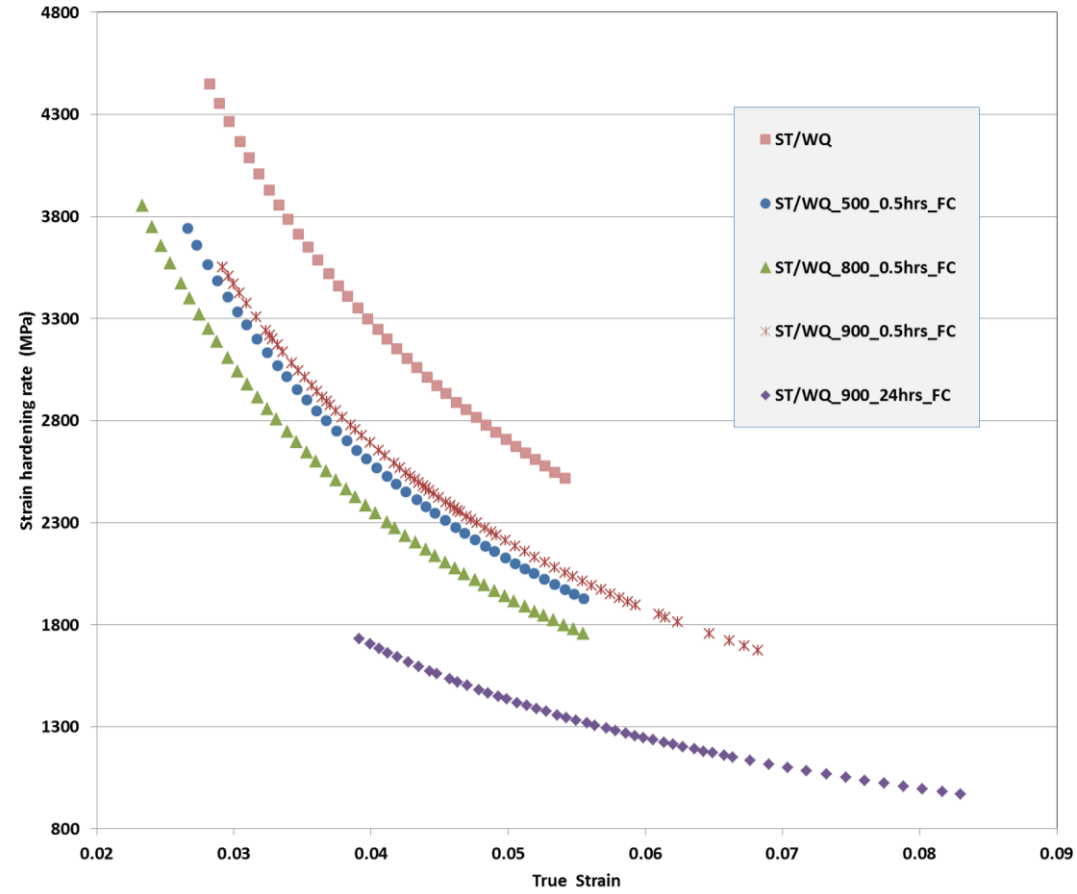

Figure 4.36: The strain-hardening rate versus the true strain of the specimens that were simply ST/WQ and ST/WQ followed by ageing treatments

The effect of ageing of the ST/FC specimen on the strain-hardening rate versus the true strain is shown in Figure 4.37. The ST/FC specimen had a considerably lower strain-hardening rate than the aged ST/FC specimen. The strain-hardening rate of both specimens decreased continuously as the true strain increased. The strain-hardening rate of the ST/WQ specimens decreased with ageing, while it increases with ageing of the ST/FC specimens.

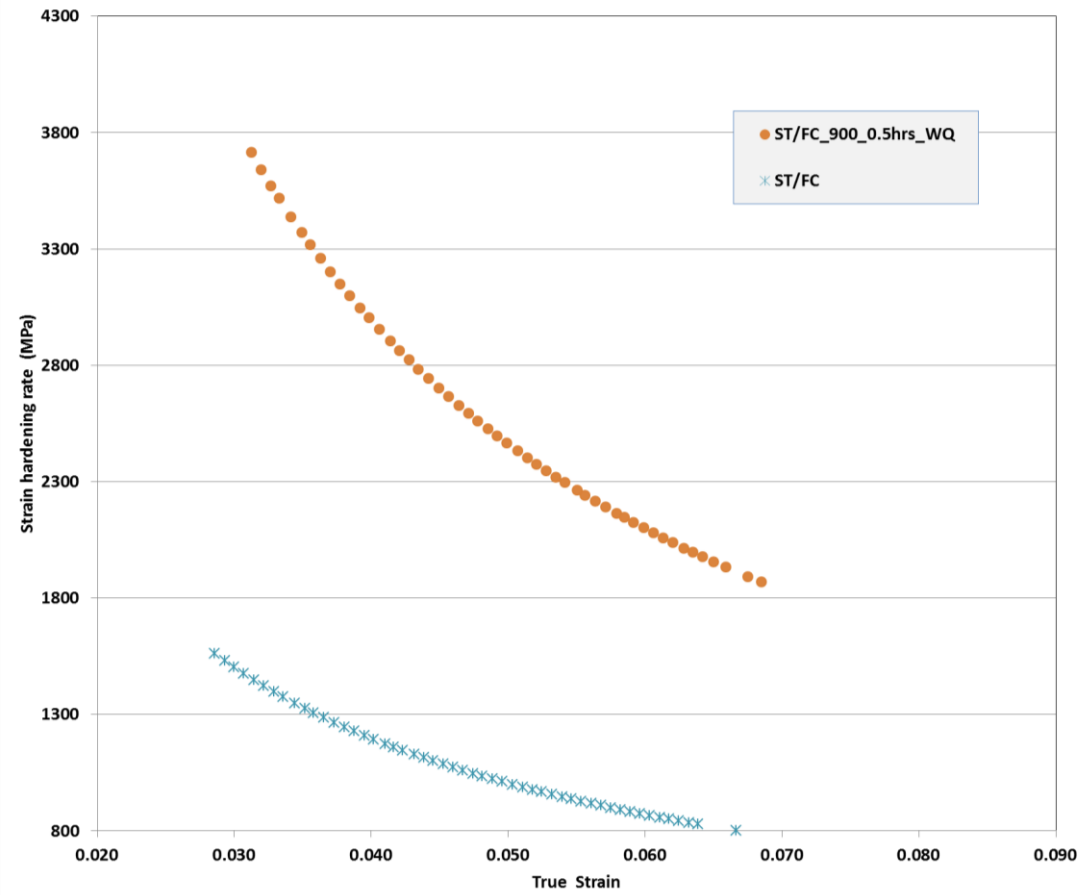

Figure 4.37: The strain-hardening rate versus the true strain of the simply ST/FC and the ST/FC aged at 900°C for 0.5hrs then WQ specimens

The graph of the strain-hardening rate versus true stress for the ST/WQ specimen and the aged ST/WQ specimens is shown in Figure 4.38. The fully martensitic morphology produced a greater strain-hardening rate, while the basketweave morphology (ST/WQ-900 °C-24 hrs FC) had the lowest. Similarly, the strain-hardening rate decreased continuously as the true stress increased. The increase in ageing temperature and time led to a decrease in the strain-hardening rate.

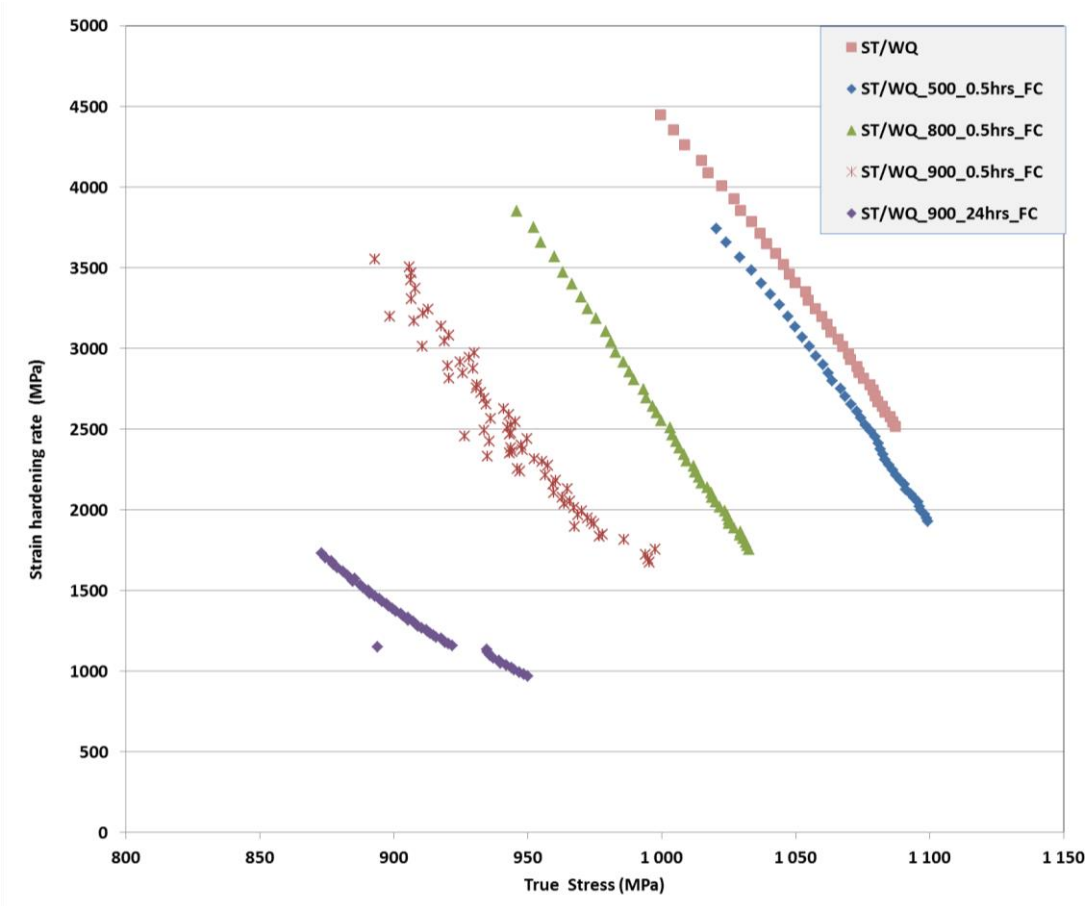

Figure 4.38: Graph of strain-hardening rate versus the true stress of the ST/WQ, and ST/WQ, followed by various ageing treatments

The strain-hardening rate versus the true stress curve of the simply ST/FC and the ST/FC and aged specimen shown in Figure 4.39 showed the aged ST/FC specimen with a notably greater strain-hardening rate. However, ageing was found to increase the strain-hardening rate.

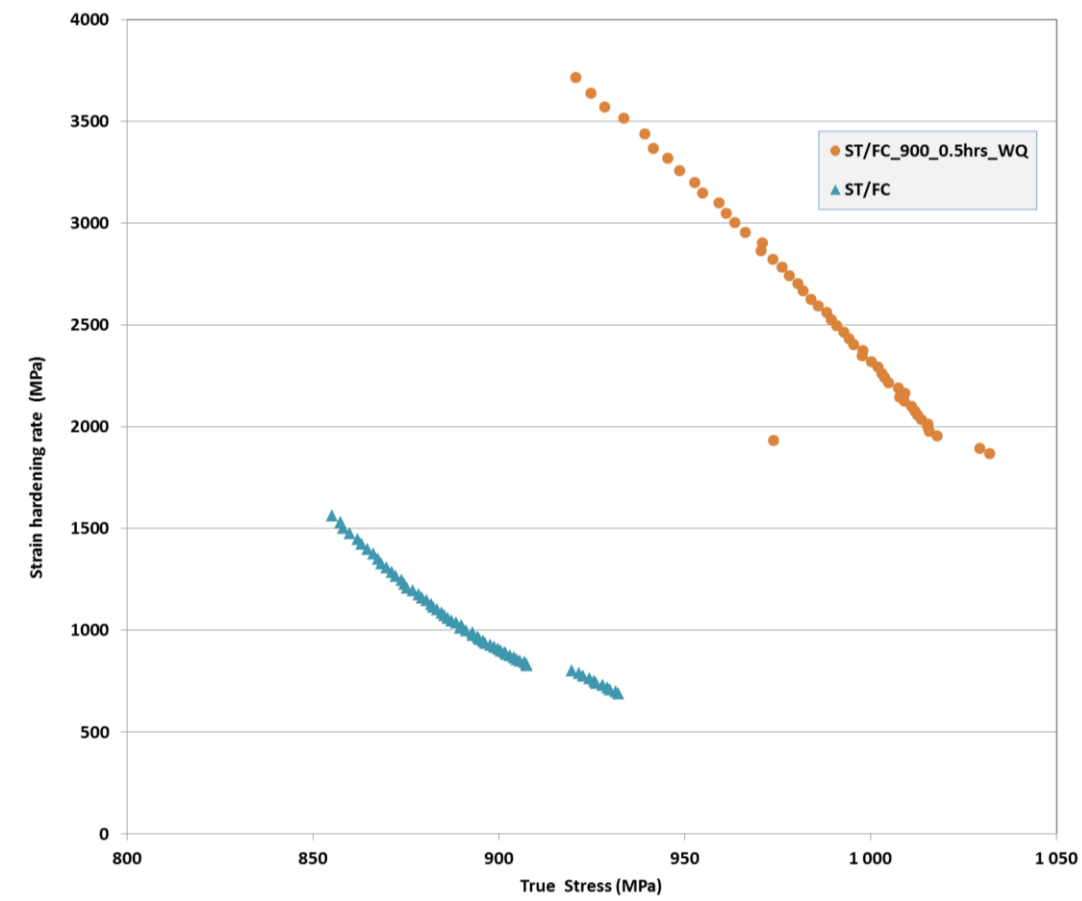

Figure 4.39: The strain-hardening rate versus the true stress of the simply ST/FC and the ST/FC aged at 900°C for 0.5 hrs then WQ

The cross-sectioned fractures of the tensile tested specimens are shown in Figure 4.40 (a) to (g). The Ti-6Al-4V specimens with a fully martensitic microstructure (Figure 4.40 (a) and (b)) showed a cleavage fracture along the interface of the martensitic needles and the β-phase. The specimens with a colony lamellar microstructure (Figure 4.40 (f) and (g)) showed a rougher fracture surface (ductile). Specimens with a partial martensitic morphology (Figure 4.40 (c) and (d)) showed a rougher fracture surface and also indicated more ductility compared to the fully martensitic microstructures (Figure 4.40 (a) and (b)). The crack propagation was along the martensite needles or along the interface of the α-laths/α'-needles. All the specimens revealed transgranular fracture.

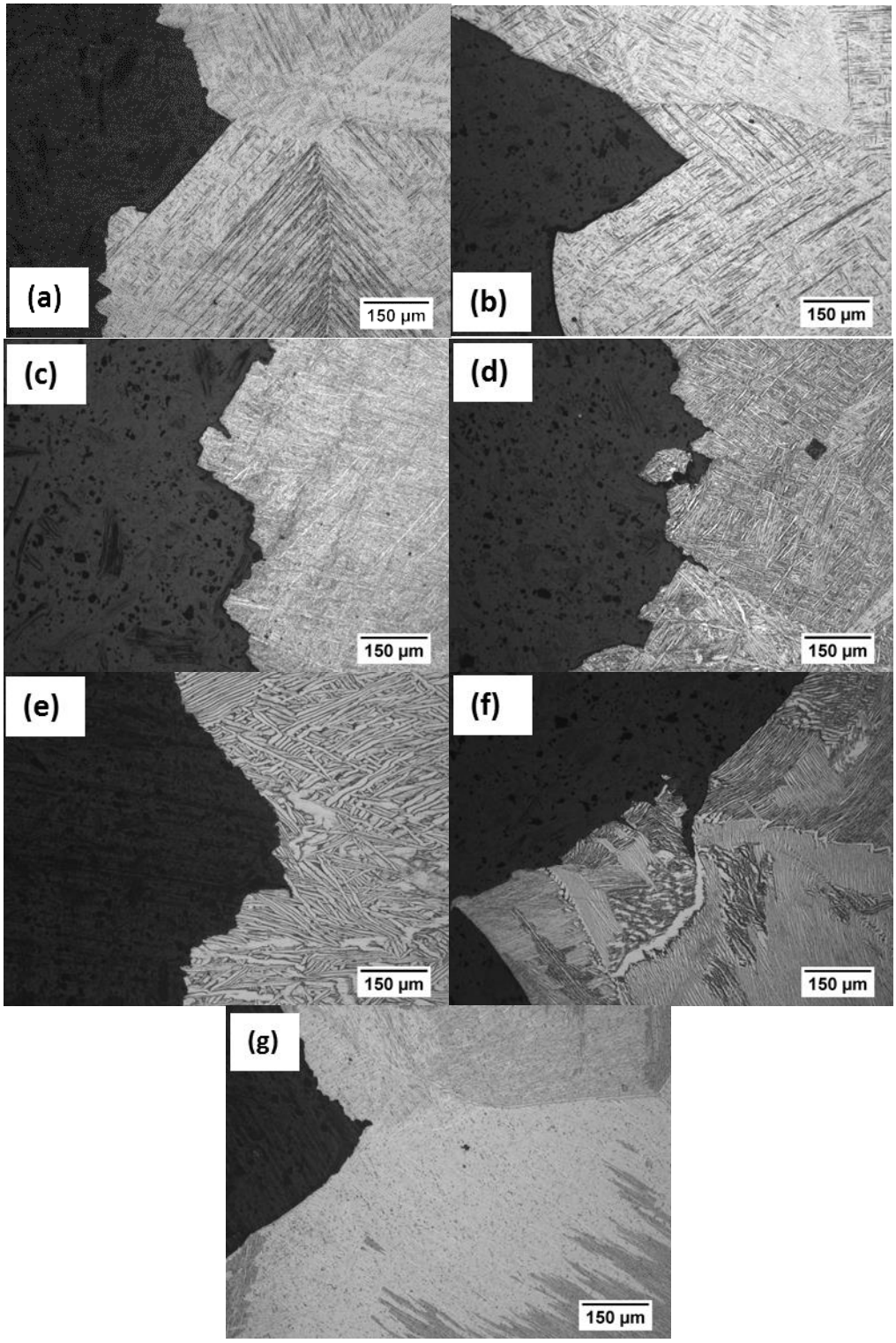

Figure 4.40: Optical micrographs showing cross-sectioned views of fracture regions of the tensile tested specimens of (a) ST/WQ, (b) ST/WQ, aged at 500 °C for 30 min and FC, (c) ST/WQ aged at 800 °C for 30 min and FC, (d) ST/WQ aged at 900 °C for 30 min and FC, (e) ST/WQ aged at 900 °C for 4 hrs and FC, (f) ST/FC, (g) ST/FC aged at 900 °C for 30 min and WQ

The SEM micrographs of the polished cross-sectioned views of the tensile fractured specimens are shown in Figure 4.41. All the specimens showed secondary micro-crack formation and coalescence leading to the final crack (Figure 4.41). The secondary micro-

cracks initiated at interfaces between the α-phase and the β-phase or the α-phase/α'-phase. The colony lamellar microstructure showed a kink of α/β-laths, resulting in resistance to crack propagation (Figure 4.41 (f)).

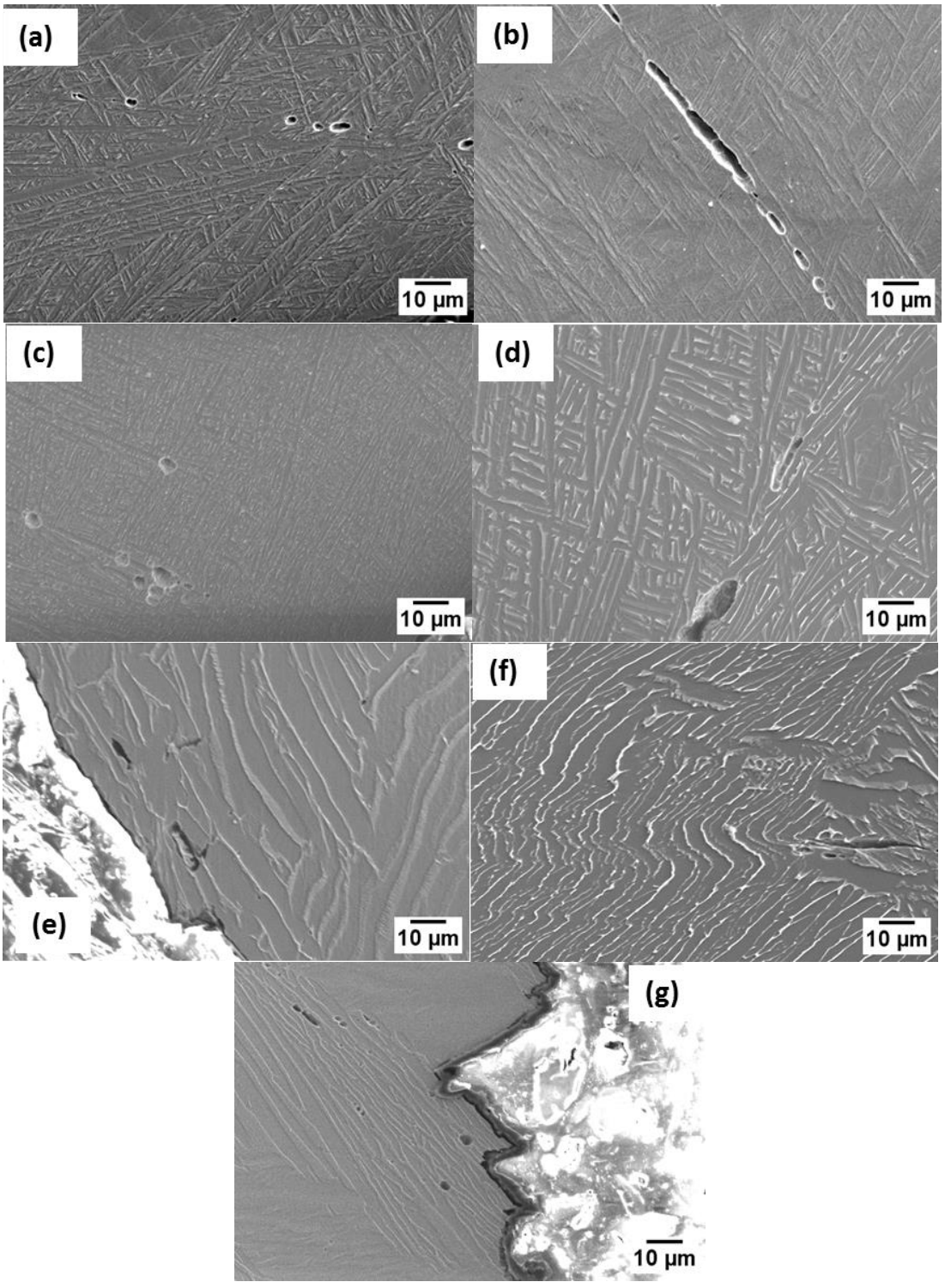

Figure 4.41: SEM micrographs showing cross-sectioned views of the fractured region in the tensile tested specimens of (a) ST/WQ, (b) ST/WQ aged at 500 °C for 30 min and FC, (c) ST/WQ aged at 800 °C for 30 min and FC, (d) ST/WQ aged at 900 °C for 30 min and FC, (e) ST/WQ aged at 900 °C for 24 hrs and FC (f) ST/FC, (g) ST/FC aged at 900 °C for 30 min and WQ

The SEM fractographs of the tensile tested specimens are shown in Figure 4.42. The Ti-6Al-4V specimens with fully martensitic morphologies (Figure 4.42 (a) and (b) showed cleavage fractures with no dimples. However, specimens with partial martensitic morphologies (Figure 4.42 (c) and (d)) showed smaller-sized dimples. The larger and equiaxed dimples were exhibited by the specimen with a basketweave morphology (Figure 4.42 (e)). The specimen with an initial colony lamellar and the aged specimen with a colony lamellar morphologies (Figure 4.42 (f) and (g)) showed elongated dimples and rougher fracture surfaces than the specimen with a fully martensitic morphology (Figure 4.42 (a) and (b)) and the specimen with a partial martensitic morphology (Figure 4.42 (c) and (d)). Ductility was shown to increase with increasing ageing temperature. The results are consistent with ductility results reported before, where the fully martensitic morphologies gave lower % EL. In addition, as the ageing temperature increased, the % EL increased. The larger dimples found in the ST/FC specimens compared to the ST/WQ specimens, also confirmed the difference in ductility reported before.

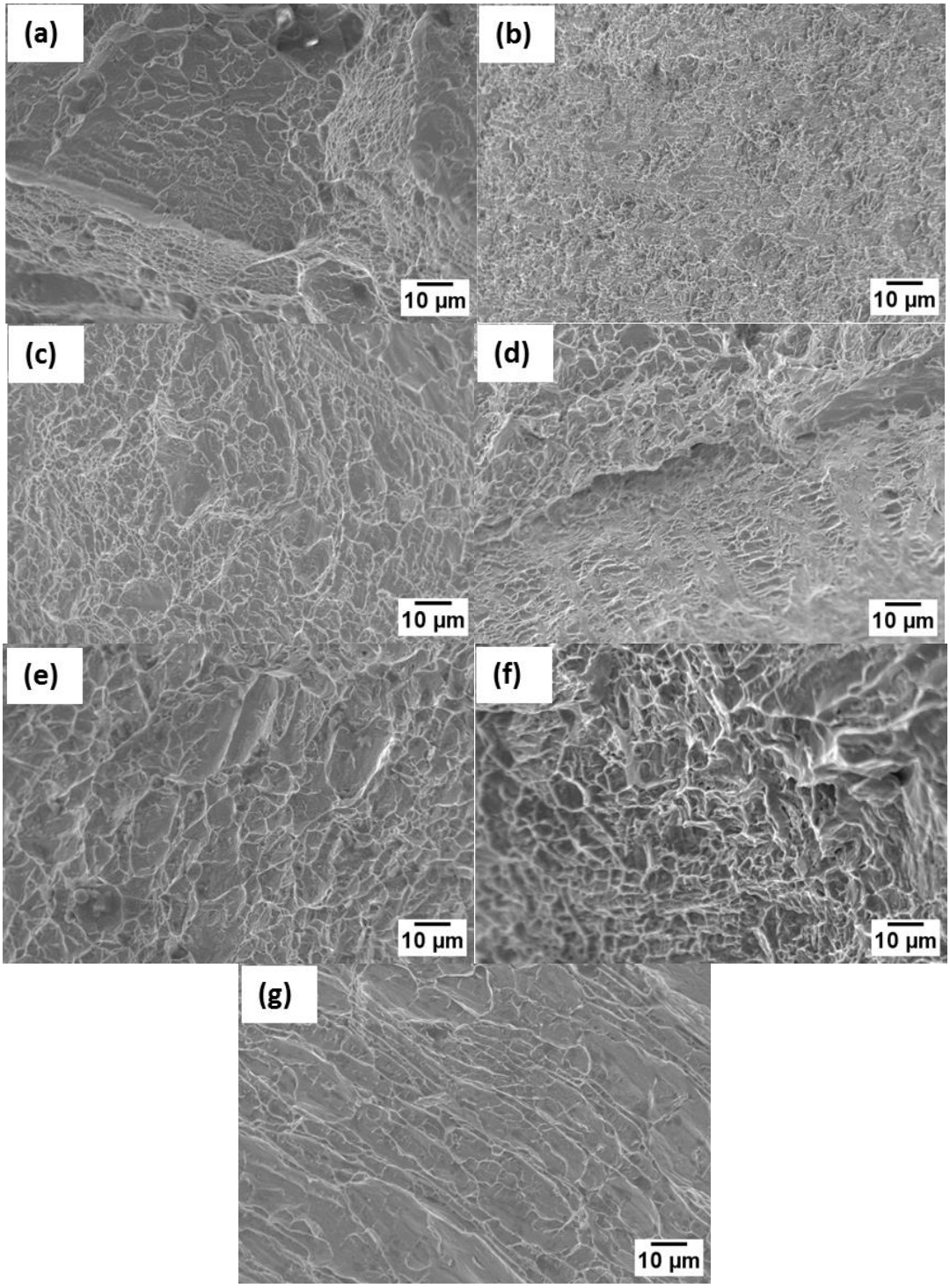

Figure 4.42: SEM fractographs of the tensile tested specimens of (a) ST/WQ, (b) ST/WQ aged at 500 °C for 30 min and FC, (c) ST/WQ aged at 800 °C for 30 min and FC, (d) ST/WQ aged at 900 °C for 30 min and FC, (e) ST/WQ aged at 900 °C for 24 hrs and FC, (f) ST/FC, (g) ST/FC aged at 900 °C for 30 min and WQ

Table 4.6 shows the ultimate tensile strength and ductility of various Ti-6Al-4V alloy variants. If UTS x % EL is defined as a strength-ductility balance [44], the specimen with a basketweave microstructure (ST/WQ, aged at 900 °C for 24 hours and FC) was found to have the highest strength-ductility balance, while the aged specimen with a colony lamellar microstructure (ST/FC aged at 900 °C for 30 min and WQ) produced the lowest. The

specimen with a colony lamellar microstructure (ST/FC) and specimen with a basketweave microstructure (ST/WQ aged at 900 °C for 24 hours and FC) had similar UTS values but a superior % EL was shown by the specimen with a basketweave microstructure, which resulted in a greater strength-ductility balance. Ageing of the ST/WQ specimens increased the strength-ductility balance, while ageing of the ST/FC specimens reduced it.

Table 4.6: Strength (UTS) x ductility (% EL) balance

Specimen details	UTS (MPa)	% EL	UTS x %EL
ST/WQ	1040	4.4	4576
ST/WQ-500°C-30 min-FC	1050	5.8	6090
ST/WQ-800°C-30 min-FC	987	4.4	4342
ST/WQ-900°C-30 min-FC	930	10	9310
ST/WQ-900°C-24 hrs-FC	876	15.4	13490
ST/FC	877	9	7893
ST/FC-900°C-30 min-WQ	955	4.4	4202

4.3 Fracture toughness

The quantitative results of the microstructural features of the ST/WQ, ST/WQ-900 °C-24 hrs-FC and ST/FC specimens that were used for measuring the fracture toughness are summarised in Table 4.7.

Table 4.7: Quantification of microstructural features (± Standard Deviation (SD))

Specimen details	β-grain size (μm)	α content (%)	α-lath width (μm)
ST/WQ	713±104	-	0.8±0.2
ST/WQ-900 ºC-24hrs-FC	720±116	88±2	6.0±1.0
ST/FC	1027±196	83±4	2.9±1.4

The β-grains of the ST/FC specimen were larger than those of both the ST/WQ and the ST/WQ-900 °C -24 hrs-FC specimens. The basketweave morphology (ST/WQ-900 °C -24 hrs-FC) had thicker α-laths and a greater α-phase content than the colony lamellar morphology. The martensite laths (α′) were thinner than both of the α-laths found in the basketweave and the colony lamellar morphologies.

The fracture toughness (K_{1Q}) results are indicated in Figure 4.43. A significantly greater fracture toughness was revealed in the ST/FC specimen, while the ST/WQ had the lowest. The specimen with a basketweave microstructure gave fracture toughness values in-between the ST/WQ and the ST/FC specimens.

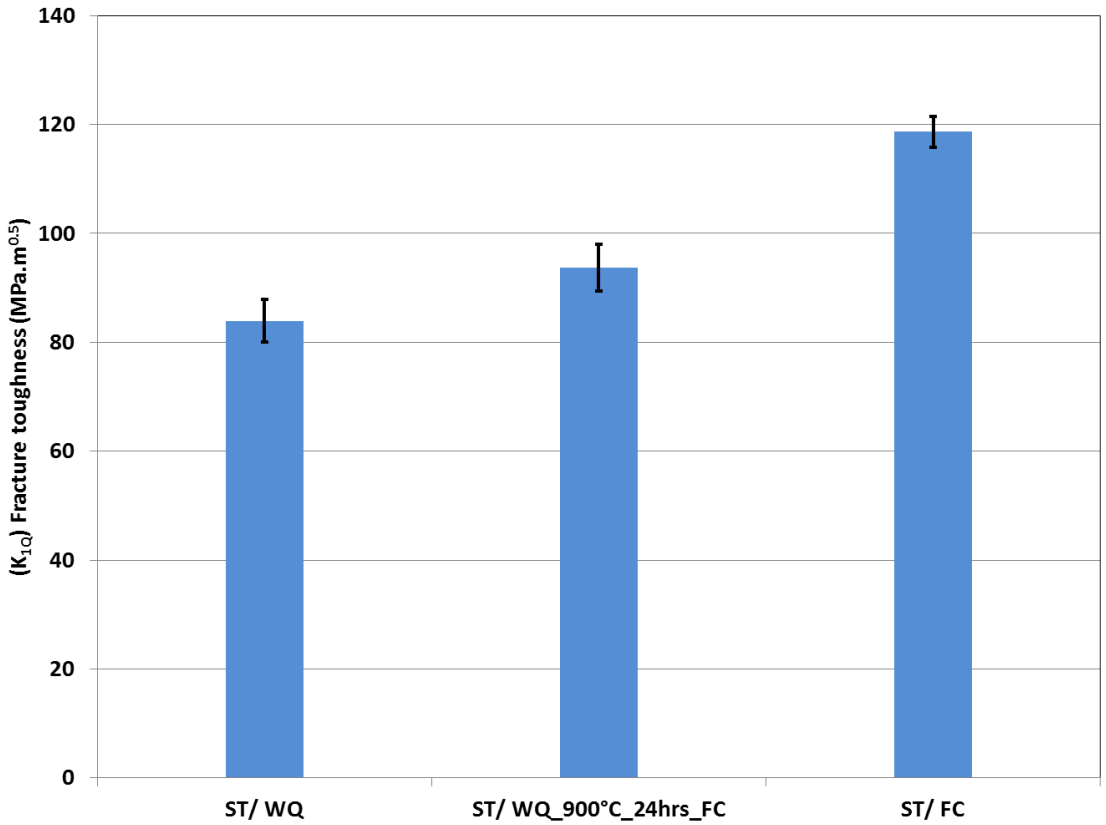

Figure 4.43: Fracture toughness of ST/WQ, ST/WQ-900 °C -24 hrs-FC and ST/FC specimens

The fracture toughness values on a 25 mm thick specimen did not pass the validity condition for plane strain fracture toughness, with respect to both the thickness and the remaining ligament as shown in Table 4.8. The ST/WQ specimen gave the closest values to plane strain fracture toughness as the thickness was greater than the 2.5 $(K_{1Q}/YS)^2$ (fracture toughness validity conditions, ASTM standard E399) [56]. The specimens with the greater fracture toughness values (ST/FC and ST/WQ-900 °C-24 hrs-FC) gave 2.5 $(K_{1Q}/YS)^2$ values that were much larger than the thickness used. The results indicate that thicker samples are required to obtain plane strain fracture toughness values for the ST/FC and ST/WQ-900 °C-24 hrs-FC specimens. See Appendix II for details on the calculation of the fracture toughness.

Table 4.8: Values used for plane strain fracture toughness validity conditions

	ST/WQ	ST/WQ-900 ºC-24 hrs-FC	ST/FC
B (mm)	25	25	25
W-a (mm)	19.23	25.75	23.18
YS (MPa)	906	756	812
K_{1Q} (MPa.m$^{0.5}$)	83.92	93.7	118.70
2.5*$(K_{1Q}/YS)^2$	23	38	53

The relationship between fracture toughness and yield strength is shown in Figure 4.44. The ST/WQ specimen gave the highest yield strength while the ST/FC specimen had the highest fracture toughness. The aged specimen (ST/WQ-900 °C-24hrs-FC) showed the lowest yield strength while its fracture toughness was between that of the other two.

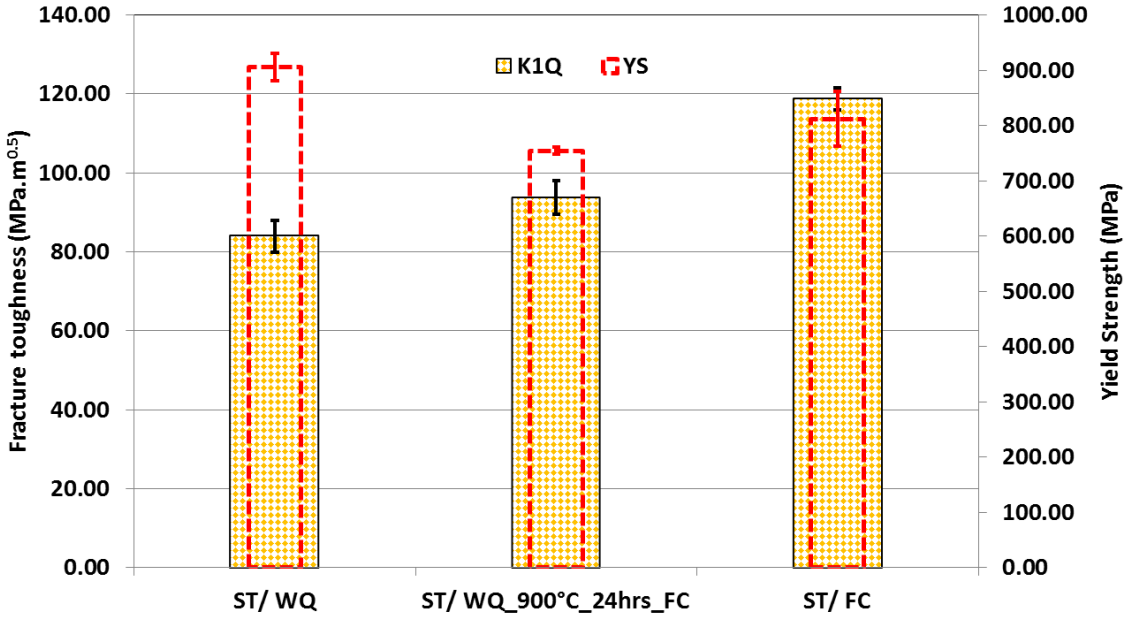

Figure 4.44: The fracture toughness of the Ti-6Al-4V alloys in relation to their yield strength

Figure 4.45 shows a polished cross-section of the fracture surfaces of the ST/WQ specimen which had been aged (ST/WQ-900 °C-24 hrs-FC) and the ST/FC specimen. The simply ST/WQ specimen and the ST/WQ-900 °C-24 hrs-FC specimens showed more brittle fracture surfaces, while the ST/FC was more ductile. Smaller crack deflections were observed in the simply ST/WQ and the ST/WQ-900 °C-24 hrs-FC specimens. Larger deflections, crack branching and the formation of secondary cracks were evident in the ST/FC specimen.

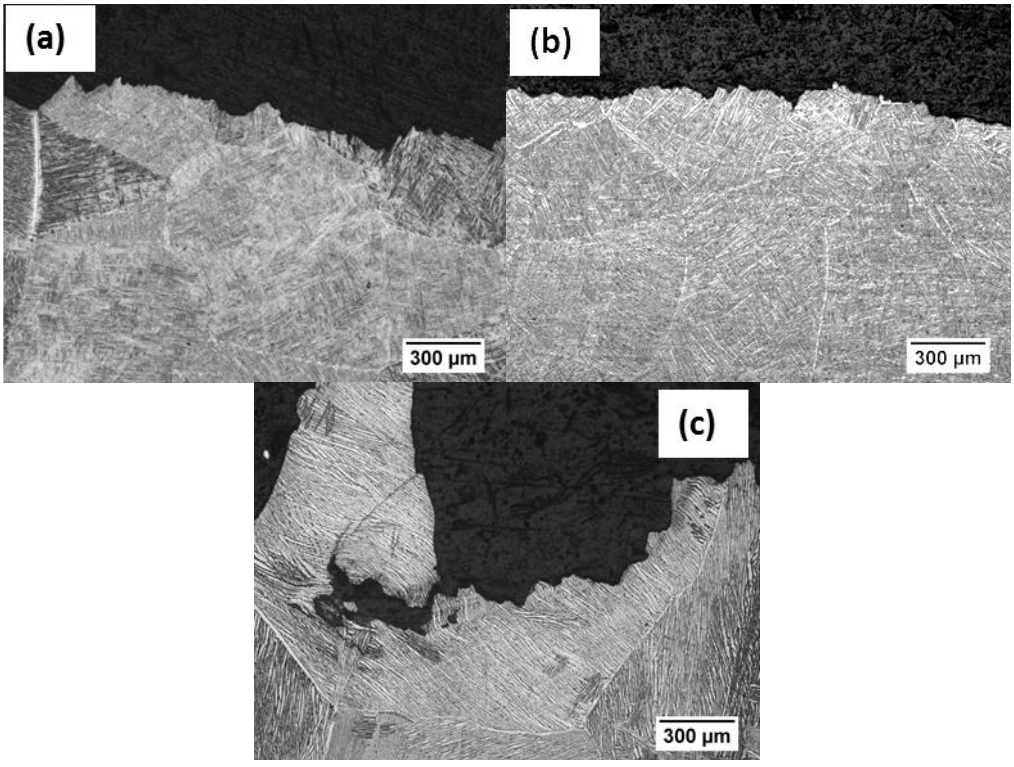

Figure 4.45: Optical images of polished cross-sectional fracture surfaces of specimens of (a) ST/WQ, (b) ST/WQ-900 °C-24 hrs-FC and (c) ST/FC, after fracture toughness testing

Figure 4.46 shows SEM micrographs of polished cross-sectional views of the diversely heat-treated Ti-6Al-4V specimens. Crack propagation in the ST/WQ specimen was of more smooth fractures along the martensitic needles and the deflection occurred when differently oriented needles were encountered (Figure 4.46 (a)). There was little or no evidence of crack branching or creation of secondary cracks. The aged specimen (ST/WQ-900 °C-24hrs-FC) showed microcrack formation closer to the primary crack (Figure 4.46 (b)). Crack deflection and creation of secondary cracks were evident. The ST/FC specimen showed a larger crack deflection, the creation of secondary cracks and crack branching (Figure 4.46 (c)).

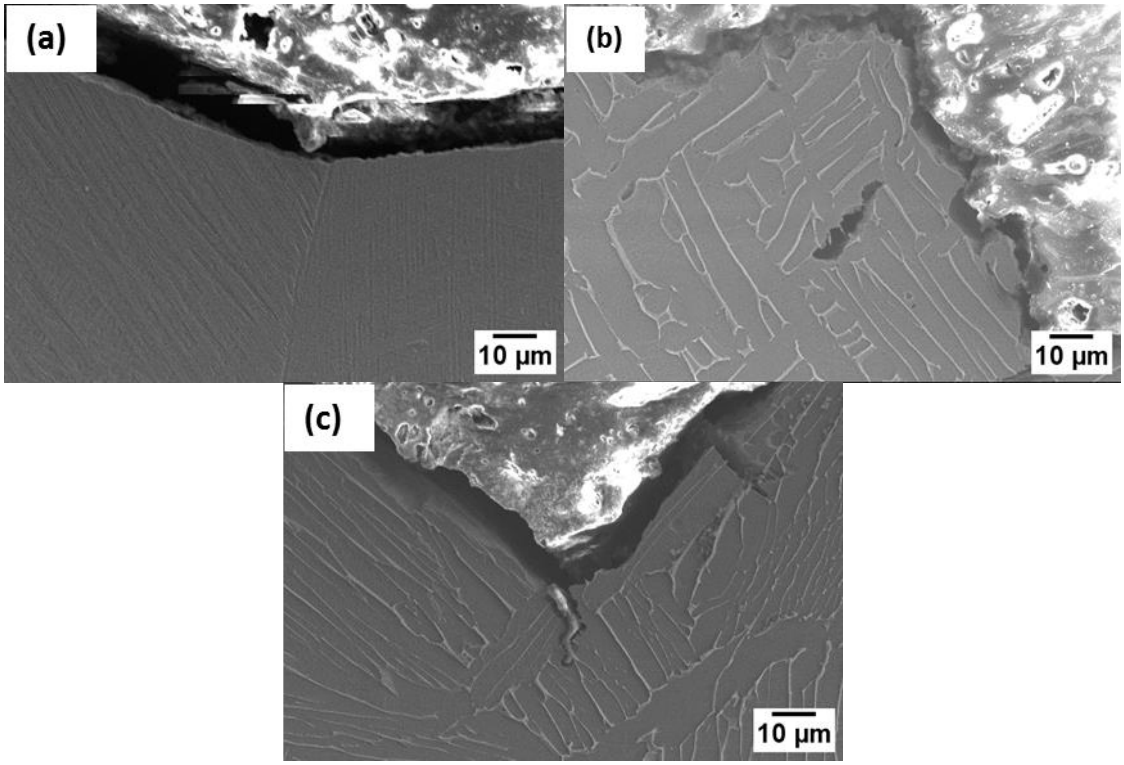

Figure 4.46: SEM micrographs of the polished cross-sectional fracture surfaces of specimens of (a) ST/WQ, (b) ST/WQ-900 °C-24 hrs-FC and (c) ST/FC, after fracture toughness testing

The SEM micrographs of the fracture surfaces are shown in Figure 4.47. The fracture surface of the ST/WQ specimen (Figure 4.47 (a)) showed fewer dimples compared to the aged specimen (Figure 4.47 (b) and the simply ST/FC specimen (Figure 4.47 (c)). The aged specimen exhibited more plastic deformation, compared to the other two as dimples were larger and deeper. The aged specimen did not show crack bifurcation or deflection. Secondary cracks formed from the creation of microvoids closer to the main crack. The deflection of cracks at colony boundaries was evident in the ST/FC specimen. The creation of secondary cracks was also prevalent in the ST/FC specimen.

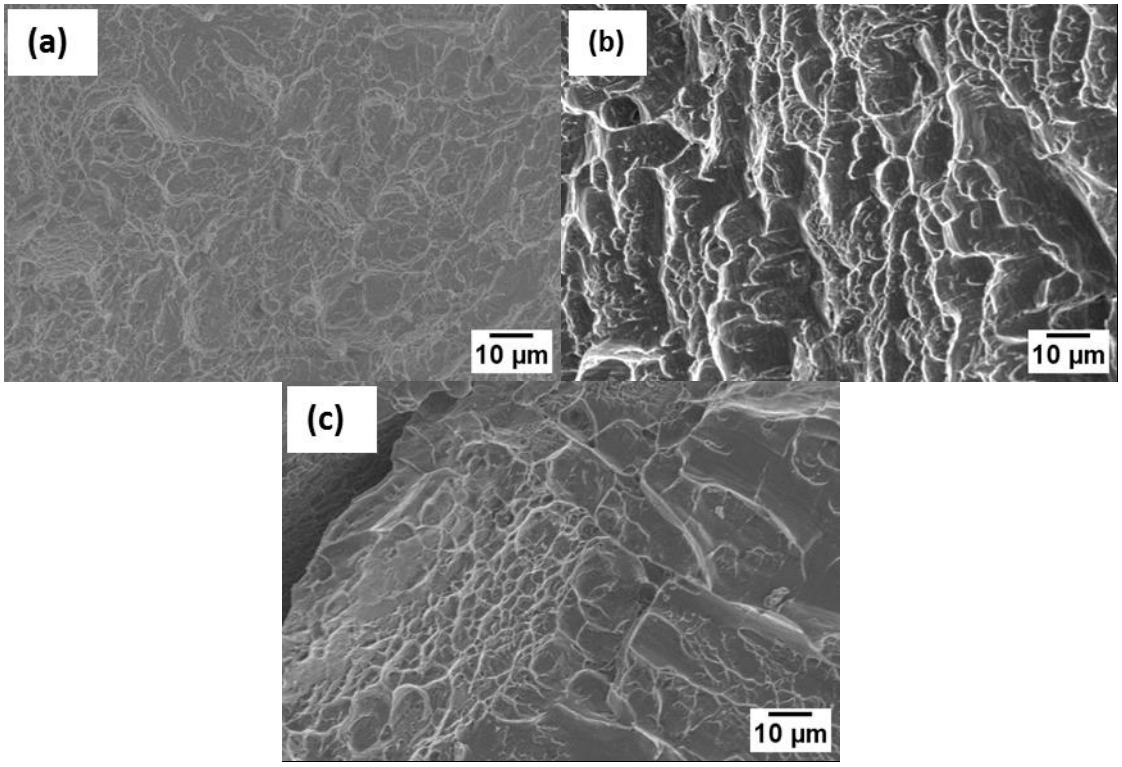

Figure 4.47: SEM micrographs of fracture surfaces of specimens of (a) ST/WQ, (b) ST/WQ-900 °C-24hrs-FC and (c) ST/FC, after fracture toughness testing

4.4 Fatigue crack growth

Figure 4.48 shows a curve of crack length versus the number of cycles for the simply ST/WQ, aged (ST/WQ-900 °C-24hrs-FC) and simply ST/FC specimens. The ST/FC specimen showed a significantly longer fatigue life than that of the ST/WQ and the aged specimen for the same crack length. The fatigue life of the ST/WQ specimen was slightly longer than that in the aged specimen.

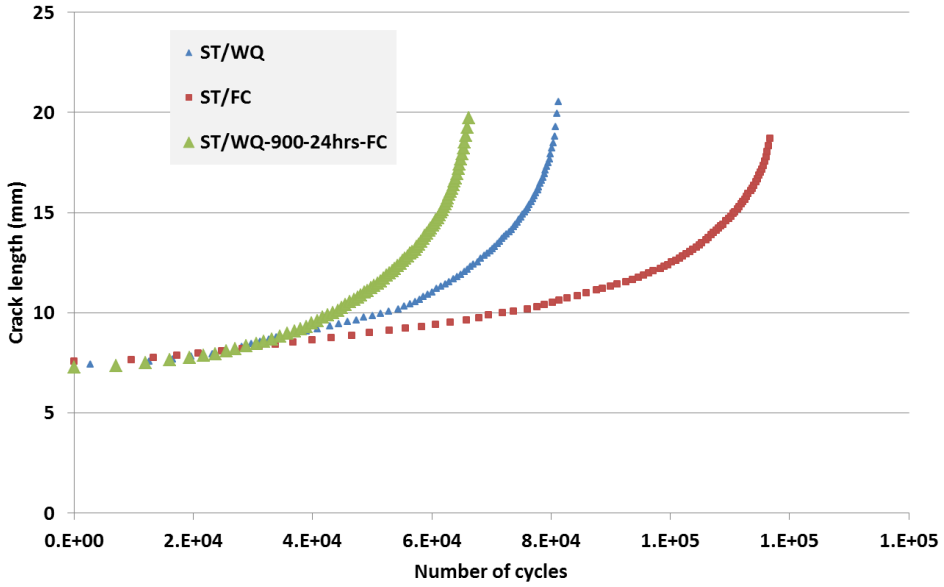

Figure 4.48: Crack length versus the number of cycles of ST/WQ, ST/WQ-900 °C-24 hrs-FC and ST/FC specimens of Ti-6Al-4V alloy

A Paris curve showing crack growth rate versus ΔK is shown in Figure 4.49. The ST/FC specimen had a greater fatigue crack growth resistance than the aged and the ST/WQ specimens. The crack growth rates (da/dN) of the ST/WQ and aged specimens were similar and higher than that of the ST/FC specimen for ΔK values of 16 to 32 MPa.m$^{0.5}$. All specimens showed similar crack growth rates at greater levels of ΔK (ΔK >32 MPa.m$^{0.5}$).

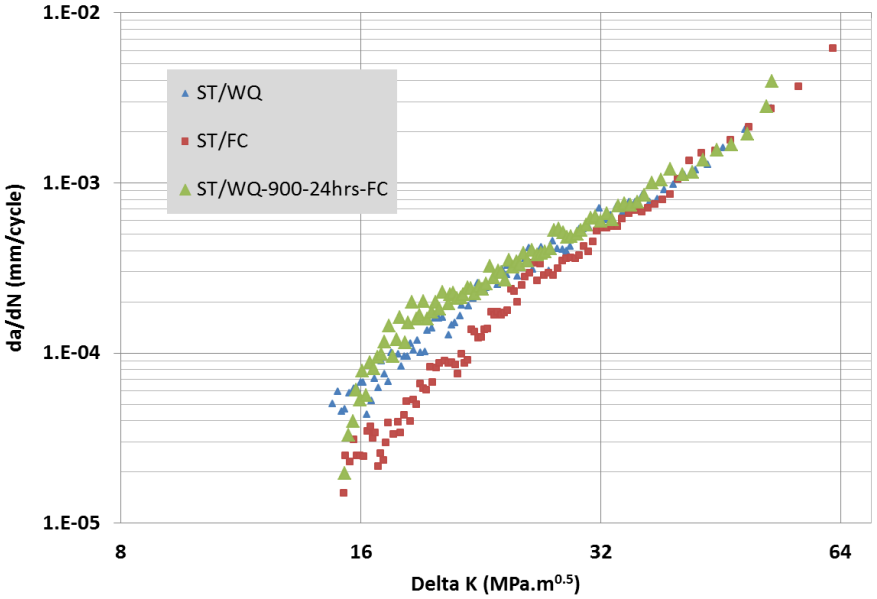

Figure 4.49: Fatigue crack growth rate versus ΔK of Ti-6Al-4V alloy

The Paris constants (*C*, *m*, ΔK_{th}, K_c) were determined for all the specimens and the results shown in Table 4.9. The ST/WQ specimen and the aged specimen had greater and similar *C* constants (measure of crack growth rate) than those of the ST/FC specimen. The *m* constant values for all the specimens were within the expected range of metals (2-4). The threshold stress intensity factors (ΔK_{th}) of the ST/WQ specimen and the aged specimen were similar but significantly lower than for the ST/FC specimen. The critical stress intensity (K_c) values for the ST/WQ and aged specimen were also similar but significantly lower than for the ST/FC specimen. The results show that the fatigue crack growth resistance of the aged and fully martensitic morphologies was similar. However, the fatigue crack growth resistance of the ST/FC specimen was superior.

Table 4.9: Paris constants of the Ti-6Al-4V alloy (±SD)

Specimen details	C (mm/cycle)	m	ΔK_{th} (MPa.m$^{0.5}$)	K_c (MPa.m$^{0.5}$)
ST/WQ	$1x10^{-8}$	3.2	11.6±0.5	63±1.9
ST/WQ-900 ºC-24 hrs-FC	$2x10^{-8}$	3.0	12.1±2.1	62±1.2
ST/FC	$4x10^{-10}$	4.0	15.2±0.6	68±1.2

Low-magnification optical images of the ST/WQ, ST/WQ-900 ºC-24 hrs-FC, and ST/FC Ti-6Al-4V specimens are shown in Figure 4.50. The ST/WQ and the aged specimen showed more straight fracture paths than the ST/FC specimen which showed zigzag crack paths. Crack deflection was evident in the ST/FC specimen.

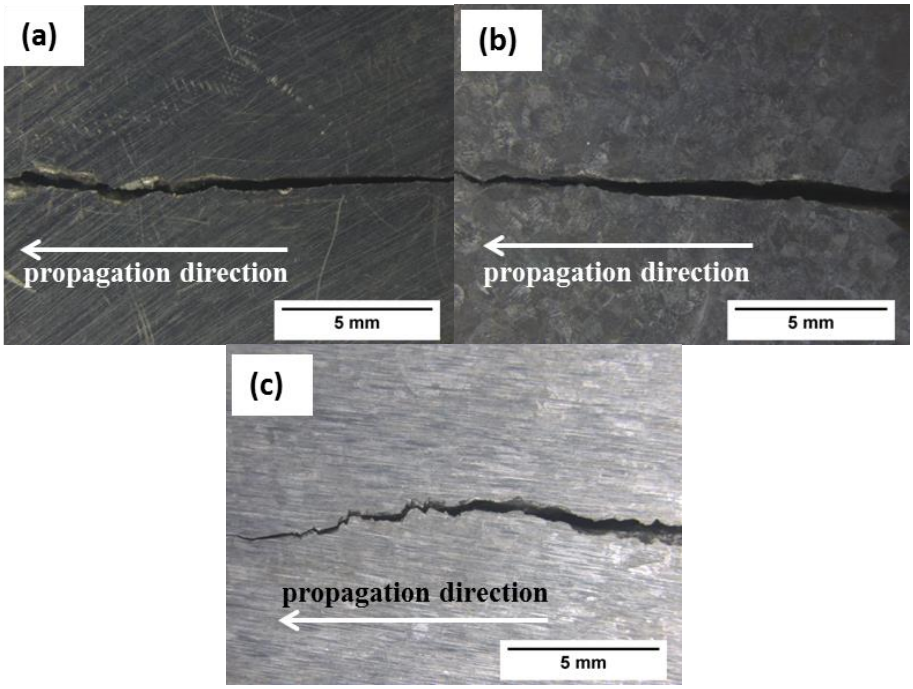

Figure 4.50: Low-magnification optical images of polished specimens of (a) ST/WQ, (b) ST/WQ-900 ºC-24 hrs-FC, and (c) ST/FC, after fatigue crack growth testing

The cross-sectional views of the fractures of the specimens are shown in the OM images in Figure 4.51. The ST/FC specimen (Figure 4.51 (c)) showed secondary cracks, and an uneven fracture surface, while the ST/WQ specimen in Figure 4.51 (a) showed more straight fracture paths and a smooth fracture surface, indicating brittle fracture. The aged specimen (Figure 4.51 (b) showed smaller deflections and crack branching compared to the ST/FC specimen. Secondary cracks were not observed in the aged specimen.

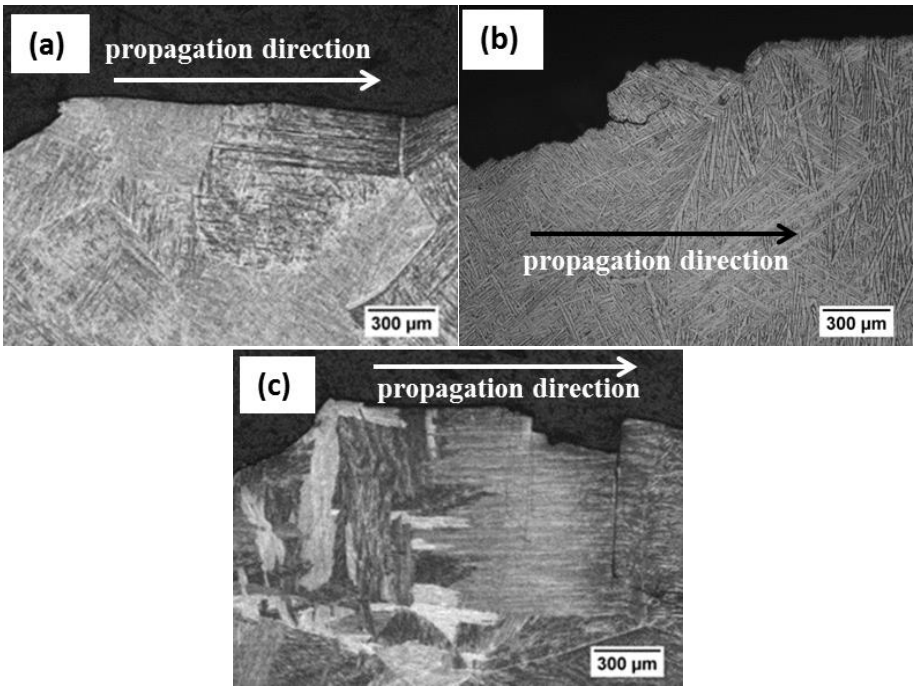

Figure 4.51: OM cross-sectional views of polished specimens of (a) ST/WQ, (b) ST/WQ-900 ºC-24 hrs-FC, and (c) ST/FC specimens after fatigue crack growth testing

The SEM micrographs of the cross-sectional views of the Ti-6Al-4V specimens are shown in Figure 4.52. The ST/FC specimen (Figure 4.52 (c)) showed larger crack deflection and crack branching, while the aged specimen (Figure 4.52 (b)) showed smaller crack branching. The ST/WQ specimen (Figure 4.52 (a)) showed microcrack formation whenever the crack propagated perpendicularly to the martensitic needles. In addition, as the crack propagated parallel to the martensitic needles, cleavage fracture occurred with no microvoid formation.

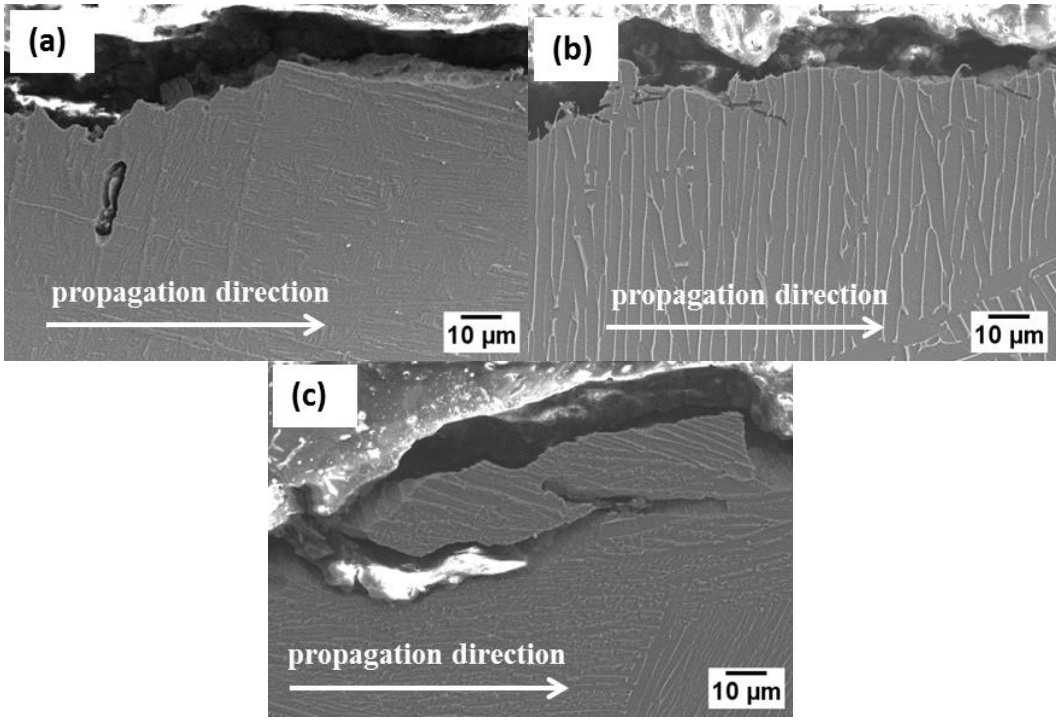

Figure 4.52: SEM cross-sectional views of (a) ST/WQ, (b) ST/WQ-900 ºC-24 hrs-FC, and (c) ST/FC after fatigue crack growth testing

Figure 4.53 shows SEM micrographs of the fracture surfaces after fatigue crack growth testing. The fracture surface of the ST/WQ specimen (Figure 4.53 (a)) showed a brittle surface, while the ST/FC specimen (Figure 4.53(c)) showed a more ductile surface. The aged specimen (Figure 4.53 (b) also showed a more ductile surface than the ST/WQ specimen. The formation of microcracks was observed on the fracture surface of the ST/WQ and the aged specimen. However, larger cracks appeared on the fracture surface of the ST/FC specimen (Figure 4.53(c)). Crack deflection at α-laths was evident in the ST/FC specimen, leading to an uneven fracture surface.

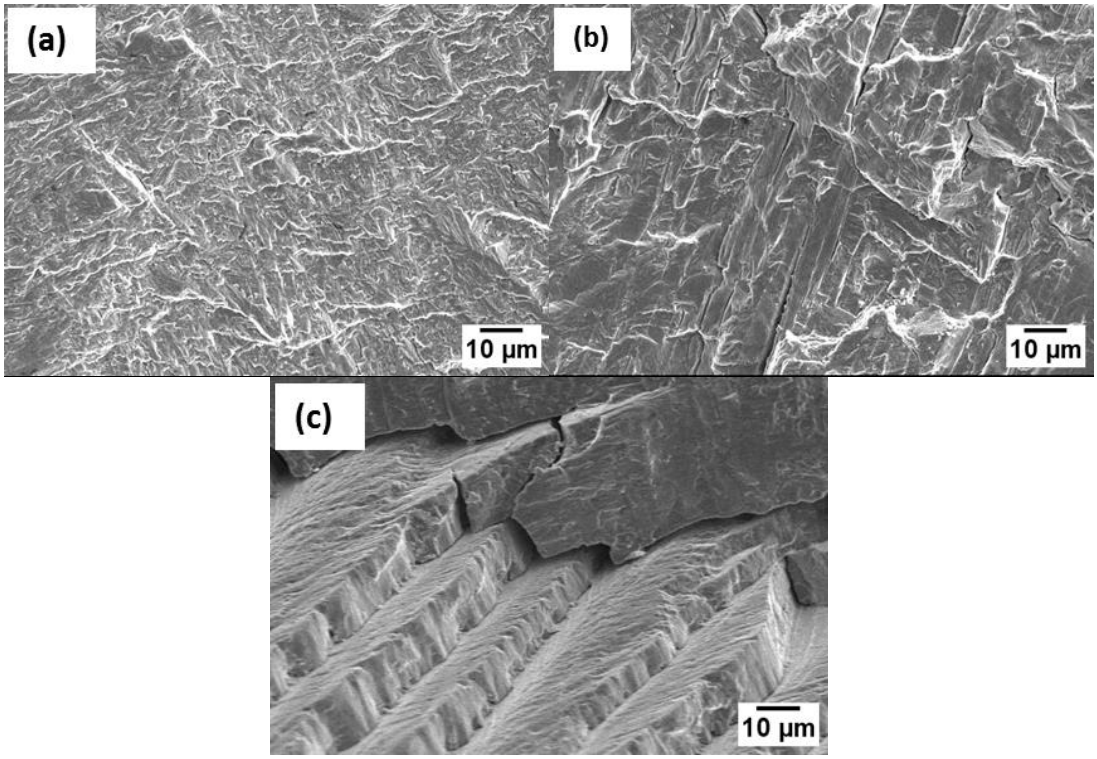

Figure 4.53: SEM fracture surfaces of (a) ST/WQ, (b) ST/WQ-900 ºC-24 hrs-FC, and (c) ST/FC after fatigue crack growth testing

CHAPTER 5 Discussion

5.1 Microstructural evolution during heat treatments and hardness

The high cooling rate (WQ) from the β-phase region (ST at 1050 °C) reduces the exposure time to diffusion dominated transformation of the β-phase and the β-grains. The shorter time of the ST/WQ process led to relatively smaller β-grains and a fine lath structure in the Ti-6Al-4V martensite. On the other hand, the lower cooling rate in the ST/FC treatment produced a coarser grain size and α/β-laths than in the martensitic microstructure. The fully martensitic morphology gave a greater hardness value than the colony morphologies due to the presence of fine martensitic needles. As the thickness of the laths increased in the ST/FC microstructure, the hardness dropped. Similar results are reported by Youssef et al. [7] (Figure 2.15) showing a fine lamellar microstructure with a greater hardness than the coarse lamellar microstructure. The hardness results are consistent with the general Hall-Petch relationship where finer structures give greater hardness values. The greater standard deviation in hardness of the Ti-6Al-4V alloy with a colony lamellar microstructure indicates heterogeneity of the microstructure as compared to the more homogenous fully martensitic morphology in the ST/WQ sample. The presence of thinner α/β-laths in the partial martensitic microstructure yielded lower hardness values than in the colony lamellar microstructure which contained coarser α/β-laths. The effects of solution treatment on microstructural features of the current study are consistent with results from the literature where Li et al. [31] found β-grains of about 600 μm for both ST/WQ and ST/AC, while the ST/FC yielded β-grains of 735 μm. The authors showed that a slow cooling rate gave rise to larger β-grains [31]. The thickness of the α-laths was found to be about 1 μm, 3 μm and 6 μm for ST/WQ, ST/AC and ST/FC respectively, while the colony width was about 350 μm for FC [31]. Guo et al. [42] also found the β-grain size of the FC Ti-6Al-4V specimens to be larger than those of the WQ specimens due to the slower cooling rate, allowing grain growth to occur.

Water-quenching from the solution treatment can produce α, α′ and β-phases which provides additional degrees of freedom in optimising the microstructure and mechanical properties than air-cooling or furnace-cooling with ageing treatment [9][23]. The presence of fine martensitic needles in the solution-treated and water-quenched specimens provided the highest possible yield strength and ultimate tensile strength, and consistency in the microstructure.

Furnace-cooling after ageing was found to provide sufficient time for continuous α′-needle's decomposition to form shorter α′-needles and fine β-phase to occur below 625 °C, thereby promoting age hardening. However, faster cooling after ageing such as water-quenching, resulted in reduced formation of the α_2-phase, giving relatively lower hardness values at ageing temperatures of 500 °C to 800 °C. Donachie [18] reported that Ti_3Al forms more easily with furnace-cooling than air-cooling, which might explain why furnace cooling yielded greater hardness values than water-quenching. Various authors reported the formation of the α_2-phase mainly within the lamellar morphology where the content of the aluminium is greater than 6%, therefore, α_2-phase formation during ageing of the fully martensitic morphology in this Ti-6Al-4V alloy is improbable [13][39]. At an ageing temperature of 900 °C, water-quenching after ageing gave greater hardness values. This increase was due to martensite forming during water-quenching as some of the β-phase had already formed at an ageing temperature of 900 °C. Even though furnace cooling after ageing was not notably

favourable compared to water quenching, it was selected for ageing of the fully martensitic morphology. Water-quenching after ageing was found to have little effect on the initial fully martensitic morphology, hence the choice of furnace cooling.

The ageing temperatures of 500 °C to 700 °C were below the α to β-phase transformation region (700 °C to 960 °C) resulting in the fully martensitic morphology remaining the same. The microstructure consisted mainly of α′, α and β-phases as reported by Mutombo et al. [21]. The decomposition of the longer α′-needles to shorter α′-needles during ageing at temperatures of 500 °C to 700 °C, led to a hardness increase relative to the unaged fully martensitic morphology. The increase in hardness is also attributed to the formation of the fine β-structures during ageing. The results are in agreement with those of Wang et al. [37] and Yu et al. [71] where it was found that the hardness increased at ageing temperatures of 500 °C to 600 °C. The proposition that martensite decomposes to form shorter needles is in agreement with the work of Donachie [18], Pinke [23] and Li et al. [31]. The authors reported that the ageing of a martensitic microstructure had led to the decomposition of the unstable β-phase and martensite to form fine shorter martensitic needles and fine β-phase, resulting in improved hardness. Zeng and Bieler [5], Gil et al. [14] and Pinke et al. [23] also reported the decomposition of α′-phase to form fine α′ and β-phases during ageing of a martensitic Ti-6Al-4V alloy. The martensitic needles changed from being long and thin, to being shorter and remaining thin. Shi et al. [72] and Li et al. [31] reported a similar geometry change after ageing of a martensitic morphology. The current study found the hardness to drop at ageing temperatures above 650 °C as the α-phase coarsened and the content of the α′-needles was reduced. The results of Wang et al. [37] in Figure 2.17 showed the hardness to drop below that of the unaged specimen at ageing temperatures of 650 °C to 700 °C, while the current study found an increase in hardness. The effect of ageing temperature on the hardness as reported by Gil et al. [14] in Figure 2.18, is contrary to that of other authors [14][18][37][72] and the current study. According to Gil et al. [14], hardness increases due to the transformation of the α′-needles to form short α′-needles and fine β-phase as the ageing temperature increases from 400 °C to 800 °C. The decomposition continues and is said to reach completion at 800 °C, leading to a continuous increase in hardness. The authors did not consider the possibility of coarsening of the α-phase due to overageing [14] as reported in this study and by other authors [14][18][37][72].

Ageing at 800 °C and 900 °C led to transformation of some of the α′-phase to the β-phase, resulting in a change to a partial martensitic morphology after furnace-cooling. At these temperatures, which are close to the β-transus temperature, α-phase transformation to the β-phase will occur during the ageing heating cycle. Furnace-cooling from the ageing temperature will then result in a microstructure consisting of the α-phase, and the residual α′ and β-phases, leading to a partial martensitic morphology. The martensite content is greatly reduced at higher ageing temperatures (800 °C and 900 °C), leading to hardness values lower than those of the unaged morphology. In addition, the α-phase which is known to be softer than the β-phase, increases in content and thickness, resulting in a further decrease in hardness. The reduction in hardness as the α-phase content increases is reported in the literature [12][40][73][72]. The α-phase is known to be stable at temperatures below 650 °C, while it transforms to the β-phase above 650 °C. Furnace-cooling after ageing between 800 °C and 900 °C results in an increase in the α-lath's thickness as the β-phase transforms to the α-phase during cooling [21].

The ageing times of 0.5 to 48 hours at ageing temperatures of 500 °C to 650 °C led only to decomposition of the α′-needles and precipitation of the fine β-phase. As the microstructure

still consisted of the α′ and β-phases, the morphology remained fully martensitic as the ageing time increased. The morphology was not expected to change as the temperatures were well below those of the α to β-phase transformation region. Even though the morphology did not change, the size of the denuded zones around the β-grain boundaries increased with increasing ageing time. Gil et al. [14] reported optimum hardness values at an ageing time of about 30 minutes, while increasing ageing times did not lead to much improvement in hardness. As ageing times increase, precipitation of the fine α and β-phases reaches a limit and no improvement in hardness is obtained [14]. The results of the current project are in agreement with the results of Ouchi et al. [27] (Figure 2.19) where an optimum hardness was found at 30 minutes, but a drop in hardness occurred as the ageing time increased. This drop in hardness is significant at higher temperatures and is attributed to the increase in the size of the fine α-phase, which is termed overageing [27]. The presence of fine α-needles at ageing temperatures of 650 °C and ageing time of 48 hours showed the closeness of this ageing temperature to the α/β stable region. Mutombo et al. [21] showed the α/β stable region to be about 650 °C to 900 °C.

At an ageing temperature of 750 °C, the transformation energy was sufficient to convert most of the martensitic needles to the β-phase, which subsequently transformed to the α-phase during furnace-cooling. The resulting microstructure was a mixture of α′, α and β-phases. As the ageing time increased, the denuded zone increased and coarse α-laths formed within the grains. At ageing temperatures of 800 °C, increasing ageing time led to the formation of coarser and irregular α-laths described as α-pools which is attributed to the massive transformation of the β-phase to the coarse α-phase. The results are in agreement with the literature where grain boundaries are said to transform completely to the α-phase with increasing ageing time [14][27]. Coarsening of the sub-grain α-pools continued to take place until a new microstructural morphology was produced, termed the basketweave morphology, clearly visible at an ageing temperature of 900 °C and ageing time of about 24 hours. The 900 °C ageing temperature was close to the β-transus temperature and longer ageing times allowed enough time for the transformation of all the phases to the β-phase, leading to α-phase formation during furnace-cooling. The heterogeneity of the microstructure increased consistently with the formation of the α-pools and coarsening of the α-phase as the ageing times increased. The continuous increase in the content and size of the of the α-phase as the ageing time increased led to a drop in hardness. The dissolution of the martensitic needles with increasing ageing time also led to a notable drop in hardness.

The colony lamellar morphology consisted of α/β-laths in which the α-phase transformed to the β-phase from ageing temperatures of 650 °C up to the β-transus temperature [21]. Therefore, ageing at temperatures below 900 °C were not expected to cause significant microstructural morphology changes, hence the lamellar morphology remained the same at ageing temperatures of 750 °C to 900 °C. However, the contents of the α and β-phases were expected to change depending on the ageing time and the cooling rate. The lamellar morphology in the work of Carreon et al. [13] and Lee et al. [39] also remained the same after ageing. The increase in ageing temperature followed by water-quenching after ageing led to an increase in the content of the β-phase, consistent with approaching the β-transus. The thickness of the α-phase was also reduced as the α-phase transformation to the β-phase progressed. The results of Carreon et al. [13] showed an increase in hardness after ageing a lamellar microstructure at 515 °C, 545 °C and 575 °C and an ageing time of 30 minutes. Carreon et al. [13] attributed the increase in hardness to the precipitation of the α_2-phase. Other authors also reported that fine crystals of Ti_3Al or α_2-phase formed inside the α-phase

in the Ti-6Al-4V alloy during ageing up to 625 °C. The α_2-phase promotes increased hardness values due to precipitation or an age-hardening mechanism. Mutombo et al. [21] reported the disappearance of the α_2-phase above 650 °C. The solvus temperature of the α_2-phase is said to be about 550 °C [9][13][21][39][74]. The current study did not obtain a notable increase in hardness at ageing temperatures of 750 °C or 800 °C for up to 24 hours as the hardening effect of the α_2-phase was not likely. The contribution of the α_2-phase to hardening of the Ti-6Al-4V alloy with a colony lamellar microstructure was not evaluated in this study. However, the hardness was found to increase notably from ageing temperatures of 800 °C and times of 48 hours owing to the significant increase in the β-phase content and the reduction in the thickness of the α-laths after water-quenching. The β-phase is known to give greater hardness values than the α-phase [12][40][46]. The consistency in the hardness values improved with increasing ageing temperature due to the formation of thin α-laths and a fine β-phase. It was surprising that increasing the ageing times from 0.5 to 48 hours did not produce significant changes in the hardness even though the β-phase content increased. The results were similar to what Carreon et al. [13] (Figure 2.20) found where a further increase in the ageing time from about 100 to 700 hours at ageing temperatures of 515 °C, 545 °C and 575 °C did not lead to a drop or change in hardness. However, Lee et al. [39] (Figure 2.21) reported a continuous increase in hardness after ageing of a lamellar microstructure at 545 °C for ageing times of 200 to 300 hours, contrary to what Carreon et al. [13] found.

As ageing temperatures were below the β-transus, ageing of the fully martensitic or lamellar morphology did not change the β-grain size and the colony size. The observation is in agreement with the results of Godfrey et al. [48] where the grain size of the Ti-6Al-4V alloy remained the same for heat treatments below the β-transus. In addition, the colony size was also not affected by the ageing treatment [48]. Carreon et al. [13] did not obtain a notable change in the colony size, the β-grain size and the thickness of the α-laths after ageing the lamellar morphology at 515 °C to 575 °C for up to 576 hours. The β-grain size, colony size and the thickness of the α-laths were also unchanged in the work of Lee et al. [39]. The current study and the literature are in agreement that the morphology, the β-grain size and the colony size remain the same after ageing of the lamellar morphology. However, higher ageing temperatures used in the current study led to an increase in the content of the β-phase during heating. In addition, water-quenching during cooling produced a greater content of martensitic needles and the β-phase, and the reduction in the thickness of the α-laths compared to the unaged colony lamellar microstructure.

5.2 Tensile properties

The presence of fine acicular martensitic needles in the fully martensitic morphology led to greater strength values, while the coarser α-laths in the lamellar morphology reduced the strength. The lower standard deviation in the fully martensitic morphologies indicated a homogenous and consistent microstructure attributable to the fine and dispersed martensitic needles. However, the lamellar morphologies had heterogeneous and inconsistent microstructures due to various sizes of colonies and α-laths. The results are in agreement with Reda et al. [8], Filip et al. [12], Donachie [18], Venkatesh et al. [41] and Dong et al. [26], who reported similar results where the yield strength (YS) and the ultimate tensile strength (UTS) of the fully martensitic morphology were the highest. Water-quenching from above the β-transus temperature was found to produce a greater volume fraction of the α′-needles resulting in the highest UTS. The colony lamellar microstructure (ST/FC) having a softer platelet α-phase, gave a lower YS than the harder martensitic α′-phase, consistent with results of Dong et al. [26] shown in Figure 2.16.

The decomposition of the martensitic needles to form short α′-needles and a fine β-phase led to an increase in the tensile properties (YS and UTS) after ageing of the fully martensitic morphology. The results were consistent with the reported literature [12][24][41]. Ageing of the fully martensitic morphology resulting in a partial martensitic morphology led to a decrease in tensile strength, due to the coarsening of the α-phase, and a reduction in the content of the martensitic needles (Specimens aged at 800 °C and 900 °C). As the ageing temperature and time increased, the content and the size of the α-phase increased, hence a reduction in tensile strength (YS and UTS) occurred. The geometry of the martensitic needles changed from being long and thin, to shorter and thin, followed by shorter and thick. This change initially led to the YS and UTS increase followed by a decrease [72]. Others found the increase in the content of the β-phase to lead to a greater YS and UTS [40][26][42]. Ageing of the lamellar morphology led to an increase in the YS and UTS due to the increase in the β-phase content and the reduction in the thickness of the α-laths.

The ductility percentage elongation (% EL) and percentage reduction in area (% RA) of the fully martensitic and the aged fully martensitic morphologies were similar due to the microstructure having remained fully martensitic after ageing. As the ageing temperature increased, the content of the martensitic needles decreased while the content of the α-phase increased, leading to an increase in ductility. A notable increase in ductility was obtained at an ageing temperature of 900 °C which is attributable to the substantial increase in the content of the α-phase. This finding was consistent with the α-phase known to deform more easily than the β-phase [6][40][46][73]. The highest ductility (15% EL, 35% RA) was obtained from the basketweave morphology, as it contained the highest α-phase content and the thickest α-laths. Such ductility values are common in specimens that are solution-treated below the β-transus temperature, and consist mainly of primary α-phase and smaller β-grains. In addition, the strength ductility balance of the basketweave microstructure was superior to that of the other variants evaluated (40% greater), mainly due to the greater content and the size of the α-phase. Chao et al. [44] suggested the use of the strength ductility balance as an indicator of optimised mechanical properties of the Ti-6Al-4V alloy. The lamellar type morphology was found to have a greater ductility than the fully martensitic morphology which was ascribed to the greater content of the α-phase.

The greater volume fraction of the α'-phase in the fully martensitic microstructural morphology led to the strain-hardening exponent and the strain-hardening rate being greater than in the partial martensitic and the colony lamellar microstructures. Gupta et al. [6] related the strain-hardening response of the fully martensitic morphology to the interactions of dislocations with each other and with the fine martensitic needles. Kao et al. [40], Venkatesh et al. [41] and Chao et al. [44] also reported that the fast cooling rate from above the β-transus led to a high dislocation density, hence greater strain-hardening. Dong et al. [26] show in Figure 2.16 that the strain-hardening exponent of the colony lamellar morphology having platelet α-phase is greater than that of the martensitic microstructure having α′-needles. This finding is contrary to what the current study found.

As the ageing temperature increased, the content of the β-phase decreased, resulting in the strain-hardening exponent and the strain-hardening rate dropping. As the α-phase content increased (i.e. the β-phase content decreased), the strain-hardening exponent and the strain-hardening rate decreased due to ease of deformation of the α-phase. The results are in agreement with those of Morita et al. [46] showing the strain-hardening to decrease with increasing ageing temperature due to the reduction in the volume of the retained β-phase. The current study has not investigated the effect of dislocations in strain-hardening. However, the strain-hardening results are consistent with results from other studies [6][41][46][47][48][44]

showing the content of the β-phase to be the dominant factor in strain-hardening. It was unexpected to find that the strain-hardening exponent of the aged lamellar morphology was significantly greater than that of the fully martensitic morphology (30% greater). However, the aged lamellar microstructure was expected to have a greater strain-hardening exponent than the unaged lamellar microstructure due to the increase in the β-phase content during ageing. Sugahara et al. [32] reported results where they showed that the Widmanstätten microstructure had the α/β-interface acting as obstacles to dislocation motion and having reduced grain boundary sliding. The relative content of the β-phase was found to be the dominant factor in strain-hardening of alpha-beta titanium alloys, while the β-grain size did not have a notable effect [1][6][41][47].

Ageing of the fully martensitic morphology led to a decrease in the strain-hardening exponent and the strain-hardening rate. However, ageing of the colony lamellar morphology led to an increase in the strain-hardening exponent and the strain-hardening rate. A high strain-hardening exponent and strength coefficient found after ageing are required for good ballistic properties. The strain-hardening rate curves of the Ti-6Al-4V alloy showed a continuous drop in the strain-hardening rate without any inflection, implying deformation slip as the only strain-hardening mechanism taking place. Various sources also found the Ti-6Al-4V alloy to have only one strain-hardening mechanism [6][41][46][47][48][44].

The increase in the volume fraction and size of the α-phase was consistent with the increase in the size of dimples resulting from ageing of the fully martensitic microstructure. This finding was consistent with the increase in ductility as ageing progressed. Lee and Lee [74] are in agreement as they found the size and the number of voids to increase with overageing. As the size of the α-laths increased, the size of the microvoids increased, which subsequently led to larger dimples. As the α-phase is easier to deform than the β-phase, the basketweave specimen of this study (with greatest ductility) was prone to more macroscopic plastic deformation as reported in the literature [12][40][46][73]. The greater content of the β-phase for low ductility specimens produced brittle fracture surfaces due to the difficulty in deformation. The formation of the β-phase during ageing of the colony lamellar microstructure produced more brittle fracture surfaces than the unaged lamellar microstructure. The material became harder and less ductile as the size and the number of dimples were reduced.

The microcracks were found mainly along the interfaces of the α′-needles and the β-phase or the α and β-laths as these were the preferred crack initiation sites. As the fully martensitic morphology contained long and thin α′ needles, the crack followed these needles to create large brittle fractures. The crack would then change direction only when encountering differently oriented martensitic needles. This crack propagation mode led to larger, faceted and brittle areas on the fracture surface with no dimples forming. Fracture of the martensitic morphologies was mainly by cleavage along the martensitic needles. The partial martensite and basketweave morphologies consisted of short and thicker α-laths. However, the crack changed direction after shorter distances than in the fully martensitic morphology. The fracture surfaces were rougher due to the formation of dimples. The colony lamellar and aged colony lamellar microstructures consisted of colonies of various orientations which gave rise to frequent crack deflection, leading to intermittent crack propagation. This crack propagation mode produced uneven fracture surfaces. All the specimens fractured in a transgranular mode with micro-void formation and coalescence being the main failure mechanisms. The results were consistent with those of Venkatesh et al. [41], Morita [46] and Filip [12] showing an increase in dimple size as the ductility increased. The fracture surfaces were also becoming rougher with increasing ductility.

5.3 Fracture toughness

The greater content of the α′-phase and the β-phase in the fully martensitic microstructure led to lower fracture toughness results, while the presence of a softer α-phase and various orientations of the α/β-colonies led to greater fracture toughness in the colony lamellar microstructure. The results were consistent with the UTS and the tensile ductility results where the colony lamellar specimen that showed greater ductility and lower UTS than the fully martensitic morphology gave greater fracture toughness values than the fully martensitic morphology. Various orientations of the α/β-colonies in the colony lamellar morphology slowed down the crack propagation rate by promoting crack branching and the formation of secondary cracks. A greater fracture toughness in the colony lamellar microstructure is consistent with the fractured surface being uneven and rougher, indicating ductile fracture. The greater fracture toughness is attributed to the larger crack deflection and branching due to the presence of α/β-colonies. The specimen with a fully martensitic microstructure showed smooth fractures, indicating brittle fracture and hence lower fracture toughness. Guo et al. [42] reported similar results in a Ti-6Al-4V alloy where the colony lamellar microstructure gave greater fracture toughness than the fully martensitic microstructure. The authors [42] attributed the greater fracture toughness to the presence of α/β-colonies, larger β-grains, and thicker α-laths.

The basketweave morphology, which showed significantly greater ductility than the colony lamellar microstructure gave a surprisingly lower fracture toughness than the microstructure consisting of a colony lamellar morphology. The fracture surface of the basketweave morphology showed larger dimples than the colony lamellar microstructure, while the fracture toughness was lower. This finding is not consistent with the generally accepted understanding that greater ductility implies greater fracture toughness. The work of Shi et al. [72] showing that fracture toughness is influenced by both the material's ductility (intrinsic fracture toughness) and the crack path tortuosity (extrinsic fracture toughness) may shed light on this exception. The basketweave microstructure (with a greater α-phase content) would have a greater intrinsic fracture toughness, while the colony lamellar microstructure (with random orientation of α/β-colonies) would have greater extrinsic fracture toughness. Since crack propagation is mainly along the interface of the α-laths, the material's ductility plays a lesser role in crack deflection than the random orientation of α/β-colonies. This is a probable explanation why the lamellar microstructure gave a greater fracture toughness than the basketweave microstructure. Shi et al. [72] reported that fracture toughness can be greatly enhanced by optimisation of the extrinsic fracture toughness rather than the intrinsic fracture toughness. These authors found the intrinsic fracture toughness of the titanium alloy Ti–5Al–5Mo–5V– 1Cr–1Fe for different treatments to be close to one another. However, the extrinsic fracture toughness was vastly different for different morphologies. The content of the α and β-phases controls the intrinsic toughness, while the morphology controls the extrinsic fracture toughness. The larger effect of randomly oriented α/β-colonies as compared to the individual α-laths in enhancing fracture toughness was confirmed by Shi et al. [75]. Lütjering and Williams [38] are in agreement that the fracture toughness of the α+β titanium alloys increases with increased α/β-colony size, and the presence of α/β-colonies dominates the contribution of the ductile phases within the microstructure. Fan et al. [76] also ranked the influence of the colony size greater than the influence of the α-laths. Where the arrangement of the α/β-colony has no significant difference, the plastic zone at the crack tip may be the main factor [76]. Contrary to popular belief, greater ductility does not necessarily translate to greater fracture toughness. This study showed that ductility results from a tensile test cannot

always be used to predict fracture toughness. Ductility is simply a measure of plastic deformation, while fracture toughness is a measure of the resistance to crack propagation.

The current study found crack propagation in the Ti-6Al-4V alloy to be mainly transgranular (i.e. crack propagation was mainly through the grains rather than along grain boundaries). A schematic diagram depicting crack propagation in the Ti-6Al-4V alloy is shown in Figure 5.1. A crack will either cut through microstructural features or go around them as indicated in Figure 5.1. It is more difficult for a crack to propagate through thicker plates than to cut through thinner plates. Longer and thicker α-plates lead to larger crack deflections and greater fracture toughness. Larger and more α/β-colonies lead to even greater deflections and crack branching. The colony lamellar microstructure with longer and thicker α-plates, and α/β-colony lamellae yielded the best fracture toughness. However, the basketweave microstructure contained thicker and shorter α-plates which gave a lower fracture toughness than the lamellar microstructure. The fully martensitic morphology, which consisted of long and thinner α′-needles, gave the lowest fracture toughness. The work of Shi et al. [72] showed a similar result where the longer and thinner microstructural features produced the lowest fracture toughness, while the presence of larger colonies gave the highest fracture toughness. The fracture toughness did not seem to be influenced by the β-grain size as the crack propagation was transgranular. However, the β-grain size influenced the size of the other microstructural features (the colony size, α′ or α-length). The colony size and the α-lath size increase with increasing β-grain size. Peng et al. [57] confirmed the difficulty of correlating the fracture toughness to the β-grain size. These authors reported that the colony lamellar microstructure was the significant influence on the fracture toughness. Shi et al. [75] found fracture to be mainly along phase boundaries and not along grain boundaries. Random orientation of the α-plates is preferred for increased fracture toughness [75].

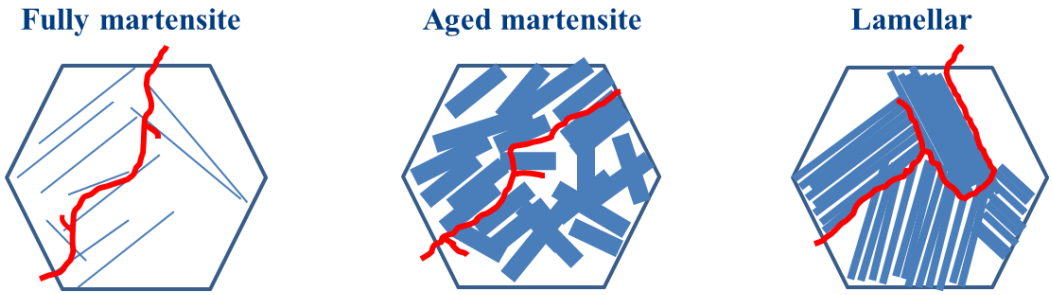

Figure 5.1: A schematic diagram showing the difference in crack propagation through various microstructures of the Ti-6Al-4V alloy

The basketweave morphology was found to have larger dimples than the colony lamellar microstructure, although its fracture toughness was lower. This finding is consistent with the tensile test results showing a greater ductility in the basketweave microstructure. The results are also consistent with the basketweave microstructure with a greater intrinsic fracture toughness than the colony lamellar microstructure. However, the lamellar microstructure showed larger crack deflections than the basketweave microstructure, which confirmed the greater extrinsic fracture toughness in the lamellar microstructure. The fully martensitic microstructure showed a brittle fracture surface as crack deflection was not as pronounced as in the colony lamellar or basketweave microstructures.

Plane strain fracture toughness values were not fully achieved in this study. The results showed that the Ti-6Al-4V alloy evaluated did not obey the linear elastic fracture approximation. An elastic plastic fracture mechanics approach would be more appropriate, as large scale yielding at the crack tip seemed to have been present. The results were consistent with those of Li et al. [31] where a compact tension specimen was used to determine the

plane strain fracture toughness of a titanium alloy (Ti–6Al–2Zr–1Mo–1V ELI). This author used a 40 mm thick specimen and plane strain fracture toughness was not achieved after solution treatment followed by furnace cooling, implying very high K_{1C} fracture toughness values. The fully martensitic microstructure of the current study produced near plane strain conditions due to the brittle nature of the microstructure. A J-integral test would be suitable to determine plane strain fracture toughness of the Ti-6Al-4V alloy as thinner specimens are required than those used in this study.

Even though plane strain fracture toughness values were not obtained, damage tolerance or yield strength to fracture toughness balance (YS x K_{1C}) of the specimens tested was evaluated by using apparent fracture toughness values (K_{1Q}). The current study's results were consistent with the results reported by Banerjee and Williams [61] in Figure 2.29, showing that increasing the content of the α-lath phase increased the fracture toughness and reduced the yield strength. The yield strength of the aged martensitic specimen was the lowest due to the highest content of the α-phase. However, its fracture toughness was lower than that of the ST/FC specimen which contained the α/β-colony lamellar morphology, leading to crack branching and deflection.

5.4 Fatigue crack growth

Similar to fracture toughness results, the existence of randomly oriented α/β-colonies in the lamellar morphology resulted in greater fatigue crack growth resistance than in the fully martensitic morphology or the basketweave morphology which had no colonies. The presence of colonies reduced the crack growth rate by promoting the formation of secondary cracks and crack bifurcation. Similar results were reported by Benedetti and Fontary [10], Krüger et al. [63], Leyens and Peters [19], Nalla et al. [11] and Qiu et al. [77] who showed that fatigue crack growth resistance in the colony lamellar morphology was superior due to the presence of α/β-colonies and their orientation. Surprising results were obtained by Li et al. [31] which showed that the lamellar microstructure had a lower fatigue crack growth resistance than the partial martensitic microstructure obtained by solution treatment followed by air-cooling in the Ti–6Al–2Zr–1Mo–1V alloy. The authors attributed the difference to the few colonies formed within the furnace-cooled microstructure, which limited the fatigue crack growth resistance. Peters and Lütjering [64] described the contribution of the larger colonies as improving the extrinsic fracture properties of the material. The current study demonstrated that the extrinsic mechanisms (crack deflection and branching) were the main contributors to higher fracture toughness and fatigue crack growth resistance. The fully martensitic microstructure containing a finer lamellar morphology showed a lower fatigue crack growth resistance, while the colony lamellar microstructure with a coarser lamellar microstructural morphology gave the highest fatigue crack growth resistance. These results are consistent with those reported by Lütjering and Williams [38] in Figure 2.31 which showed a fine lamellar microstructure with a lower fatigue crack growth resistance than a coarse lamellar microstructure.

The grain size and the size of sub-grains or colonies and the orientation of α/β-lamellae control the crack propagation in the Ti-6Al-4V microstructure. A crack will propagate through the weakest link in the microstructure. The grain boundaries or sub-grain boundaries are known to be weaker and hence determine the preferred crack propagation paths. The crack propagates along the α/β-interfaces in the colony lamellar microstructure and along the interfaces between the α′-needles and the β-phase in the fully martensitic microstructure. Where sub-grains or α-laths are larger, cracks will be deflected more than in the finer structures. Within a colony lamellar morphology, a crack is deflected whenever it meets a

differently oriented colony boundary. The deflection leads to crack branching and formation of secondary cracks. The colony lamellar microstructure leads to larger crack deflections than those of the finer martensitic microstructure. Qiu et al. [77] showed that crack deflection was mainly controlled by the α/β-colonies, followed by α-laths. Li et al. [31] also showed that grain boundaries did not affect crack propagation. The longer the length of the laths or width of colonies, the larger the deflections. An unexpected result was obtained where the fatigue crack growth resistance of the basketweave microstructure was similar to that of the fully martensitic microstructure. The result was surprising, as the fracture toughness of the basketweave microstructure was notably greater. It was not clear why such results were obtained. Could it be that the fracture mechanism during fatigue crack growth was different from the fracture toughness mechanism? Using the analogy of Shi et al. [72] where the length and thickness of the lath are considered, may possibly aid in explaining this anomaly. As the crack propagated slower in fatigue crack growth than during propagation in the fracture toughness tests, extrinsic properties (length and orientation of laths) play a larger role than that of the intrinsic properties (ductility of the laths). In addition, the crack has sufficient time to propagate between laths during fatigue crack growth. If this view is valid, then the thickness of the α-laths plays a lesser role in fatigue crack growth. This implies that a basketweave microstructure with shorter and thicker α-laths should not have a greater fatigue crack growth resistance than the fully martensitic microstructure with longer and thinner α′-needles. However, the fracture analysis of both microstructures showed little crack deflection, hence similar fatigue crack growth resistance patterns.

The larger the deflection of the crack (or at a lower crack growth rate) at an α/β-phase interface or at colony boundaries, the rougher the fractured surface, as was found in the lamellar microstructure indicating ductile fracture. However, the smaller deflection of the crack at a greater crack growth rate at the α'-interface led to a smoother fractured surface, as in the fully martensitic microstructure. In addition, the shorter α-laths in the basketweave microstructure led to a smaller crack deflection, resulting in a smoother fracture surface and showing brittle fracture. All specimens showed mainly transgranular fracture which confirmed the dominant α/β-colonies, α-laths and α′-needle on crack propagation, compared to the lesser role of the β-grain size. Consistent with the current study, other studies showed lamellar microstructures having rougher fracture surfaces due to the larger microstructural features (larger α/β-colonies) [11][63][64][77]. However, smaller microstructural features (fine martensitic needles and short α-laths) resulted in smaller crack deflection and flatter fracture surfaces.

The fatigue cracks in the fully martensitic, basketweave and lamellar morphology grew almost at the same rate up to about 4 $x10^4$ cycles. It picked up exponentially at about 5 $x10^4$ cycles in the basketweave morphology, 7 $x10^4$ cycles in the fully martensitic morphology, and about 9 $x10^4$ cycles in the lamellar microstructure. The observation confirms that the lamellar microstructure with coarser α/β-colonies has a better crack growth resistance than the fully martensitic or the basketweave microstructure. The uneven and rough fracture surface indicates ductile fracture in the lamellar microstructure, confirming an improved fatigue crack growth resistance. In addition, the formation of secondary cracks and large crack deflection in the colony lamellar microstructure are consistent with the greater fatigue crack growth resistance observed. The Paris constants (C, m, ΔK_{th} and K_c) of the fully martensitic and the basketweave microstructures were similar, confirming similar fatigue crack growth behaviour as shown by the fracture analysis. The fracture surfaces of the fully martensitic and the basketweave microstructures showed similar brittle fractures, confirming similarity of the Paris constants. The trend of the fatigue crack growth curves of the fully martensitic and basketweave morphologies were similar from region 1 to region 3 of the Paris

curve, indicating similar crack growth patterns. The influence of the microstructure (fully martensitic or basketweave) could not be observed from the Paris curves. However, the fatigue crack growth curve of the lamellar microstructure was distinguishable from the ΔK_{th} value up to the ΔK value of about 32 Mpa.$m^{0.5}$. This difference implied that region 2 of the Paris curve showed a clear microstructural sensitivity between the colony lamellar morphology and the fully martensitic or basketweave morphology. For the ΔK values (above 32 Mpa.$m^{0.5}$) approaching region 3 of the Paris curve, the fatigue crack growth curves could not be differentiated due to the high crack growth rates. The observation was consistent with other studies showing that region 3 crack growth was not sensitive to microstructural differences [63] [77]. To propagate a crack in a fully martensitic morphology or basketweave morphology required a lower stress intensity, as the threshold stress intensity values (ΔK_{th}) were lower than in the microstructure with a lamellar morphology. Consistent with fracture toughness results, the terminal stress intensity value (K_c) for the lamellar morphology was fairly greater than those of the fully martensitic and the basketweave morphologies. However, the K_c values of fully martensitic and the basketweave morphologies were similar, even though their fracture toughness values were different. Ageing of the fully martensitic morphology could not improve fatigue crack growth resistance even though the fracture toughness was improved.

CHAPTER 6 Conclusions

The influence of ageing treatment on the microstructural evolution and, subsequently, the effect of microstructures on the hardness, tensile properties, fracture toughness and fatigue crack growth of the Ti-6Al-4V alloy have been studied and the following conclusions can be made:

- Ageing of the solution-treated and water-quenched (ST/WQ) specimens (fully martensitic microstructure) was found to result in greater Yield Strength (YS), Ultimate Tensile Strength (UTS), strain-hardening exponent, and strain-hardening rate than for ST/WQ specimens that were unaged.
- Optimum ageing conditions for the ST/WQ specimens to produce a high YS, UTS and strain-hardening were found to be at about 500 °C for 0.5 hours, followed by furnace-cooling.
- Ageing of the solution-treated and furnace cooled (ST/FC) specimens (colony lamellar morphology) did not improve hardness and tensile properties significantly, compared to the unaged lamellar microstructure. However, the aged lamellar specimen produced the highest strain-hardening exponent and strength coefficient. The high strain-hardening exponent and strength coefficient can be used to yield improved ballistic properties.
- The highest strength-ductility balance (UTS x %EL), was found in the specimen that had been treated by ST/WQ, followed by ageing at 900 °C for 24 hours, and furnace-cooled (basketweave microstructure).
- Although increasing the ageing temperature and time increased the thickness of the α-laths for ST/WQ specimens, a basketweave microstructure with highest ductility and YS and UTS similar to that of the colony lamellar microstructure was produced. Where a colony lamellar microstructure is used for its strength (YS and UTS) and ductility properties, an alternative microstructure (basketweave) offers superior ductility while maintaining similar YS and UTS.
- The fracture toughness was found to be superior in the microstructure with a colony lamellar morphology due to the presence of randomly oriented α/β-colonies. The fully martensitic morphology had the lowest fracture toughness, while the basketweave morphology had an in-between fracture toughness. Ageing of the fully martensitic microstructure improved the fracture toughness.
- Similar to fracture toughness, the fatigue crack growth resistance of the microstructure with a colony lamellar morphology was superior. The threshold stress intensity and the critical stress intensity factors were greater for the lamellar microstructure (ΔK_{th} = 15.2 MPa.m$^{0.5}$, K_c = 68 MPa.m$^{0.5}$) but lower for the fully martensitic microstructure (ΔK_{th} =11.6 MPa.m$^{0.5}$, K_c = 63 MPa.m$^{0.5}$). The presence of randomly oriented α/β lamellar colonies led to crack deflection, branching, and formation of secondary cracks, resulting in greater fatigue crack growth resistance in the colony lamellar morphology. The microstructure with a fully martensitic morphology and (aged fully martensitic) basketweave morphologies showed similar fatigue crack growth behaviour. Ageing of the microstructure with a fully martensitic morphology did not produce a notable difference in the fatigue crack growth resistance.

- Controlling the amount of the α and β-phases, their morphologies, and their geometry can benefit in obtaining the required combination of microstructure and mechanical properties in the Ti-6Al-4V alloy.

The current research study has demonstrated the benefit that can be derived from ageing of the microstructure with a fully martensitic morphology and with a colony lamellar morphology. The evolution of microstructures with the ageing conditions was substantially explored and presented. The study has also provided a correlation between the microstructure and the mechanical properties of the Ti-6Al-4V alloy.

CHAPTER 7 Recommendations

The determination of plane strain fracture toughness of the Ti-6Al-4V alloy was partially achieved. The alloy showed elasto-plastic fracture behaviour, requiring thicker specimens to get valid plane strain fracture toughness results. Due to sample size constraints, machining time and testing time required, the determination of plane strain fracture toughness was discontinued. The use of a J-integral (J_{1C}) method instead of a K_{1C} is proposed for future work. This would allow the determination of the true damage tolerance in this alloy.

Fracture toughness and fatigue crack growth resistance of the various microstructural morphologies produced by ageing of the colony lamellar morphology were not evaluated and can form part of future work.

Evaluation of the ballistic performance of the solution-treated and furnace-cooled specimens followed by ageing may be done as part of future studies. This recommendation is made due to the strain-hardening exponent and the strength coefficient being substantially greater than in other specimens evaluated.

Bibliography

[1] A. A. Salem, S. R. Kalidindi, and R. D. Doherty, "Strain hardening of titanium: Role of deformation twinning," *Acta Mater.*, vol. 51, no. 14, pp. 4225–4237, 2003.

[2] S. Zhang, J. Li, H. Kou, J. Yang, G. Yang, and J. Wang, "Microstructure evolution of isothermal holding treatment during melt solidification of Ti–6Al–4V alloy," *Trans. Nonferrous Met. Soc. China*, vol. 25, no. 4, pp. 1091–1096, 2015.

[3] C. Veiga, J. Davim, and A. Loureiro, "Properties and Applications of Titanium Alloys: a Brief Review," *Rev. Adv. Mater. Sci*, vol. 32, pp. 133 – 148, 2012.

[4] J. Cai, F. Li, T. Liu, and B. Chen, "Investigation of mechanical behavior of quenched Ti-6Al-4V alloy by microindentation," *Mater. Charact.*, vol. 62, no. 3, pp. 287–293, Mar. 2011.

[5] L. Zeng and T. R. Bieler, "Effects of working, heat treatment, and aging on microstructural evolution and crystallographic texture of α, α′, α″ and β phases in Ti-6Al-4V wire," *Mater. Sci. Eng. A*, vol. 392, no. 1–2, pp. 403–414, 2005.

[6] R. K. Gupta, C. Mathew, and P. Ramkumar, "Strain Hardening in Aerospace Alloys," *Front. Aerosp. Eng.*, vol. 4, no. 1, pp. 1–13, 2015.

[7] S.S.Youssef, K. M. Ibrahim, and M. Abdel-Karim, "Effect of Heat Treatment Process on Tribological Behavior of Ti-6Al-4V Alloy," vol. 2, no. 4. 2013.

[8] A. H. Reham Reda, Adel Nofal, "Effect of Quenching Temperature on the Mechanical Properties of Cast Ti-6Al -4V Alloy," *J. Metall. Eng.*, vol. 2, no. 1, pp. 48–54, 2013.

[9] G. Lütjering, J. C. Williams, and A. Gysler, *Microstructure and mechanical properties of Titanium alloys*, vol. 2. Boston, MA: Springer US, 2000.

[10] M. Benedetti and V. Fontanari, "The effect of bi-modal and lamellar microstructures of Ti-6Al-4V on the behaviour of fatigue cracks emanating from edge-notches," *Fatigue Fract. Eng. Mater. Struct.*, 2004.

[11] R. K. Nalla, B. L. Boyce, J. P. Campbell, J. O. Peters, and R. O. Ritchie, "Influence of microstructure on high-cycle fatigue of Ti-6Al-4V: Bimodal vs. lamellar structures," *Metallurgical and Materials Transactions A*, vol. 33, no. 13. pp. 899–918, 2002.

[12] R. Filip, K. Kubiak, W. Ziaja, and J. Sieniawski, "The effect of microstructure on the mechanical properties of two-phase titanium alloys," *J. Mater. Process. Technol.*, vol. 133, no. 1–2, pp. 84–89, Feb. 2003.

[13] H. Carreon, A. Ruiz, and B. Santoveña, "Study of aging effects in a Ti-6AL-4V alloy with widmanstätten and equiaxed microstructures by non-destructive means," *AIP Conf. Proc.*, vol. 1581 33, no. JANUARY 2014, pp. 739–745, 2014.

[14] F. X. Gil Mur, D. Rodríguez, and J. a. Planell, "Influence of tempering temperature and time on the α′-Ti-6Al-4V martensite," *J. Alloys Compd.*, vol. 234, no. 2, pp. 287–289, 1996.

[15] R. Dabrowski, "The Kinetics of Phase Transformations during Continuous Cooling of Ti6Al4V Alloy from the Diphase Alpha Plus Beta Range," *Arch. Metall. Mater.*, vol. 56, no. 2, pp. 217–221, Jan. 2011.

[16] K. P. Rao, K. Angamuthu, and P. B. Srinivasan, "Fracture toughness of electron beam welded Ti6Al4V," *J. Mater. Process. Technol.*, vol. 199, no. 1–3, pp. 185–192, Apr. 2008.

[17] www.arcam.com, “Titanium alloy Ti6Al4V ELI,” 2017. [Online]. Available: http://www.arcam.com/wp-content/uploads/Arcam-Ti6Al4V-ELI-Titanium-Alloy.pdf.

[18] M.J. Donachie, *Titanium: A Technical Guide*, 2nd ed. ASM International, 2000.

[19] C. Leyens and M. Peters, *Titanium and Titanium Alloys, Fundamentals and Applications*. 2003.

[20] S. L. Semiatin, S. L. Knisley, P. N. Fagin, F. Zhang, and D. R. Barker, “Microstructure Evolution during Alpha-Beta Heat Treatment of Ti-6Al-4V,” vol. 34, no. October, pp. 8–10, 2003.

[21] K. Mutombo, C. Siyasiya, and W. E. Stumpf, “Dynamic globularization of α -phase in Ti6Al4V alloy during hot compression,” in *Thermec’2013: International Conference on Processing & Manufacturing of Advanced Materials*, 2013.

[22] J. Sieniawski, W. Ziaja, K. Kubiak, and M. Motyk, “Microstructure and Mechanical Properties of High Strength Two-Phase Titanium Alloys,” in *Titanium Alloys - Advances in Properties Control*, InTech, 2013.

[23] P. Pinke, Ľ. Čaplovič, and T. Kovács, “The Influence of Heat Treatment on the Microstructure of the Casted Ti6Al4V Titanium Alloy,” *Slovak Univ. …*, vol. 20, no. May, pp. 1–6, 2011.

[24] ASM international, *ASM handbook Volume 2: Properties and Selection: Nonferrous Alloys and Special-Purpose Materials*. ASM International. Metals Park, Ohio, USA, 1990.

[25] Y. Fan, W. Tian, Y. Guo, Z. Sun, and J. Xu, “Relationships among the Microstructure , Mechanical Properties , and Fatigue Behavior in Thin Ti6Al4V.”

[26] J. Dong, F. Li, and C. Wang, “Micromechanical behavior study of α phase with different morphologies of Ti-6Al-4V alloy by microindentation,” *Materials Science and Engineering A*, vol. 580. pp. 105–113, 2013.

[27] C. Ouchi, H. Fukai, and K. Hasegawa, “Microstructural characteristics and unique properties obtained by solution treating or aging in β-rich α+β titanium alloy,” *Mater. Sci. Eng. A*, vol. 263, no. 2, pp. 132–136, May 1999.

[28] S. L. Semiatin, P. N. Fagin, M. G. Glavicic, I. M. Sukonnik, and O. M. Ivasishin, “Influence on texture on beta grain growth during continuous annealing of Ti-6Al-4V,” *Mater. Sci. Eng. A*, vol. 299, pp. 225–234, 2001.

[29] F. J. Gil, M. P. Ginebra, J. M. Manero, and J. A. Planell, “Formation of α-Widmanstätten structure: effects of grain size and cooling rate on the Widmanstätten morphologies and on the mechanical properties in Ti6Al4V alloy,” *J. Alloys Compd.*, vol. 329, no. 1–2, pp. 142–152, Nov. 2001.

[30] M. T. Jovanović, S. Tadić, S. Zec, Z. Mišković, and I. Bobić, “The effect of annealing temperatures and cooling rates on microstructure and mechanical properties of investment cast Ti-6Al-4V alloy,” *Mater. Des.*, vol. 27, no. 3, pp. 192–199, 2006.

[31] S. Li, B. Xiong, S. Hui, W. Ye, and Y. Yu, “Effects of microstructure on fatigue crack growth behavior of Ti–6Al–2Zr–1Mo–1V ELI alloy,” *Mater. Charact.*, vol. 59, no. 4, pp. 397–401, Apr. 2008.

[32] T. Sugahara, D. a. P. Reis, C. Moura Neto, M. J. R. Barboza, E. a. C. Perez, F. Piorino Neto, and A. C. O. Hirschmann, “The Effect of Widmanstätten and Equiaxed Microstructures of Ti-6Al-4V on the Oxidation Rate and Creep Behavior,” *Mater. Sci. Forum*, vol. 636–637, pp. 657–662, 2010.

[33] K. Gu, H. Zhang, B. Zhao, J. Wang, Y. Zhou, and Z. Li, “Effect of cryogenic treatment and aging treatment on the tensile properties and microstructure of Ti-6Al-4V alloy,” *Mater. Sci. Eng. A*, vol. 584, pp. 170–176, Nov. 2013.

[34] S. Hadke, R. K. Khatirkar, S. K. Shekhawat, S. Jain, and S. G. Sapate, “Microstructure Evolution and Abrasive Wear Behavior of Ti-6Al-4V Alloy,” *J. Mater. Eng. Perform.*, vol. 24, no. 10, pp. 3969–3981, 2015.

[35] H. Fujii, “Strengthening of α+β titanium alloys by thermomechanical processing,” *Mater. Sci. Eng. A*, vol. 243, no. 1–2, pp. 103–108, Mar. 1998.

[36] Y. T. Lee and G. Welsch, “Young’s modulus and damping of Ti-6Al-4V alloy as a function of heat treatment and oxygen concentration,” *Materials Science and Engineering: A*, vol. 128, no. 1. pp. 77–89, 1990.

[37] B. Wang, L. J. Huang, and L. Geng, “Effects of heat treatments on the microstructure and mechanical properties of as-extruded TiBw/Ti6Al4V composites,” *Mater. Sci. Eng. A*, vol. 558, pp. 663–667, Dec. 2012.

[38] G. Lütjering and J. C. Williams, *Titanium*, 2nd ed. Berlin, Heidelberg: Springer Berlin Heidelberg, 2007.

[39] D. G. Lee, S. Lee, and C. S. Lee, “Quasi-static and dynamic deformation behavior of Ti-6Al-4V alloy containing fine α2-Ti3Al precipitates,” *Materials Science and Engineering A*, vol. 366, no. 1. pp. 25–37, 2004.

[40] Y. L. Kao, G. C. Tu, C. A. Huang, and T. T. Liu, “A study on the hardness variation of alpha and beta-pure titanium with different grain sizes,” *Materials Science and Engineering A*, vol. 398, no. 1–2. pp. 93–98, 2005.

[41] B. D. Venkatesh, D. L. Chen, and S. D. Bhole, “Effect of heat treatment on mechanical properties of Ti–6Al–4V ELI alloy,” *Mater. Sci. Eng. A*, vol. 506, no. 1–2, pp. 117–124, Apr. 2009.

[42] P. Guo, Y. Zhao, W. Zeng, and Q. Hong, “The effect of microstructure on the mechanical properties of TC4-DT titanium alloys,” *Mater. Sci. Eng. A*, vol. 563, pp. 106–111, 2013.

[43] S. S. da Rocha, G. L. Adabo, G. E. P. Henriques, and M. A. D. A. Nóbilo, “Vickers hardness of cast commercially pure titanium and Ti-6Al-4V alloy submitted to heat treatments.,” *Braz. Dent. J.*, vol. 17, no. 2, pp. 126–9, Jan. 2006.

[44] Q. Chao, P. Cizek, J. Wang, P. D. Hodgson, and H. Beladi, “Enhanced mechanical response of an ultrafine grained Ti-6Al-4V alloy produced through warm symmetric and asymmetric rolling,” *Mater. Sci. Eng. A*, vol. 650, pp. 404–413, 2016.

[45] ASTM E646-00, *Standard Test Method for Tensile Strain-Hardening Exponents (n - Values) of Metallic*. ASTM International, West Conshohocken, PA, USA., 2000.

[46] T. Morita, K. Hatsuoka, T. Iizuka, and K. Kawasaki, “Strengthening of Ti–6Al–4V Alloy by Short-Time Duplex Heat Treatment,” *Mater. Trans.*, vol. 46, no. 7, pp. 1681–1686, 2005.

[47] S. X. Liang, L. X. Yin, L. Y. Zheng, M. Z. Ma, and R. P. Liu, “The Strain-Hardening Behavior of TZAV-30 Alloy After Various Heat Treatments,” *J. Mater. Eng. Perform.*, vol. 25, no. 2, pp. 530–535, 2016.

[48] T. M. T. Godfrey, A.Wisbey, P. S. Goodwin, and K. Bagnall, “Microstructure and tensile properties of mechanically alloyed Ti – 6A1 – 4V with boron additions,” *Mater. Sci. Eng. A*, vol. 282, no. 2000, pp. 240–250, 2000.

[49] S. Sinha, A. Ghosh, and N. P. Gurao, “Effect of initial orientation on the tensile properties of commercially pure titanium,” *Philos. Mag.*, vol. 6435, no. April, pp. 1–24, 2016.

[50] R. P. Mulay, J. A. Moore, J. N. Florando, N. R. Barton, and M. Kumar, “Microstructure and mechanical properties of Ti-6Al-4V: Mill-annealed versus direct metal laser melted alloys,” *Mater. Sci. Eng. A*, vol. 666, pp. 43–47, 2016.

[51] ASM international, *ASM Handbook, Volume 08: Mechanical Testing and Evaluation*. ASM International. Metals Park, Ohio, USA, 2000.

[52] G. Dieter and D. Bacon, *Mechanical Metallurgy. SI Metric Edition*. 1988.

[53] W. F. Hosford, *Mechanical Behavior of Materials*. Cambridge: Cambridge University Press, 2009.

[54] X. Feng, A. Wang, Y. Ma, X. Wu, J. Lei, and Y. Cui, “Influence of Microstructure on Fatigue Crack Propagation and Fracture Toughness of Large Ti-6Al-4V Cast Structure,” pp. 1–7, 2013.

[55] M. Srinivasan and S. Seetharamu, *Fracture Toughness of Metal Castings, Science and Technology of Casting Processes*. 2012.

[56] ASTM E399-12, *Standard Test Method for Linear-Elastic Plane-Strain Fracture Toughness KIc of Metallic Materials*. ASTM International, West Conshohocken, PA, USA., 2014.

[57] X. Peng, H. Guo, T. Wang, and Z. Yao, “Effects of beta treatments on microstructures and mechanical properties of TC4-DT titanium alloy,” *Materials Science and Engineering A*, vol. 533. pp. 55–63, 2012.

[58] H. J. Rack and J. I. Qazi, “Titanium alloys for biomedical applications,” *Mater. Sci. Eng. C*, vol. 26, no. 8, pp. 1269–1277, Sep. 2006.

[59] S. Shademan, V. Sinha, A. B. O. Soboyejo, and W. O. Soboyejo, “An investigation of the effects of microstructure and stress ratio on fatigue crack growth in Ti–6Al–4V with colony α/β microstructures,” *Mech. Mater.*, vol. 36, no. 1–2, pp. 161–175, Jan. 2004.

[60] D. G. Lee, S. Lee, and Y. Lee, “Effect of precipitates on damping capacity and mechanical properties of Ti-6Al-4V alloy,” *Mater. Sci. Eng. A*, vol. 486, no. 1–2, pp. 19–26, 2008.

[61] D. Banerjee and J. C. Williams, “Perspectives on titanium science and technology,” *Acta Mater.*, vol. 61, no. 3, pp. 844–879, 2013.

[62] ASTM E647 − 13a, *Standard Test Method for Measurement of Fatigue Crack Growth Rates*. ASTM International, West Conshohocken, PA, USA., 2014.

[63] L. Krüger, N. Grundmann, and P. Trubitz, “Influence of Microstructure and Stress Ratio on Fatigue Crack Growth in a Ti-6-22-22-S alloy,” *Mater. Today Proc.*, vol. 2, no. 0, pp. S205–S211, 2015.

[64] J. O. Peters and G. Lütjering, “Comparison of the fatigue and fracture of α+β and β titanium alloys,” *Metall. Mater. Trans. A*, vol. 32, no. 11, pp. 2805–2818, 2001.

[65] H. Matsumoto, H. Yoneda, K. Sato, S. Kurosu, E. Maire, D. Fabregue, T. J. Konno, and A. Chiba, “Room-temperature ductility of Ti-6Al-4V alloy with α’ martensite microstructure,” *Mater. Sci. Eng. A*, vol. 528, pp. 1512–1520, 2011.

[66] J. Oh, N. J. Kim, S. Lee, and E. W. Lee, “Correlation of fatigue properties and

microstructure in investment cast Ti-6Al-4V welds," *Mater. Sci. Eng. A*, vol. 340, no. 1–2, pp. 232–242, 2003.

[67] S. S. Al-Bermani, M. L. Blackmore, W. Zhang, and I. Todd, "The Origin of Microstructural Diversity, Texture, and Mechanical Properties in Electron Beam Melted Ti-6Al-4V," *Metall. Mater. Trans. A*, vol. 41, no. 13, pp. 3422–3434, 2010.

[68] ASTM E112, *Standard Test Methods for Determining Average Grain Size*. ASTM International, West Conshohocken, PA, USA., 2004.

[69] ASTM E384, *Standard Test Method for Knoop and Vickers Hardness of Materials*. ASTM International, West Conshohocken, PA, USA., 2012.

[70] ASTM E8/E8M-11, *Standard Test Methods for Tension Testing of Metallic Materials*. ASTM International, West Conshohocken, PA, USA., 2013.

[71] Y. Yu, W. Zhang, W. Dong, X. Han, C. Pei, X. Jiao, and Y. Feng, "Research on heat treatment of TiBw/Ti6Al4V composites tubes," *Mater. Des.*, vol. 73, pp. 1–9, 2015.

[72] X. Shi, W. Zeng, C. Shi, H. Wang, and Z. Jia, "The fracture toughness and its prediction model for Ti-5Al-5Mo-5V-1Cr-1Fe titanium alloy with basket-weave microstructure," *J. Alloys Compd.*, vol. 632, pp. 748–755, 2015.

[73] E. Lee, "Microstructure Evolution and Microstructure/Mechanical Properties Relationships in α + β Titanium Alloys," The Ohio State University, USA, 2004.

[74] D. G. Lee and S. Lee, "Effects of nano-sized alpha2 (Ti3Al) particles on quasi-static and dynamic deformation behavior of Ti-6Al-4V alloy with bimodal microstructure," *J. Mater. Sci.*, vol. 40, no. 15, pp. 4077–4084, 2005.

[75] Z. Shi, H. Guo, J. Han, and Z. Yao, "Microstructure and mechanical properties of TC21 titanium alloy after heat treatment," *Trans. Nonferrous Met. Soc. China*, vol. 23, no. 10, pp. 2882–2889, 2013.

[76] J. K. Fan, J. S. Li, H. C. Kou, K. Hua, and B. Tang, "The interrelationship of fracture toughness and microstructure in a new near β titanium alloy Ti-7Mo-3Nb-3Cr-3Al," *Materials Characterization*, vol. 96. pp. 93–99, 2014.

[77] J. Qiu, X. Feng, Y. Ma, J. Lei, Y. Liu, A. Huang, D. Rugg, and R. Yang, "Fatigue crack growth behavior of beta-annealed Ti–6Al–2Sn–4Zr–xMo (x=2, 4 and 6) alloys: Influence of microstructure and stress ratio," *Int. J. Fatigue*, vol. 83, pp. 150–160, 2016.

Appendices

Appendix I. Mechanical properties samples drawings

Tensile test specimen drawing

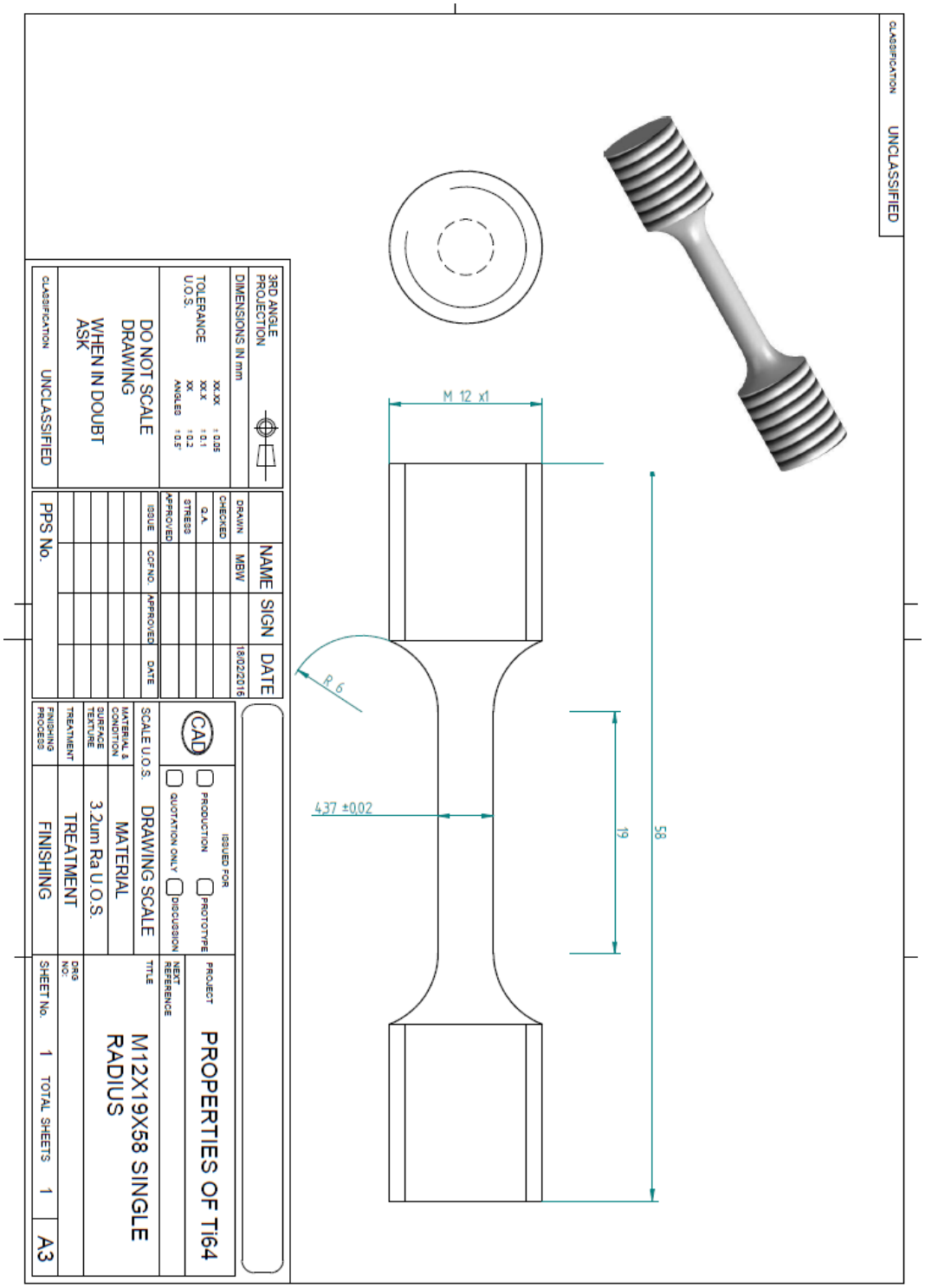

15mm thick bar type compact tension specimen drawing used for Fatigue crack growth testing

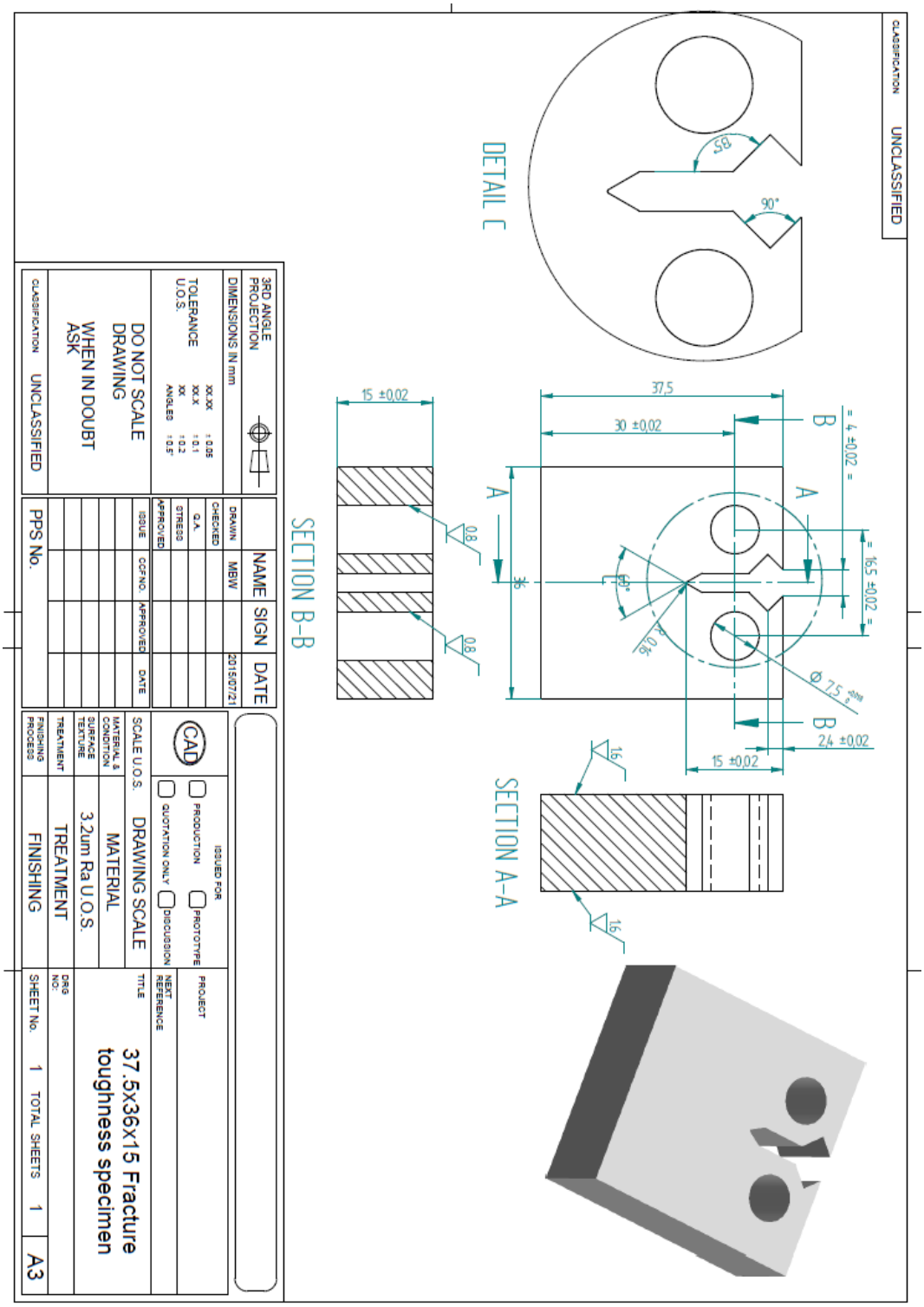

25mm thick disc type compact tension specimen drawing used for Fracture toughness testing

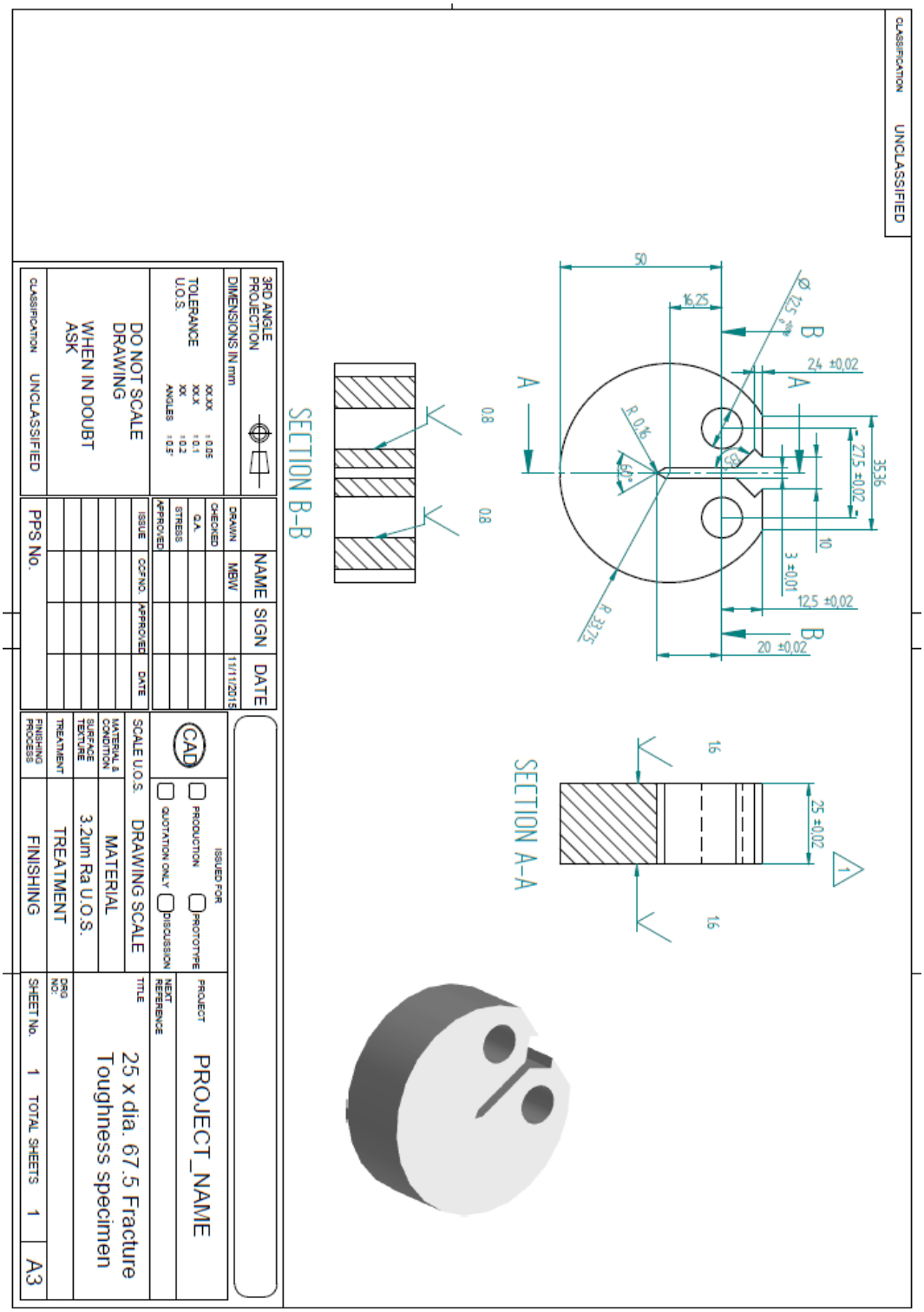

Appendix II. Table for calculation of fracture toughness values

Test method	Disc shaped type Compact tension specimen
Test speed (mm/min)	0.5
Temperature	Room
Size (mm)	62x50x25
Test procedure	ASTM E399

Specimen	W (mm)	B (mm)	a1 (mm)	a2 (mm)	a3(mm)	Average,a (mm)	Ligament (W-a), mm	a/w	f(a/w)	P_Q (N)	K_Q (Mpa.$m^{0.5}$)	YS (Mpa)	2.5*(K_Q/YS)^2
ST/WQ1	Sample 1	50.00	24.98	31.11	32.12	30.95	31.39	18.61	0.63	16.25	29801	86.71	905.79	22.91
ST/WQ2	Sample 2	50.00	24.98	30.19	31.16	30.95	30.77	19.23	0.62	15.43	29372	81.13	905.79	20.05
ST/WQ3	Sample 3	50.00	25.00	28.08	29.65	29.19	28.97	21.03	0.58	13.40	36009	86.34	905.79	22.72
							19.23			Median		86.34		22.72
										Stdev		3.12		
										CV%		3.62		

Specimen	W (mm)	B (mm)	a1 (mm)	a2 (mm)	a3(mm)	Average,a (mm)	Ligament (W-a), mm	a/w	f(a/w)	P_Q (N)	K_Q (Mpa.$m^{0.5}$)	YS (Mpa)	2.5*(K_Q/YS)^2
ST/FC1	Sample 1	50.00	24.85	26.85	27.08	26.85	26.93	23.07	0.54	11.57	59152	123.15	811.94	57.51
ST/FC2	Sample 2	50.00	24.99	26.73	26.60	26.60	26.64	23.36	0.53	11.35	58044	117.87	811.94	52.69
ST/FC3	Sample 3	50.00	24.97	26.63	26.70	27.13	26.82	23.18	0.54	11.48	57719	118.70	811.94	53.43
							23.18			Median		118.70		53.43
										Stdev		2.84		
										CV%		2.39		

Specimen	W (mm)	B (mm)	a1 (mm)	a2 (mm)	a3(mm)	Average,a (mm)	Ligament (W-a), mm	a/w	f(a/w)	P_Q (N)	K_Q (Mpa.$m^{0.5}$)	YS (Mpa)	2.5*(K_Q/YS)^2
ST/WQ-900-24-FC1	Sample 1	50.00	25.00	23.348	23.696	23.478	23.51	26.49	0.47	9.26	56578	93.70	756.41	38.36
ST/WQ-900-24-FC2	Sample 2	50.00	25.00	24.594	24.309	23.862	24.26	25.75	0.49	9.70	53853	93.45	756.41	38.16
ST/WQ-900-24-FC3	Sample 3	50.00	25.00	24.665	24.586	23.868	24.37	25.63	0.49	9.77	57745	100.96	756.41	44.54
							25.75			Median		93.70		38.36
										Stdev		4.26		
										CV%		4.55		